

**Zinc depletion-induced apoptosis is associated with altered microRNA expression in  
human breast cancer MDA-MB-231 cells**

by

MELINDA BAKKER

A THESIS SUBMITTED IN PARTIAL FULFILMENT OF  
THE REQUIREMENTS FOR THE DEGREE OF

MASTER OF SCIENCE

in

THE FACULTY OF GRADUATE AND POSTDOCTORAL STUDIES

(HUMAN NUTRITION)

THE UNIVERSITY OF BRITISH COLUMBIA  
(Vancouver)

October 2013

© Melinda Bakker, 2013

## **Abstract**

Zinc is an essential trace element required for many physiological functions, including growth. At the cellular level, zinc is required for structural and catalytic roles in thousands of proteins, and adequate labile zinc is an important determinant of cellular viability. However, abnormal zinc accumulation in breast tissue is associated with breast cancer, suggesting that zinc status plays a role in breast cancer pathogenesis. Chelation-induced depletion of labile intracellular zinc promotes apoptosis, or programmed cell death, in multiple breast cancer cell lines. The mechanisms whereby zinc regulates apoptosis remain unclear. In particular, little is known about the role of microRNAs (miRs), a novel class of short non-coding RNA, involved in the regulation of gene expression. Zinc status can influence miR expression, and possibly the processing and stability of miRs. The hypothesis of my thesis research is that miRs are involved in zinc depletion-induced apoptosis in human breast cancer cells. The overall objective of this study was to determine the involvement of miRs in zinc depletion-induced apoptosis in breast cancer MDA-MB-231 cells. Zinc depletion for 24, 48 and 72 h induced apoptosis in 4.5, 24.4 and 28.0 % of the cells, respectively, indicating a time-dependent increase in zinc depletion-induced apoptosis. Expression of 8, 90, and 94 miRs were significantly altered during the early stages of zinc depletion-induced apoptosis, at 3, 12, and 24 h of zinc depletion, respectively. Overall, expression of 285 unique miRs was significantly affected by zinc depletion, duration of zinc depletion, and their interactions. qRT-PCR analysis confirmed that zinc depletion resulted in an increased abundance of miR-132-3p, miR-1246, miR-1273, miR-4484 and miR-4787-5p and a decreased abundance of miR-4521 in a time-dependent manner. MiR-132-3p and miR-

1246 have previously been shown to play a role in mediating apoptosis in prostate cancer PC-3 and lung cancer A549 cells, respectively. In conclusion, abundance of numerous miRs was altered during the early stages of zinc depletion-induced apoptosis, indicating possible involvement of these miRs in mediating zinc depletion-induced apoptosis. The role and targets of these miRs in zinc depletion-induced apoptosis requires validation in further research.

## **Preface**

This dissertation presents the findings of my master's research study and was prepared in accordance with the requirements of the University of British Columbia Faculty of Graduate Studies. I designed the experiments together with Dr. Zhaoming Xu, and was responsible for performing all experiments and interpreting of the results under the supervision of Dr. Xu, with the exception of the microarray profiling experiment. LC Sciences performed the microarray profiling, as well as assisted with subsequent data analyses.

## Table of Contents

<b>Abstract</b> .....	<b>ii</b>
<b>Preface</b> .....	<b>iv</b>
<b>Table of Contents</b> .....	<b>v</b>
<b>List of Tables</b> .....	<b>vii</b>
<b>List of Figures</b> .....	<b>viii</b>
<b>Acknowledgements</b> .....	<b>xi</b>
<b>Introduction</b> .....	<b>1</b>
<b>Chapter 1: Literature Review, Hypothesis, and Objectives</b> .....	<b>3</b>
1.1. Zinc Overview .....	3
1.1.1. Introduction.....	3
1.1.2. Food sources .....	5
1.1.3. Absorption, transport & excretion .....	5
1.1.4. Cellular zinc homeostasis .....	8
1.2. Zinc and Breast Cancer.....	10
1.3. Zinc Depletion-Induced Apoptosis.....	15
1.3.1. Introduction to apoptosis .....	15
1.3.2. <i>In vivo</i> research .....	19
1.3.3. <i>In vitro</i> research .....	20
1.3.4. Mechanisms of zinc depletion-induced apoptosis .....	23
1.4. MicroRNAs: Regulators of Apoptosis .....	29
1.4.1. Introduction to microRNA.....	29
1.4.2. MiR biogenesis .....	30
1.4.3. MiR function.....	31
1.4.4. MiR stability .....	32
1.4.5. MiR expression in breast cancer.....	33
1.4.6. MiRs & apoptosis in breast cancer .....	36
1.5. Zinc and MiR Expression .....	40
1.6. Hypothesis .....	44
1.7. Overall Objective and Specific Aims .....	44
<b>Chapter 2: Zinc depletion-induced apoptosis is associated with altered microRNA expression in human breast cancer MDA-MB-231 cells</b> .....	<b>45</b>
2.1. Materials and Methods .....	45
2.1.1. Cell culture system .....	45
2.1.2. Depletion of intracellular zinc .....	45
2.1.3. Apoptosis assay .....	46
2.1.4. Total RNA isolation.....	47
2.1.5. MiR microarray assay.....	49
2.1.6. MiR heat maps.....	50
2.1.7. qRT-PCR miR assay.....	50
2.1.8. Statistics.....	52
2.2. Results .....	54
2.2.1. Zinc depletion-induced apoptosis.....	54
2.2.2. Zinc depletion altered miR expression .....	55

2.2.3. Zinc depletion altered abundance of miR-132-3p, miR-1246, miR-1273g-3p, miR-4484, miR-4521 and miR-4787-5p .....	57
2.3. Discussion.....	60
<b>Chapter 3: Conclusions, Limitations, and Future Directions .....</b>	<b>81</b>
3.1. Conclusions .....	81
3.2. Limitations.....	82
3.3. Future Directions .....	84
<b>References.....</b>	<b>87</b>
<b>Appendices .....</b>	<b>106</b>

## List of Tables

Table 2.1: Differential expression of miR-182-5p induced by 3-h TPEN treatment. ....	68
Table 2.2: Differential expression of miRs induced by 12-h TPEN treatment. ....	69
Table 2.3: Differential expression of miRs induced by 24-h TPEN treatment. ....	70
Table A.1: MiR expression in control and TPEN-treated MDA-MB-231 cells.....	107

## List of Figures

Figure 1.1: Key elements of the intrinsic mitochondrial apoptotic pathway.....	42
Figure 1.2: General pathway for microRNA (miR /miRNA) biogenesis and function.....	43
Figure 2.1: Zinc depletion-induced apoptosis in MDA-MB-231 cells.....	71
Figure 2.2: 3-h TPEN treatment altered expression of several miRs. ....	72
Figure 2.3: 12-h TPEN treatment altered expression of many miRs.....	73
Figure 2.4: 24-h TPEN treatment altered expression of many miRs.....	74
Figure 2.5: Zinc depletion promoted a time-dependent increase in hsa-miR-132-3p expression. ....	75
Figure 2.6: Zinc depletion increased expression of hsa-miR-1246 after 12 and 24 h TPEN treatment. ....	76
Figure 2.7: Zinc depletion-induced time-dependent upregulation of hsa-miR-4484. ....	77
Figure 2.8: Zinc depletion increased hsa-miR-4787-5p expression at 3 and 12 h. ....	78
Figure 2.9: Zinc depletion promoted expression of a-miR-1273g-3p in a time-dependent manner. ....	79
Figure 2.10: Zinc depletion inhibited has-miR-4521 expression in a time-dependent manner. .....	80
Figure A.1: Hsa-miR-16-5p expression measured by microarray (z-scores of log transformed signal intensities). ....	122
Figure A.2: Hsa-miR-16-5p expression during qRT-PCR experiment 1. ....	123
Figure A.3: Hsa-miR-16-5p expression during qRT-PCR experiment 2. ....	124
Figure A.4: Hsa-miR-16-5p expression during qRT-PCR experiment 3. ....	125
Figure A.5: Hsa-miR-16-5p expression during qRT-PCR experiment 4. ....	126
Figure A.6: Baseline DNdA fragmentation in MDA-MB-231 cells at 0 h. ....	127
Figure A.7: DNA fragmentation in MDA-MB-231 cells treated with TPEN at 3 h. ....	128
Figure A.8: DNA fragmentation in MDA-MB-231 cells treated with TPEN at 6 h. ....	129
Figure A.9: DNA fragmentation in MDA-MB-231 cells treated with TPEN at 12 h. ....	130
Figure A.10: DNA fragmentation in MDA-MB-231 cells treated with TPEN at 24 h. ....	131
Figure A.11: 48-h TPEN-induced DNA fragmentation in MDA-MB-231 cells.....	132
Figure A.12: 72-h TPEN-induced DNA fragmentation in MDA-MB-231 cells.....	133

## List of Abbreviations

<b>AIF</b>	Apoptosis inducing factor
<b>ANOVA</b>	Analysis of variance
<b>Ago</b>	Argonaute
<b>BAD</b>	BCL-2-associated death promoter protein
<b>BAK1</b>	BCL-2 antagonist killer 1
<b>BAX</b>	BCL-2 associated X protein
<b>BCL-2</b>	B-cell lymphoma 2
<b>BHK</b>	British hamster kidney
<b>BT-IC</b>	Breast tumor-initiating cells
<b>DCCR8</b>	DiGeorge syndrome critical region 8
<b>DCIS</b>	Ductal carcinoma <i>in situ</i>
<b>DIABLO</b>	Direct IAP binding protein with low pI
<b>DNase</b>	Deoxyribonuclease
<b>DMEM</b>	Dulbecco's modified eagle's medium
<b>DMSO</b>	Dimethyl sulfoxide
<b>DTPA</b>	Diethylenetriaminepentacetic acid
<b>dNTP</b>	Deoxyribonucleotide triphosphates
<b>dTTP</b>	Deoxythymidine triphosphate
<b>DYRK1A</b>	Dual specificity tyrosine-phosphorylation-regulated kinase 1A
<b>EDTA</b>	Ethylenediaminetetraacetic acid
<b>ER+/-</b>	Estrogen receptor-positive/-negative
<b>FBS</b>	Fetal bovine serum
<b>FOXO</b>	Forkhead box O
<b>HEK</b>	Human embryonic kidney
<b>HER2</b>	Human epidermal growth factor receptor type II
<b>H<sub>2</sub>O<sub>2</sub></b>	Hydrogen-peroxide
<b>Hsa</b>	Human
<b>HSD</b>	Honestly Significant Difference
<b>IAPs</b>	Inhibitor of apoptosis proteins
<b>ICAD</b>	Inhibitor of caspase-activated deoxyribonuclease
<b>LIPZ</b>	Labile intracellular pool of zinc
<b>MiR</b>	MicroRNA
<b>MMP</b>	Mitochondrial membrane potential
<b>MRE</b>	Metal response elements
<b>MT</b>	Metallothionien
<b>MTF-1</b>	Metal-responsive-element binding transcription factor-1
<b>MNU</b>	N-methyl-N-nitrosourea
<b>NAC</b>	N-Acetyl-L-Cysteine
<b>NF</b>	Nuclear factor
<b>NOS</b>	Nitric oxide synthase
<b>OMM</b>	Outer mitochondrial membrane
<b>PARP</b>	Poly ADP ribose polymerase
<b>PACT</b>	Protein activator of PKR
<b>PBL</b>	Peripheral blood T lymphocytes

<b>PBS</b>	Phosphate buffered saline
<b>PI</b>	Propidium iodide
<b>PR</b>	Progesterone receptor
<b>Pre</b>	Precursor
<b>PrE</b>	Primary prostatic epithelial
<b>Pri</b>	Primary
<b>PTP</b>	Permeability transition pore
<b>qRT-PCR</b>	quantitative reverse transcription polymerase chain reaction
<b>RISC</b>	RNA-induced silencing complex
<b>RNase</b>	Ribonuclease
<b>SD</b>	Standard deviation
<b>SirT</b>	Silent information regulator
<b>Sp</b>	Specificity protein
<b>SSPE</b>	Saline-sodium phosphate-EDTA
<b>TNF</b>	Tumor necrosis factor
<b>TPEN</b>	N,N,N',N'-tetrakis(2-pyridylmethyl)ethylenediamine
<b>TRBP</b>	Trans-activating response RNA-binding protein
<b>UTR</b>	Untranslated region
<b>VSMCs</b>	Vascular smooth muscles cells
<b>XIAP</b>	X-linked inhibitor of apoptosis protein
<b>Zip</b>	ZRT, IRT-like protein
<b>ZnT</b>	Zinc transporter

## **Acknowledgements**

I am grateful to the many people who helped make this research possible. First of all, I would like to acknowledge and thank my supervisor Zhaoming Xu for numerous hours spent guiding and assisting me with this research project. I would also like to thank my supervisory committee: Christine Scaman, Vivien Measday and Amandio Vieira for their insightful advice and feedback during the course of my research studies. I would also like to thank my labmates both past and present for their assistance and support, especially Deanna Ibbitson who really encouraged me during our many coffee shop visits. I would like to offer a huge thank you to my husband Patrick for supporting me through the inevitable ups and downs of my studies. I can't even describe all of the many ways you were there for me – not least of all visiting me when I was stuck in the lab for long hours, patiently listening to technobabble about my research, challenging me to grow as a person, providing endless encouragement and loving me unconditionally. I am thankful for the continued love and support of my family, especially my mom and dad, and my siblings Charlene, Brent and Katie. Thank you also mom and dad Bakker for your love and encouragement. A big thank you to the rest of the extended Ouwerkerk and Bakker family for your support, especially to Jonathan Bakker for being a sounding board on my research design and statistical analysis. I am grateful for the support I received from friends, with special thanks to Nick and Renee Reeves for their infectious positive attitude and frequent encouragement. I am thankful to have had the opportunity to pursue this research and for the many people who supported me throughout!

## Introduction

Zinc is an essential nutrient, required for a broad range of physiological functions in humans, including growth, reproduction, normal neurological function and immunity<sup>1</sup>. However, zinc accumulation has been associated with breast cancer<sup>2</sup>. Furthermore, elevated expression of some zinc transporters and the zinc storage protein metallothionein are implicated in breast cancer and have been found to regulate some cancer traits, including resistance to apoptosis<sup>3-10</sup>.

Zinc is known to regulate apoptosis and zinc depletion has been shown to induce apoptosis both *in vivo* and *in vitro*<sup>11,12</sup>. In multiple breast cancer cell lines, depletion of intracellular zinc promoted apoptosis through the intrinsic mitochondrial apoptotic pathway, involving release of cytochrome c from the mitochondria and activation of the caspase cascade<sup>13,14</sup>, though the exact mechanisms involved are not fully understood.

Currently, little is known about the role of microRNAs (miRs) in mediating zinc depletion-induced apoptosis. MiRs are small non-coding RNAs that regulate gene expression at the post-transcriptional level<sup>15</sup>. MiRs regulate numerous signaling pathways, including key apoptotic pathways in cancer<sup>16,17</sup>. Treatments targeting expression of miRs have been shown to influence cancer pathogenesis<sup>18</sup>.

Only a few studies to date have investigated the effects of zinc status on miR expression, finding that zinc regulates miR expression both *in vivo*<sup>19,20</sup> and *in vitro*<sup>21,22</sup>, and may influence the processing and stability of miRs<sup>21</sup>. Therefore, miRs might play a role in zinc depletion-induced apoptosis. This research is intended to investigate the possible

involvement of miRs in zinc depletion-induced apoptosis using human breast cancer MDA-MB-231 cells as a model. An improved understanding of the mechanisms involved in zinc-mediated regulation of apoptosis may contribute to the development of new treatment strategies against breast cancer.

# Chapter 1: Literature Review, Hypothesis, and Objectives

## 1.1. Zinc Overview

### 1.1.1. Introduction

Zinc is an essential trace element and the second most abundant trace element in humans after iron, with 2-3 grams of total zinc in an adult<sup>1</sup>. Zinc is present in all tissues, with 90% of the body zinc in the muscle and bones<sup>23</sup>. Zinc is present only as a divalent cation ( $Zn^{2+}$ ) in living organisms.

Zinc exerts a wide range of physiological functions. One of the most profound functions of zinc is its essential role in growth - zinc deficiency impairs growth in every living organism studied to date<sup>24</sup>. Zinc has many other physiological functions, including reproduction, brain development, immunity, taste and vision, etc.<sup>1</sup>. Zinc deficiency causes many adverse health effects; early symptoms of zinc deficiency are growth retardation, skin lesions, and immune dysfunction<sup>1</sup>. Additionally, hair loss and poor wound healing also occur with zinc deficiency<sup>1</sup>. Severe zinc deficiency can cause hypogonadism in male adolescents, failed pregnancies, diarrhea, infections and neurological disorders<sup>1</sup>. In humans, acrodermatitis enteropathica, a genetic disorder resulting in decreased absorption of zinc, results in the typical broad range signs of zinc deficiency including impaired growth, dermatitis, diarrhea, immune dysfunction and sometimes neuropsychological disorders<sup>25</sup>.

At the cellular level, zinc plays a role in numerous cellular signaling pathways, including those involved in cell proliferation, differentiation and apoptosis<sup>26</sup>. Zinc deficiency

has been shown to impair DNA synthesis<sup>27</sup>, reduce cell viability, and induce apoptotic cell death<sup>14</sup>.

Zinc is present in thousands of proteins, including many enzymes, which are known as zinc metalloenzymes, and transcription factors. Collectively, zinc metalloenzymes and zinc-containing transcription factors are known as zinc metalloproteins. Zinc metalloproteins have wide ranging functions, including their involvement in metabolism of proteins, carbohydrates, nucleic acids and lipids, as well as regulation of gene expression<sup>24</sup>. Using a bioinformatics approach, it is predicted that 10 % of the human proteome is made up of zinc-containing proteins, of which 40% are transcription factors, while the remainder is made up mostly of zinc metalloenzymes<sup>28</sup>. Zinc-containing transcription factors are zinc-finger proteins, in which zinc is bound to amino acids, most commonly 4 cysteine (Cys<sub>4</sub>) residues, or two cysteine residues followed by two histidine residues (Cys<sub>2</sub>His<sub>2</sub>)<sup>28</sup>. A major role for the zinc-finger structure is to interact with DNA base pairs, which is essential for the binding of transcription factors to their target nucleic acid sequence<sup>29</sup>. In zinc metalloenzymes, zinc plays both structural and catalytic functions. Zinc metalloenzymes belong to every enzyme classification, demonstrating a wide ranging role for zinc in enzyme function<sup>24</sup>. Another recently identified, but less well understood role of zinc, is that free zinc ion (Zn<sup>2+</sup>) has been shown to act as a second messenger in some cellular signaling pathways<sup>30</sup>.

### **1.1.2. Food sources**

The zinc content of foods is associated with its protein content. Thus, meats are generally good sources of zinc. Shellfish such as oysters are particularly rich in zinc (33.2-182.0 mg Zn/100g cooked oyster) and red meat is also a good source of zinc (e.g. cooked beef: 5.3 – 11.5 mg Zn/100g)<sup>31</sup>. White meats and finfish contain lower amounts of zinc (e.g. cooked turkey: 1.1 -3.6 mg Zn/100 g; chicken: 1.1 – 2.9 mg Zn/100g; wild atlantic salmon: 0.8 mg Zn/100 g)<sup>31</sup>. Milk (1.0-1.1 mg Zn/250 mL cup) and dairy products also provide a source of zinc<sup>31</sup>. Zinc is also found in whole grains (e.g. wheat germ: 8.0 mg Zn/100g) and legumes (ex. cooked lentils: 1.3 mg Zn/100g; cooked peas: 1.5 mg Zn/100g)<sup>31</sup>. While zinc is found in protein rich plant foods, the bioavailability of zinc in plant foods is generally lower due to the presence of inhibitors of absorption (e.g. phytic acid, oxalic acid and polyphenols, etc.)<sup>1</sup>. Thus, fruits and vegetables are generally poor sources of zinc<sup>31</sup>.

### **1.1.3. Absorption, transport & excretion**

During digestion, dietary zinc is hydrolyzed from amino acids and nucleic acids<sup>32</sup>. The solubility of zinc influences absorption. Plant ligands such as phytate (phosphorous storage form in plants) can bind to zinc forming insoluble complexes, making it unavailable for absorption<sup>33,34</sup>. Animal protein generally offers a higher bioavailability of zinc; furthermore, it has been shown to improve absorption of zinc from plant sources when they are ingested at the same time<sup>35,36</sup>.

The gastrointestinal system is mainly responsible for regulating systemic zinc homeostasis through absorption of dietary zinc and excretion of endogenous zinc<sup>25,37,38</sup>. Zinc is absorbed throughout the small intestine, with the jejunum being the main site of absorption<sup>39</sup>. Humans consuming diets low in zinc generally absorb zinc with a higher efficiency and are adapted to increase zinc absorption over time<sup>40</sup>. However, high phytate consumption prevents positive adaptations in zinc absorption during low zinc consumption. The efficiency of zinc absorption is generally inversely related to dietary zinc intakes; however, the quantity of dietary zinc absorbed increases with higher dietary zinc intakes.

Only recently have the molecular mechanisms of zinc absorption begun to be elucidated, due to increased understanding of the role of zinc transporters in enterocytes, or intestinal absorptive cells. In humans, there are two families of zinc transporters: the ZnT or SLC30A family and Zip (Zrt-, Irt-like proteins) or SLC39A family. To date, 10 ZnT and 14 Zip transporters have been identified in humans<sup>41</sup>. In 2002, it was discovered that mutation in Zip4 (Zrt-, Irt-like protein 4), a novel zinc transporter, was responsible for acrodermatitis enteropathica<sup>42,43</sup>. In mice, dietary zinc deficiency caused upregulation of Zip4 expression and promoted its localization to the apical plasma membrane of enterocytes<sup>44,45</sup>. Additionally, another zinc transporter ZnT5B was found to be involved in zinc uptake in human Caco-2 cells<sup>46</sup>.

In addition to dietary zinc absorption, the small intestine also reabsorbs zinc from endogenous secretions. Zinc is found in high levels in salivary, gastric, pancreatic and biliary secretions<sup>47</sup>. Reabsorption of endogenous zinc appears to be crucial to reaching positive zinc balance during low zinc intakes, more so than absorption of dietary zinc. In a human study,

when male subjects consumed a low zinc diet (4.1 mg Zn/day) for 6 months, the fractional zinc absorption rate was increased, but the total dietary zinc absorption still decreased compared to the baseline<sup>48</sup>. In compensation, fecal losses of endogenous zinc were reduced, resulting in a net crude positive zinc balance after 6 months. In another study, zinc homeostasis in young Chinese women from either a rural farming area with low zinc intakes (5.2 mg Zn/day) or an urban area with higher intakes (8.1 mg Zn/d) were compared<sup>49</sup>. There was no difference in fractional zinc absorption between these two groups of women, indicating that the rural women absorbed significantly lower zinc in proportion to the low dietary intake. However losses of endogenous zinc were decreased in the rural women, offsetting the lower amount of dietary zinc absorbed so that the total amount of zinc absorbed was similar between the two groups.

Upon entering the enterocyte, zinc may be utilized and/or stored locally. Absorbed zinc is also transported across the basolateral membrane into the portal vein. The ZnT1 transporter is thought to control release of zinc from enterocytes into the portal vein due to its location on the basolateral membrane<sup>50,51</sup> and role in zinc efflux from cultured cells<sup>52</sup>.

About 60% of zinc in general circulation is bound to albumin for transport<sup>32</sup>. Zinc may also be bound to transferrin,  $\alpha$ -2 macroglobulin, histidine and cysteine for transport<sup>32</sup>. The serum zinc makes up only 0.1% of the total body zinc, but it supplies tissues with the necessary zinc and undergoes quick turnover<sup>53</sup>. Plasma zinc is redistributed to tissues during a variety of conditions (e.g. inflammation, infection, trauma, stress and the postprandial period all decrease plasma zinc)<sup>54</sup>.

The gastrointestinal tract is the primary location for loss of zinc from the body due to fecal excretion<sup>55</sup>. Zinc may also be lost in smaller amounts through urine, sweat, shed skin, nails, hair, menstruation and semen<sup>37</sup>.

In summary, systemic zinc homeostasis is maintained primarily at the gastrointestinal tract through regulation of dietary zinc absorption and endogenous secretion of zinc. Fractional absorption of dietary zinc tends to be inversely related to dietary zinc intakes. Reductions in endogenous zinc losses are a critical factor in conserving zinc status during low dietary intakes.

#### **1.1.4. Cellular zinc homeostasis**

The total cellular zinc concentration is typically maintained around a few hundred micromolar (e.g. 264  $\mu\text{M}$  in human colon cancer HT-29)<sup>56</sup>. While zinc is essential for normal cellular function, it is also toxic in excess. Therefore, total cellular zinc content and its intracellular distribution must be tightly regulated, balancing its requirement for numerous structural and enzymatic roles while preventing potential toxicity. The majority of cellular zinc is bound to metalloproteins with a high binding affinity so that free zinc ( $\text{Zn}^{2+}$ ) concentration is typically maintained at extremely low levels (5 - <1000 pM in various cells and tissues), which is about 6-7 orders of magnitude lower than the total cellular zinc concentration<sup>57</sup>. In order to maintain zinc homeostasis, complex regulatory systems are involved, particularly at the level of zinc transport, storage, and sensing.

Sequestration of zinc into subcellular organelles and controlled release is important for homeostatic control of free  $\text{Zn}^{2+}$  level<sup>58</sup>. Typically, about half the intracellular zinc is

located in the cytosol as well as subcellular organelles including zincosomes, a vesicular structure with highly concentrated levels of zinc<sup>24</sup>. An additional 30 to 40 % of the intracellular zinc is located in the nucleus<sup>24</sup>. The remainder of the zinc is associated with the cell membranes<sup>24</sup>.

Zinc transporters regulate the movement of extracellular zinc into the cell as well as controlling the intracellular zinc levels, keeping free intracellular zinc ( $Zn^{2+}$ ) at low levels. ZnT transporters are generally responsible for zinc efflux from the cytosol, sequestering zinc into subcellular organelles or transporting zinc to the extracellular space<sup>59</sup>. However, ZnT5B is an exception to this rule of thumb, acting as a bidirectional zinc transporter<sup>46</sup>. Zip transporters have been shown to increase cytosolic zinc, by extracellular zinc uptake and release from intracellular vesicles<sup>59</sup>. The expression of ZnTs and Zips is tissue/cell type specific and regulation of their expression is an area of ongoing research.

Another important family of proteins involved in zinc homeostasis is metallothioneins (MTs), metal-binding proteins that mediate zinc storage. MTs have high capacity for zinc due to the large number of cysteine residues (1/3 amino acids) with sulphur ligands that bind to zinc<sup>57</sup>. Four major isoforms of mammalian metallothionein have been identified (MT1-4), based on similarities in their amino acid sequences. In humans, there are 11 known functional MT-1 genes (MT1-A, -B, -E, -F, -G, -H, -I, -J, -K, -L and -X) and one gene for the other three isoforms (MT-2A, MT-3 and MT-4)<sup>7</sup>. MT-1 and MT-2 are widely expressed across different tissues, while MT-3 is expressed in the brain and MT-4 is expressed in squamous epithelia<sup>60</sup>. Each MT molecule binds up to 7 zinc ions, exhibiting at least three different levels of binding affinities from nanomolar to picomolar of zinc<sup>61</sup>. When

the level of available zinc increases, metallothionein synthesis is induced to buffer the zinc<sup>62</sup>. On the other hand, MT may function as a zinc donor when available zinc decreases<sup>62</sup>.

The metal-responsive-element binding transcription factor-1 (MTF-1) is an important zinc sensor. It responds to increases in intracellular zinc by activation of genes involved in zinc storage and zinc transport, thus playing an important role in homeostatic control of cellular zinc levels<sup>63,64</sup>. Free zinc ( $Zn^{2+}$ ) binds to MTF-1 causing it to rapidly translocate from the cytosol to the nucleus, where it binds to the metal response elements (MRE) in the promoter region of the MT gene<sup>65</sup> and activates the transcription of metallothionein<sup>66-68</sup>. MTF-1 has also been shown to mediate zinc induced expression of ZnT1 in mice<sup>69</sup>.

In summary, zinc is an essential trace element and its absorption, transport and excretion are tightly regulated in order to provide the body with adequate zinc when possible. At the cellular level, the movement of free zinc ions is also finely regulated in order to balance requirements for cellular functions against potential toxicity. When zinc homeostasis is altered due to changes in expression of zinc transporters and metallothionein, it may lead to the development and progression of disease, including breast cancer, which will be discussed more in the following section<sup>70,71</sup>.

## **1.2. Zinc and Breast Cancer**

Abnormal zinc status is implicated in the development of some diseases, including certain types of cancer<sup>2,72</sup>; however, the role of zinc in tumor development and growth is poorly understood. In studies with rats, zinc was found to accumulate in mammary tumors

induced with the carcinogen N-methyl-N-nitrosourea (MNU) at significantly higher levels compared to healthy mammary tissue (6-19 times)<sup>73</sup>.

Zinc is an important mineral for tumor growth, because it is required for cell proliferation<sup>27</sup> and zinc deficiency suppresses cell proliferation and induces apoptosis<sup>27,74</sup>. Zinc deficiency has been shown to inhibit the growth of a wide range of tumors in animals<sup>75-79</sup>. When rats were fed a zinc-deficient diet following the establishment of implanted mammary adenocarcinomas, tumor growth was suppressed<sup>80</sup>. This study also found that there was a positive correlation between the tumor zinc concentration and the percent viable tumor tissue. However, the zinc concentration in the tumors did not vary significantly between the rats fed a zinc-deficient diet (<4 mg Zn/kg diet) and the rats fed one of the three control diets, depending on the experiment (35-50 Zn/kg diet). In another study, zinc deficiency also protected against the development of MNU-induced mammary tumors in rats<sup>81</sup>. Interestingly, zinc was found to accumulate in rat mammary tumors regardless of whether or not the rats consumed a zinc-deficient (3 mg Zn/kg diet) or zinc-adequate (31 mg Zn/kg diet) diet, despite the ten-fold difference in zinc dietary content and there was no significant difference in the zinc content of the tumors between the rats fed the different diets<sup>73</sup>. These animal studies suggest that zinc deficiency may protect against cancer development and growth, possibly due to a requirement for a higher level of zinc in cancer growth.

While zinc is important for tumor growth, high levels of dietary zinc intake have not been found to promote mammary cancer growth. In nude mice xenografted with human MCF-7 breast cancer cells, the primary tumor growth rate did not differ between the rats fed

a zinc supplemented diet (180 mg Zn/kg diet) and the rats fed a zinc adequate diet (30 mg Zn/kg diet)<sup>82</sup>.

Similar to animal studies, multiple human clinical studies also indicate that zinc accumulates in malignant breast tissue<sup>83-95</sup>. Comparisons of cancerous breast tissue to adjacent healthy tissue from the same patient indicate that zinc concentration is elevated ranging from a 1.4 – 4.4 fold increase (median concentration)<sup>83,84,86-93</sup>. Recent advances in measuring trace elements using x-ray fluorescence have permitted the assessment of trace elements distribution in breast tissue with higher spatial resolution. Malignant breast tissue samples display accumulation of zinc in areas of cancer cell clusters, with an 87% increase in zinc concentration<sup>94</sup>. Non-paired comparisons of the zinc level in breast cancer tissues to breast tissue samples from healthy women also indicates an elevated zinc level in breast cancer tissues, with an increase ranging from 2.6 to 5.2 fold (median concentration)<sup>86,87,91,93,95</sup>. Zinc appears to be more likely to accumulate in estrogen receptor positive (ER+) breast cancer cells, as ER+ breast tumors contain 80% more zinc than ER- breast tumors<sup>96</sup>. Some studies have found that zinc was elevated in benign breast disease compared to healthy breast tissue in different women<sup>93,95</sup>, but another study found that there was no difference in tissue zinc concentrations between paired samples of benign breast tumors and normal breast tissue from the same patients<sup>89</sup>. One study investigated the association between zinc levels in women with benign breast disease and subsequent risk of breast cancer, finding that higher zinc levels in breast tissue was associated with a modest increase in the risk of developing breast cancer later in life<sup>97</sup>.

The mechanisms of elevated zinc in malignant breast tissue may be due to alterations in expression of zinc transporters as well as metallothioneins. Zinc accumulation in NMU-induced rat mammary tumors was associated with alterations in zinc homeostasis, specifically decreased expression of the ZnT1 transporter, involved in zinc efflux, and increased expression of metallothionein, the zinc storage protein<sup>98</sup>. In human breast cancer, both in vivo and in vitro research indicate abnormal expression of multiple zinc transporters including Zip6, Zip7, Zip10 and ZnT2<sup>3-6,99,100</sup>, as well as upregulation of metallothionein<sup>7</sup>; and these findings will be discussed in more detail in the following sections.

Zip6 (LIV-1), is a zinc importer that is initially expressed as a pro-protein at the endoplasmic reticulum, then cleaved on the N-terminus prior to localization at the plasma membrane<sup>101</sup>. Expression of Zip6 increases in response to estrogen and it has been found to be frequently upregulated in estrogen-receptor positive breast cancer<sup>99,100,102</sup>. Increased expression of Zip6 has been associated with metastasis of breast cancer to the lymph nodes<sup>3</sup>. On the other hand, high expression of Zip6 protein has also been associated with increased survival in patients with invasive ductal carcinomas<sup>103</sup>. However, the antibody used in this study targeted the Zip6 pro-protein form located on the endoplasmic reticulum, not the active plasma membrane protein<sup>103,104</sup>. Research studies in vitro provide conflicting evidence. One study found that Zip6 upregulation in MCF-7 cells promoted epithelial-mesenchymal transition, a critical step in tumor metastasis<sup>104</sup>. In contrast, another study found that Zip-6-attenuation decreased apoptosis, increased tumor colony formation, and reduced E-cadherin expression (an epithelial marker) in T47D breast cancer cells<sup>105</sup>.

Zip7 is located on the endoplasmic reticulum, and is thought to control release of zinc from ER stores to the cytoplasm<sup>106</sup>. Increased expression of Zip7 was associated with acquired tamoxifen resistance in MCF-7 breast cancer cells<sup>4</sup>. In this study, Zip7 upregulation was found to increase intracellular zinc and to activate an oncogenic growth factor signaling pathway. Furthermore, inhibition of Zip7 reduced intracellular zinc and inhibited breast cancer cell migration.

Elevated expression of Zip10, a zinc importer, was associated with breast cancer lymph node metastasis<sup>5</sup>. Further research revealed that Zip10 was associated with more aggressive breast cancer cell lines (i.e. MDA-MB-231), than non-invasive breast cancer cell lines (i.e. MCF-7). Zip10 mediated zinc import was essential to the invasive behavior of breast cancer cells, as depletion of either Zip10 or intracellular zinc inhibited migration of metastatic breast cancer cell lines.

The zinc transporter ZnT2 is involved in transporting zinc into vesicles and has been found to protect zinc-sensitive baby hamster kidney (BHK) cells from excess zinc accumulation<sup>107</sup>. ZnT2 may also play a role in protecting breast cancer cells from the cytotoxic effects of elevated cytoplasmic zinc. Increased expression of ZnT2 was observed in MT-null T47D breast cancer cells compared to non-malignant MT+ MCF-10A breast cells<sup>6</sup>. Additionally, inhibition of ZnT2 increased cytoplasmic zinc and resulted in increased apoptosis and reduced tumor formation.

Breast cancer has also been associated with altered zinc storage, as evidenced by changes in MT expression. The majority of studies have found that increased expression of MT-1 and -2 were associated with tumor grade, tumor stage and poor survival in breast

cancer<sup>7</sup>. However, some studies failed to find an association between MT-1 and -2 and survival of breast cancer patients<sup>7</sup>. The MT-2A isoform is more highly expressed in invasive breast cancer cell lines and may play a role in breast cancer progression. Overexpression of MT-2A in human MCF-7 breast cancer cells increased cellular proliferation, while silencing MT-2A caused growth arrest and apoptosis<sup>8</sup>. In another study, inhibition of MT-2A inhibited cell cycle progression, but only caused a marginal increase in apoptosis in MCF-7 cells<sup>9</sup>. Silencing of MT-2A expression inhibited migration and invasion of human MDA-MB-231 breast cancer cells<sup>10</sup>. MT transcription is regulated by MTF-1, which was found to be elevated in human breast cancer tissues compared to normal adjacent tissue<sup>108</sup>.

In summary, zinc appears to be accumulated in breast cancer tissues. The significance of this apparent zinc accumulation in breast cancer development and progression remains unclear. Accumulation of zinc in breast cancer cells appears to result from an altered zinc homeostasis, particularly the expression of zinc transporters (i.e. Zip6, Zip10) and metallothionein. Therefore, zinc appears to play an important role in breast cancer pathogenesis.

### **1.3. Zinc Depletion-Induced Apoptosis**

#### **1.3.1. Introduction to apoptosis**

Apoptosis or gene-directed cell death is the major type of cell death in the body for elimination of unneeded, mutant or moderately damaged cells<sup>109</sup>. While apoptosis is needed during development and tissue remodeling, defects in apoptosis contribute to pathological

conditions such as cancer<sup>110</sup>. It is an energy-dependent process involving complex coordination of signalling pathways and subsequent morphological changes including cell shrinkage, chromatin condensation, nuclear fragmentation and formation of apoptotic bodies.

Apoptosis is a highly regulated process that can be initiated by three different cellular signalling pathways: the extrinsic death receptor pathway, the intrinsic mitochondrial pathway and the intrinsic endoplasmic reticulum pathway. The death receptor pathway is activated by the binding of an extracellular apoptotic ligand [i.e. Fas, tumor necrosis factor (TNF)- $\alpha$  and TNF-related apoptosis-inducing ligand receptors] to its receptor in the plasma membrane<sup>111</sup>. The intrinsic mitochondrial pathway may be initiated by intracellular stresses such as toxins, hypoxia, oxidative stress, UV and gamma irradiation, but the signalling pathways involved are still unclear<sup>111</sup>. The intrinsic endoplasmic reticulum pathway is not as well studied, but it involves accumulation of unfolded protein and impaired protein synthesis following ER damage from hypoxia, free radicals or glucose starvation<sup>112</sup>. For the purpose of this thesis, the focus is on the intrinsic mitochondrial pathway.

Upon activation of the intrinsic mitochondrial pathway, the outer mitochondrial membrane (OMM) becomes permeable (Figure ). The B-cell lymphoma 2 (BCL-2) protein family and the permeability transition pore (PTP) regulate permeabilization of the OMM. The BCL-2 family contains the conserved BCL-2 homology domains and is made up of both anti-apoptotic proteins [i.e. BCL-2] and pro-apoptotic proteins [i.e. BCL-2 associated X protein (BAX)]. The relative abundance of pro- and anti-apoptotic proteins, localization to the mitochondria and conformational changes determines their ability to form channels in

OMM, resulting in permeabilization<sup>111</sup>. OMM permeabilization may also be achieved by opening of the PTP, an unselective mitochondrial channel, causing swelling of the mitochondrial matrix and rupture of the OMM<sup>111</sup>. There appears to be cross-talk between these two pathways as proteins in the Bcl-2 family have been shown to regulate PTP activity<sup>113</sup>. As a result of either pathway, increased OMM permeabilization permits release of proapoptotic proteins from the intermembrane space into the cytosol<sup>111,113</sup>.

One such protein, cytochrome c is typically located in the mitochondrial intermembrane space in healthy cells, but is released into the cytosol during apoptosis<sup>114</sup>. Cytochrome c is a key activator of caspases, a family of cysteine proteases that mediate apoptosis. In the cytosol, cytochrome c binds to apoptotic protease activating factor (Apaf1), forming a multimeric apoptosome<sup>115</sup>. The apoptosome recruits and activates caspase-9<sup>115</sup>. Once activated caspase-9 cleaves the downstream executioner caspases such as caspase-3, which in turn cleave key substrates involved in apoptosis<sup>115</sup>.

Permeabilization of the OMM also causes the release the proapoptotic proteins Smac (second mitochondrial activator of caspases)/DIABLO (direct IAP binding protein with low pI) and HtrA2/Omi., which bind to inhibitor of apoptosis proteins (IAPs)<sup>116</sup>. IAPs bind to caspase-9 and caspase-3 to inhibit their activation and activity. Binding of Smac/DIABLO and HtrA2/Omi displaces caspases from IAPs, thus facilitating apoptosis<sup>116</sup>.

Additionally, there is some evidence that apoptotic stimuli release other proapoptotic proteins from the intermembrane space, which are involved in caspase-independent apoptotic pathways. For example, apoptosis inducing factor (AIF) may be released from the mitochondria and translocate to the nucleus, causing DNA fragmentation

and chromatin condensation resulting in apoptosis<sup>117</sup>. However, release of AIF is not a universal requirement for cell death and its role in mediating apoptosis varies in a cell type specific manner<sup>117</sup>.

Caspase mediated cleavage of hundreds of protein targets fosters apoptosis and is also thought to be responsible for most of the characteristic morphological changes observed during apoptosis<sup>118</sup>. Caspase-3 cleaves the inhibitor of caspase-activated DNase (ICAD), activating CAD (caspase-activated-DNase) and resulting in fragmentation of genomic DNA, a hallmark of apoptosis<sup>111</sup>. Caspase-3 mediated cleavage of DNA typically causes chromatin condensation<sup>118,119</sup>. Caspases also cleave many other key cellular components including cytoskeleton proteins and the nuclear scaffold (lamins), likely causing cellular shrinkage and membrane blebbing, as well as nuclear fragmentation<sup>118</sup>. Additionally, caspases target a number of cell adhesion proteins, which may play a role in cellular detachment from the extracellular matrix, however, the exact mechanisms involved in cellular detachment are still unclear<sup>118</sup>.

In summary, apoptosis is an energy-dependent, highly controlled process for elimination of unwanted or damaged cells. Much of the signalling pathways implicated in apoptosis surround the regulation of caspase activation. In the intrinsic mitochondrial apoptotic pathway, permeabilization of the OMM facilitates the release of pro-apoptotic factors, such as cytochrome c, leading to caspase activation. Caspases play a key role in apoptosis by targeting hundreds of proteins to facilitate DNA fragmentation and controlled cellular breakdown.

Numerous studies have implicated zinc deficiency as a stimulus for apoptosis. The effects of zinc deficiency on apoptosis and the signalling pathways involved will be discussed in depth in the following sections.

### **1.3.2. *In vivo* research**

The apoptotic effects of zinc deficiency were first reported in 1977, when it shown that zinc deficient rats had increased apoptotic cells in their intestinal crypts<sup>120</sup>. Elevated apoptosis was also observed in chickens fed zinc-deficient diets in the tibial growth plate chondrocytes<sup>121</sup>. More recently, marginal dietary zinc deficiency in rats was found to induce apoptosis in the vascular smooth muscles cells (VSMCs) of large arteries<sup>122</sup>.

One area of focus in understanding the role of zinc deficiency in apoptosis is the effects of zinc status on the immune system, since zinc deficiency causes lymphopenia and thymic atrophy, resulting in suppression of immune function<sup>12</sup>. In male rats fed a zinc free diet, increased apoptosis in the thymus was observed after just 1 week, which was attributed to the subsequent development of thymic atrophy after 4 weeks<sup>123</sup>. In mice fed a zinc-deficient diet, thymic atrophy was also associated with a marked increase in apoptosis in the thymus, specifically within the population of immature pre-T cells<sup>124</sup>.

Consumption of a zinc free diet has been shown to display time-dependent apoptotic effects in other tissues. In male rats fed a zinc free diet, increased apoptosis was also observed in the testes after 3 weeks, prior to the occurrence of testicular atrophy after 10 weeks<sup>123</sup>. With more prolonged zinc depletion, elevated apoptosis was observed in the kidney after 13 weeks and in the liver and skin after 34 weeks<sup>123</sup>.

Adequate zinc is required for development and zinc deficiency is teratogenic<sup>74</sup>. For example, consumption of a low zinc diet by pregnant rats, was associated with increased apoptosis in the embryos, especially within the neural crest cells<sup>125</sup>. Increased caspase-3 activity was associated with zinc deficiency-induced embryonic cell death at mid-gestation in rats<sup>126</sup>. Additionally, the effects of zinc deficiency on early embryonic development during implantation were investigated using a murine model<sup>127</sup>. In this model, blastocyst stage embryos taken from mouse dams were cultured in low-zinc, zinc-replete or control medium. Culturing in low zinc resulted in abnormal embryonic morphology, including smaller embryos, which was attributed to the increased apoptosis observed in the zinc-deficient embryos.

In summary, zinc deficiency causes apoptosis in a wide variety of tissues. Zinc deficiency-induced apoptosis has been associated with impaired development, particularly during embryonic development.

### **1.3.3. *In vitro* research**

Zinc depletion-induced apoptosis has been demonstrated in numerous studies *in vitro*, and may be achieved by culturing cells in low or zinc-free medium, or alternatively by chelating zinc<sup>11</sup>. Apoptosis was induced by culturing human lymphoid (Raji) and myeloid (HL-60) cells in a zinc-free medium<sup>128</sup> and by culturing human leukemia (HL-60, 0.5  $\mu\text{M}$ <sup>129</sup>; Jurkat T-cells, 1.5  $\mu\text{M}$ <sup>130</sup>) and neuroblastoma cells (IMR-32, 1.5  $\mu\text{M}$ ) in a low-zinc medium<sup>130</sup>. In addition, apoptosis can also be induced by using a chelator to deplete intracellular zinc, most commonly using N,N,N',N'-tetrakis(2-

pyridylmethyl)ethylenediamine (TPEN). TPEN is a membrane permeable heavy metal chelator with a higher affinity for zinc and a lower affinity for other divalent cations such as calcium and magnesium<sup>131</sup>. TPEN has been found to sequester zinc from the labile intracellular pool of zinc (LIPZ). Depletion of intracellular zinc using TPEN treatment (30  $\mu$ M) occurs within 20 min in HeLa cells<sup>132</sup>. Treatment of breast cancer cells (i.e. MCF-7, MDA-MB-468) with TPEN reduced the abundance labile zinc in a dose-dependent manner<sup>14</sup>. In MDA-MB-231 breast cancer cells, TPEN treatment reduced LIPZ in a dose- and time-dependent manner<sup>133</sup>. TPEN treatment at higher concentrations (10 and 20  $\mu$ M) for 8 h depleted the LIPZ to below detection in MDA-MB-231 cells<sup>133</sup>. Recently, it was discovered that TPEN also sequesters zinc from a large fraction of the zinc proteome. Treatment of LLC-PK<sub>1</sub> pig kidney cells with 25  $\mu$ M TPEN for 30 min reduced the zinc bound proteome by 34% and Zn-MT by 50%<sup>134</sup>.

Chelation of intracellular zinc via TPEN (1 – 100  $\mu$ M) induces apoptosis in many different human cell lines which include thymocytes<sup>135</sup>, lymphocytes<sup>136,137</sup>, malignant airway epithelial cells<sup>138</sup>, leukemia cells<sup>139</sup>, retinal pigment epithelial cells<sup>140</sup>, melanoma cells<sup>141</sup>, keratinocytes<sup>142</sup>, pancreatic cancer cells<sup>143</sup>, cervical cancer cells<sup>132</sup> and breast cancer cells<sup>13,14,133</sup>. In breast cancer MDA-MB-468 and MCF-7 cells, chelation of either labile intracellular (via TPEN) or extracellular [via diethylenetriaminepentacetic acid (DTPA)] zinc induces apoptosis<sup>14</sup>. Previous research from our laboratory indicates that the human breast cancer cell lines MDA-MB-231, MCF-7 and T47D undergo apoptosis following TPEN-induced zinc depletion<sup>133</sup>. The level of apoptosis in these three breast cancer cell lines exceeded that observed in MCF-10A, a non-tumorigenic fibrocystic breast epithelial cell line.

The extent of the LIPZ depletion correlates well with the induction of apoptosis. In thymocytes from aged rats, which undergo spontaneous apoptosis, small decreases in the LIPZ (TPEN treatment) sharply increased the susceptibility to apoptosis, while elevating LIPZ (zinc plus an ionophore treatment) inhibited apoptosis<sup>144</sup>. TPEN-induced apoptosis in rat spleen cells was also associated with a decrease in the LIPZ<sup>144</sup>. In a human promyelocytic leukemia cell line (HL-60) grown in a low-zinc medium (5  $\mu$ M), loss of the LIPZ occurred prior to detection of mitochondrial membrane potential loss and apoptosis<sup>129</sup>. Furthermore, the LIPZ was significantly lower in cells identified as undergoing an early stage of apoptosis compared to healthy cells, regardless of the zinc concentration in the media (0.5, 25 & 50  $\mu$ M).

TPEN induced apoptosis may be prevented by concurrent addition of zinc, providing further evidence that TPEN-induced apoptosis is caused by zinc depletion. In MDA-MB-231 breast cancer cells, zinc treatment (10 – 40  $\mu$ M), essentially prevented TPEN-induced apoptosis, as it was associated with a 99% reduction in DNA fragmentation<sup>13</sup>. Zinc supplementation also inhibited apoptosis in DTPA and TPEN treated MCF-7 and MDA-MB-468 cells<sup>14</sup>.

Zinc depletion may also increase susceptibility to apoptosis from toxins and other pro-apoptotic stimuli<sup>109</sup>. For example, TPEN-induced zinc depletion of porcine airway epithelial cells was found to synergistically increase tumor necrosis factor  $\alpha$  and linoleic acid induced apoptosis<sup>145</sup>. Similarly, zinc deficiency also increased hydrogen-peroxide (H<sub>2</sub>O<sub>2</sub>)-induced caspase activation in respiratory airway cells<sup>138</sup>.

Some studies suggest that zinc supplementation may have anti-apoptotic effects<sup>109</sup>. Zinc supplementation inhibited H<sub>2</sub>O<sub>2</sub>-induced caspase activation in the model described above<sup>138</sup>. In human chronic lymphocytic leukemia cells, elevating the LIPZ via zinc supplementation in the presence of pyrithione, an ionophore, dramatically reduced the susceptibility to apoptosis induced by the toxin colchicine in a dose-dependent manner<sup>144</sup>. Increased labile zinc also inhibited apoptosis from a lipopolysaccharide endotoxin, as well as spontaneous apoptosis in sheep pulmonary artery endothelial cells<sup>146</sup>.

While zinc generally protects against apoptosis, its effects as an apoptotic regulator are cell type and dose-dependent. For example, in mouse thymocytes, zinc supplementation between 500-1000  $\mu$ M inhibited glucocorticoid-induced apoptosis. In contrast, lower zinc supplementation between 80 – 200  $\mu$ M induced apoptosis<sup>147</sup>.

In summary, zinc has been shown to play a critical role in the regulation of apoptosis. Zinc depletion may induce apoptosis and/or increase susceptibility to apoptotic stimuli. However, the effect of zinc on apoptosis is cell-type and dose-dependent.

#### **1.3.4. Mechanisms of zinc depletion-induced apoptosis**

Zinc depletion-induced apoptosis is associated with alterations in apoptotic signalling pathways, specifically the intrinsic mitochondrial pathway, involving cytochrome-c release, and the caspase cascade. Studies of zinc depletion-induced apoptosis in breast cancer cells support the role of intracellular calcium influx, and breakdown of the X-linked inhibitor of apoptosis protein (XIAP) in the regulation of apoptosis. Additionally, oxidative stress is implicated in many studies of zinc depletion-induced cell death.

A number of studies have documented release of cytochrome c from the inner mitochondrial membrane into the cytosol following zinc depletion in peripheral blood T lymphocytes (PBL)<sup>137</sup>, breast cancer cells (i.e. MDA-MB-468, MCF-7<sup>14</sup>, and MDA-MB-231<sup>13</sup>), neuronal<sup>148</sup> and osteoblastic cells<sup>149</sup>, indicating that zinc depletion-induced apoptosis is associated with the intrinsic mitochondrial apoptotic pathway. The time-course of apoptosis was investigated in PBL cells, which showed that cytochrome c rapidly accumulated in the cytosol after just one hour of TPEN treatment (15  $\mu$ M), which was also associated with activation of caspase-3 and caspase-9<sup>137</sup>. After 2 h of TPEN treatment, the caspase-3 substrate poly ADP ribose polymerase (PARP) was cleaved.

The release of cytochrome c is known to be an important factor in activating the caspase cascade<sup>115</sup>, and many studies support a role for altered expression of caspases in zinc depletion-induced apoptosis<sup>109</sup>. In rat embryos, zinc deficiency increased caspase-3 activity and apoptosis<sup>126</sup>. In multiple human malignant epithelial cells (colonic LIM1215, bronchial NCI-H292), TPEN treatment (25  $\mu$ M) was associated with rapid induction of caspase-3 (1-2 h), followed shortly by activation of caspase-6 (2 h in LIM1215 cells; 3-4 h in NCI-H292 cells)<sup>138,150</sup>. In breast cancer cells, depletion of intracellular (TPEN) and extracellular (DTPA) zinc for 48 h increased activity of caspase-9 and caspase-3 in MDA-MB-468 cells and activity of caspase-9 in MCF-7 cells (MCF-7 cells lack caspase-3) in a dose-dependent manner<sup>14</sup>. Furthermore, there was no change in caspase-8 activity following zinc depletion, indicating that the death receptor pathway was not involved in mediating apoptosis. Research from our laboratory also showed that zinc depletion-induced apoptosis was linked to early changes in caspase-9 and -3 activity (3-6 h following 20  $\mu$ M TPEN treatment) in MDA-MB-231 cells<sup>13</sup>. Co-treatment of MDA-MB-231 cells with TPEN (20  $\mu$ M) plus zinc

(10, 20 & 40  $\mu\text{M}$ ) completely inhibited activation of caspase-3, providing further evidence that intracellular zinc status regulates caspase activation<sup>13</sup>.

Changes in the concentration of intracellular free calcium ( $\text{Ca}^{2+}$ ) have also been shown to have an important role in regulating the intrinsic mitochondrial apoptotic pathway<sup>13,151</sup>. Recent research from our laboratory indicated that TPEN (20  $\mu\text{M}$ )-induced zinc depletion was associated with a small sustained rise in intracellular calcium ions in MDA-MB-231 cells (13% at 3 h)<sup>13</sup>. Blocking the mitochondrial calcium uniporter inhibited TPEN-induced caspase-3 activity, indicating that mitochondrial calcium uptake mediates apoptosis<sup>151</sup>. Chelation of intracellular calcium during TPEN treatment also increased the mitochondrial membrane potential, as well as inhibiting cytochrome c release, caspase-9 activity and caspase-3 activity<sup>13</sup>. Calcium chelation (20 & 40%) was able to partially inhibit DNA fragmentation (31 and 58%, respectively at 48 h)<sup>13</sup>. This research points to a role for calcium as a regulator of the mitochondrial mediated apoptosis, specifically cytochrome c translocation and the caspase-dependent pathway.

Additionally, a study on the role of zinc depletion in VSMCs also implicated intracellular calcium flux in modulating apoptosis<sup>122</sup>. Addition of plasma from zinc-deficient rats to VSMCs resulted in a sustained elevation of intracellular calcium and was associated with increased apoptosis. Calcium chelation prevented induction of apoptosis in this model. Treatment with of VSMCs with the zinc-deficient plasma was also associated with activation of BCL-2-associated death promoter protein (BAD), a pro-apoptotic protein, via dephosphorylation. Inhibition of calcineurin, a calcium-protein phosphatase, decreased BAD dephosphorylation and prevented apoptosis. Since calcineurin is activated by calcium, the

rise in calcium following zinc deficiency may regulate mitochondrial membrane permeability through its effects on BAD phosphorylation.

Zinc depletion-induced apoptosis has also been linked to stability of the X-linked inhibitor of apoptosis protein (XIAP). XIAP is an important regulator of both the initiation and execution phases of apoptosis, as it strongly inhibits both caspase-3 and caspase-9<sup>152</sup>. In MDA-MB-231 breast cancer cells, zinc depletion using TPEN (10  $\mu$ M) quickly resulted in loss of full length XIAP after 3 h<sup>153</sup>. This was followed by activation of caspase-3 (7 fold increase in activity) and PARP cleavage after 24 h TPEN treatment. Similarly, in prostate cancer PC-3 cells, 16 h TPEN treatment (5  $\mu$ M) resulted in loss of XIAP and PARP cleavage. Zinc is known to be structurally important for XIAP, however the mechanism by which zinc depletion causes breakdown of XIAP is not well understood<sup>153</sup>.

Recent studies have indicated that zinc depletion-induced apoptosis may also involve release of AIF from the mitochondria, however, the importance of AIF in mediating zinc depletion-induced apoptosis is still unclear. Mendivil-Perez et al. found that TPEN (3  $\mu$ M, 24h) treatment promoted nuclear translocation of AIF, in addition to caspase-3 activation in Jurkat T leukemia cells<sup>154</sup>. Guo et al. reported an elevated level of AIF in the cytosol of mouse osteoblastic MC3T3-E1 cells following TPEN treatment (5  $\mu$ M, 24h) in addition to activation of caspase-3 and -9<sup>149</sup>. Pretreatment of MC3T3-E1 cells with a broad range caspase inhibitor only partially protected cells from zinc depletion-induced apoptosis. Pretreatment of human colorectal carcinoma LIM1215 cells with a caspase-3 inhibitor or a broad range caspase inhibitor, followed by TPEN (25  $\mu$ M) treatment, resulted in partial reduction of DNA fragmentation<sup>150</sup>. These studies indicate that AIF-mediated / caspase-independent

apoptotic pathways may play a role in zinc depletion-induced apoptosis. However, caspase inhibition mostly suppressed DNA fragmentation in TPEN (15  $\mu$ M)-treated PBL cells, indicating that AIF did not play a major role in inducing apoptosis in this cell line<sup>137</sup>. Therefore, the importance of caspase-independent pathways in zinc depletion-induced apoptosis may vary in a cell-type specific manner.

Zinc deficiency has also been found to increase oxidative stress in many studies *in vivo* and *in vitro*, which may play a role in zinc depletion-induced apoptosis<sup>109</sup>. Zinc stabilizes cell membranes and macromolecules, protecting them from oxidative stress<sup>109</sup>. Zinc itself is redox inert in biological systems, but it indirectly exerts antioxidant effects<sup>155</sup>. The antioxidant effects of zinc are not well understood, but may include a metallothionein antioxidant function and zinc-dependent proteins / functions in the mitochondrial electron transport chain<sup>155</sup>. Oxidative damage is a well-known activator of apoptosis<sup>109</sup>, therefore zinc may protect against oxidative stress-induced apoptosis. In fact, a number of studies showed that antioxidant supplementation was able to suppress zinc depletion-induced apoptosis. For example, zinc-deficiency in rats was associated with increased expression of inducible nitric oxide synthase (NOS), and treatment with a NOS inhibitor suppressed zinc-deficiency induced intestinal damage, inflammatory skin lesions and apoptosis in the intestines and skin<sup>156,157</sup>. In cultured rat VSMCs, pre-incubation of cells with N-Acetyl-L-Cysteine (NAC), an antioxidant, reduced oxidative stress and prevented the induction of apoptosis following addition of plasma from zinc deficient rats<sup>122</sup>. Treatment of breast cancer cells (MCF-7, MDA-MB-468) with NAC also inhibited loss of viability induced by TPEN (10  $\mu$ M) and DTPA (100  $\mu$ M)<sup>14</sup>. In Jurkat T leukemia cells, addition of NAC not only protected against TPEN (3  $\mu$ M) induced apoptosis, but also rescued cells from apoptosis after 6 h TPEN

treatment<sup>154</sup>. Treatment of rat hepatocytes with NAC, did not prevent TPEN (30  $\mu$ M) induced caspase-3 activation at 10 h, but it did block apoptosis<sup>158</sup>. Zinc depletion in MDA-MB-231 cells (20  $\mu$ M TPEN) increased oxidative DNA damage, and was associated with increased production of inducible NOS and reactive nitrogen species<sup>159</sup>. Furthermore, inhibition of NOS, reduced caspase-3 activity by one third.

Zinc may also regulate apoptosis through transcriptional gene regulation. In human cervical HeLa cancer cells, only 3 hours of TPEN treatment (30  $\mu$ M) inhibited the DNA-binding activity of the specificity protein (Sp) family of transcription factors and 6 hours of TPEN treatment resulted in cleavage of the Sp transcription factors<sup>132</sup>. TPEN treatment (30  $\mu$ M TPEN, 24h) was also associated with loss of DNA binding activity of Zn<sub>3</sub>-Sp1 to its cognate DNA site (sodium glucose co-transporter 1 gene) in LLC-PK<sub>1</sub> pig kidney cells<sup>134</sup>. In Jurkat T leukemia cells, TPEN (3  $\mu$ M) induced apoptosis was associated with activation of NF-kB and c-Jun transcription factors, which were found to regulate loss of mitochondrial membrane potential, plasma membrane integrity and development of apoptotic nuclei<sup>154</sup>. Therefore, zinc depletion causes alterations in transcription factor activity, which may play a role in regulating apoptosis; however this has not been well studied.

In summary, zinc depletion has been shown to induce apoptosis in a wide range of cells and tissues, in a concentration and cell type-dependent manner. Zinc depletion-induced apoptosis involves increased intracellular calcium-induced release of cytochrome c from mitochondria and activation of caspases. This body of evidence suggests that that zinc depletion induces apoptosis through the intrinsic mitochondrial pathway, such as in the case

of MDA-MB-231 breast cancer cells; however, the exact mechanisms whereby zinc depletion induces apoptosis remains to be elucidated.

#### **1.4. MicroRNAs: Regulators of Apoptosis**

##### **1.4.1. Introduction to microRNA**

MicroRNAs (miRs) are a recently discovered class of short, non-coding RNAs, that regulate numerous metabolic processes by post-transcriptional gene regulation<sup>15</sup>. MiR research is rapidly evolving as the first miR was only identified in 1993<sup>160,161</sup>. The first functional role for a miR in mammalian development was discovered in 2004<sup>162</sup>. Since then the field has burgeoned, with over 2500 mature miRs reported in humans<sup>163</sup>.

MiRs are short, non-coding RNAs of 18-25 nucleotides in length, which regulate numerous metabolic processes by post-transcriptional gene regulation<sup>15</sup>. MiR regulate target messenger RNA (mRNA) through complementary base pairing, typically resulting in degradation of target mRNA<sup>164</sup>. MiR have wide-ranging physiological roles including embryogenesis, hematopoiesis, muscle development and immunity<sup>165,166</sup>.

The level of gene regulation by miRs is extensive and complex as each miR may regulate a few hundred target mRNAs, and multiple miRs may coordinate regulation of a single mRNA transcript<sup>167</sup>. In fact, it is estimated that more than 60% of human mRNAs contain conserved miR target sites, indicating widespread regulation by miRs<sup>168</sup>. MiR targets include enzymes and transcription factors, and miR-target interactions regulate key cellular activities including differentiation, proliferation and apoptosis<sup>169</sup>.

Despite considerable advances in miR research, there is still much that is unknown regarding the functionality of miR-mediated gene silencing, as well as regulation of miR expression and integration with cellular signaling pathways, etc.<sup>164,170</sup>.

#### **1.4.2. MiR biogenesis**

A multi-step process, including nuclear and cytosolic processing, produces mature miR (Figure ). In the nucleus, long primary (pri-) miR sequences are encoded within introns, exons, and intergenic regions<sup>171</sup>. Pri-miR are transcribed mainly by RNA Polymerase II into long primary transcripts of variable length (often 3-4 kb)<sup>172,173</sup>. The pri-miR contains a stem loop or hairpin-like structure, formed by a double stranded RNA stem and an unpaired RNA loop, which eventually becomes the mature miR following cleavage at two site-specific events.

In the nucleus a multiprotein complex, known as the microprocessor, cleaves the pri-miRs<sup>174-177</sup>. The microprocessor complex contains a RNA-binding domain called Pasha/DiGeorge syndrome critical region 8 (DGCR8) for substrate recognition and recruitment of the RNase enzyme Drosha<sup>175,176</sup>. Drosha cleaves the pri-miR into shorter precursor (pre-) miR of about 70 nucleotides in length<sup>178,179</sup>. Subsequently, pre-miRs are exported from the nucleus by a carrier protein called Exportin<sup>180-182</sup>. In the cytoplasm, pre-miR are processed by the miR generating complex containing a RNase enzyme, Dicer, producing double-stranded mature miR of approximately 22 nucleotides in length<sup>183</sup>. The miR generating complex may contain additional proteins which enhance cleavage of pre-miRs to mature miRs. These include trans-activating response RNA-binding protein (TRBP) and protein activator of PKR (PACT)<sup>184</sup>.

Although the pathway described was once thought to universally describe miR biogenesis, recent research reveals many variations in this pathway and the existence of individual miR-specific processing alterations<sup>185</sup>. For example, miR may undergo processing independent of Drosha or Dicer<sup>185,186</sup>.

### **1.4.3. MiR function**

For miRs to exert their function, they are incorporated into an effector RNA-induced silencing complex (RISC) containing Dicer, TRBP, and Argonaute (Ago)<sup>185</sup>. In humans there are four Ago proteins (Ago 1-4), which mediate miR-targeted silencing of protein expression. One of the mature miR strands is transferred to an Ago protein by two chaperone proteins (Hsc70/Hsp90)<sup>187</sup>, while the other strand is degraded<sup>188</sup>. The thermodynamic stability of the miRNA duplex is an important determinant of strand selection, with the miR that is less stably base paired at the 5' end being more likely to be loaded in the RISC complex<sup>188,189</sup>. Sometimes multiple mature miRs arise from a single precursor, and in this case the 5' arm and 3' arms are distinguished by annotation with -5p and -3p.

The RISC mediates degradation of mRNA based on complementarity between a miR and its targeted mRNA. The mature miR contains a seed region of 6-8 nucleotides at the 5' end, which binds to complementary base pairs in the target mRNA<sup>164</sup>. The seed region may bind to any part of the mRNA, but binding to the 3' untranslated region (UTR) is the most frequently documented and this tends to decrease target mRNA expression<sup>164</sup>. Target mRNAs are silenced by deadenylation and subsequent degradation, or translational inhibition, but the mechanisms involved are not well understood<sup>170,190</sup>. Recent studies

suggest that degradation of miR-targeted mRNAs is the primary type of gene silencing by miRs in mammalian cell cultures<sup>170</sup>.

The canonical model of miR-mediated gene regulation is that of negative regulation via miR binding to the 3' UTR of the target mRNA<sup>18</sup>. However, miRs have also been found to positively regulate gene expression. For example, during cell cycle arrest induced by serum starvation, two miRs (miR-369-3 & let-7) upregulated translation of their targeted mRNAs by binding to their 3' UTRs<sup>191</sup>. MiR-10a was also found to activate expression of ribosomal protein mRNAs by binding to their 5' UTR<sup>192</sup>. The mechanisms involved in the regulation of gene expression by miRs are currently not well understood and are still controversial<sup>164</sup>.

#### **1.4.4. MiR stability**

MiRs are typically very stable and the majority of mature miRs persist for hours up to days in the cell<sup>193,194</sup>. In human embryonic kidney (HEK)-293T cells, the vast majority (95%) of miRs remained stable for at least 8 h after inhibiting miRs transcription with a chemical inhibitor<sup>195</sup>. In another experiment, miR turnover was measured after loss of Dicer enzymatic activity in murine primary bone marrow derived macrophages<sup>196</sup>. The miRs investigated were found to have half-lives ranging from 28 to 211 h (~9 days). Therefore, miRs are generally quite stable; but the stability of miR varies on an individual miR basis. MiR stability may be affected by a number of factors including the cell cycle stage, growth factors and the presence of miR degrading enzymes<sup>194</sup>.

#### 1.4.5. MiR expression in breast cancer

Our understanding of the role of miR in the development and progression of breast cancer is in its infancy; however, it has been established that miRs are involved in the regulation of every known cellular process related to cancer, such as differentiation, proliferation and apoptosis<sup>197</sup>. Abnormal miR expression profiles have been reported for various types of cancer, including breast cancer<sup>198-201</sup>. Unique miR expression profiles or “fingerprints” are associated with estrogen receptor (ER) status, tumor differentiation, invasiveness and response to therapy<sup>198,200,201</sup>. MiR dysregulation in cancer may occur due to a number of factors including alterations in miR genomic copy number and localization, epigenetic regulation, transcription factor activity and miR processing<sup>202</sup>.

On a global scale, miR expression was found to be generally downregulated in a broad range of cancer tissues and cancer cell lines when compared to normal tissues<sup>203</sup>. A large study by Devigne et al., involving 1,302 breast cancer samples as well as 28 breast cancer cell lines, compared to 116 normal breast tissue samples showed that mature miR expression was globally decreased in breast cancer tissue and cell lines compared to normal tissue<sup>204</sup>. Furthermore, expression of the global miR population gradually declined as the tumor grade increased and was the lowest in breast cancer cell lines.

Decreased expression of miRs in cancer cells and tissues may occur through alterations in miR processing. Assessment of pri-miR and mature miR expression in a wide range of primary tumors and normal tissue samples, indicated that the level of pri-miR did not correspond to the reduced expression of mature miR, indicating that global downregulation of miR expression in cancer tissues may occur at the post-transcriptional level<sup>205</sup>. In contrast, expression of pri- and mature miR were positively correlated in normal

tissue samples. Another experiment examining the correlation between miR precursors (both pri- and pre-miRNA) compared to mature miRs in 37 human cancer cell lines also found that there was little correlation between mature and precursor miR expression<sup>206</sup>. The study showed that some miR precursors were retained in the nucleus, which would prevent cytosolic processing to mature miR. A panel of 22 normal tissues tested showed a higher correlation between precursor and mature miRNA expression.

Breast cancer has been associated with alterations in the miR processing machinery, which could play a role in the abnormal miRNA expression observed in breast cancer. One study found that in 18% of breast cancer cases, Drosha was downregulated, which was associated with breast cancer characteristics including high grade, high proliferation index, lack of BCL-2 expression and overexpression of human epidermal growth factor receptor type II (HER2)<sup>207</sup>. Dicer was also downregulated in 46% of breast cancer cases<sup>207</sup>. Decreased expression of Dicer is more likely to occur in ER negative breast cancer cells<sup>201,207-209</sup>. Dicer downregulation was also associated with some other cancer characteristics including lack of expression of progesterone receptor (PR) and BCL-2, as well as high grade and proliferation index<sup>207</sup>. In the previously mentioned study by Dvinge, et al., Dicer expression was only mildly reduced in the higher-grade tumors, which could not account for the observed global downregulation in miR expression<sup>204</sup>. This study also found that expression of other proteins involved in miR stability varied by tumor grade. The terminal uridylyltransferase 4 / zinc-finger, CCHC domain-containing protein 11, involved in miR inactivation, was slightly upregulated and the polyadenylate polymerase associated domain containing 4 / Gld-2, involved in miR stabilization, was mildly downregulated.

Therefore, these enzymes may also play a role in regulating miR expression in the context of breast cancer.

Inhibition of global miR expression may aid cancer development. Blocking miR maturation with inhibitors of Drosha, DGCR8, and Dicer1, increased transformation in mouse (LKR13) lung cancer and human cancer cell lines (i.e. MCF-7 breast cancer, U2OS osteosarcoma, and HCA7 colorectal cancer), as well as murine lung tumorigenesis *in vivo*<sup>210</sup>.

While the functional roles of the majority of miRs have not yet been determined, some miRs have been found to regulate breast cancer development<sup>211</sup>. Individual miRs may play either oncogenic or tumor suppressive roles in breast cancer. A few select examples will be described in more detail below, providing support for the key roles of miRs in modulating the course of breast cancer.

For instance, oncogenic miR-21 is the most commonly upregulated miR across many types of cancer, including breast cancer<sup>212</sup>. Inhibition of miR-21 expression in MCF-7 breast cancer cells reduced cell growth *in vitro* as well as *in vivo* in a xenograft mouse model<sup>213</sup>. MiR-21 has been found to target the tumor suppressors programmed cell death 4<sup>214,215</sup> and tropomyosin 1 proteins<sup>216</sup> to promote cell transformation in MCF-7 breast cancer cells.

In another study, a genetic screen was used to identify miRs involved in metastasis<sup>217</sup>. Upregulation of miR-373 and miR-520c were identified as promoting migration *in vitro* in MCF-7 breast cancer cells, as well as tumor invasiveness *in vivo* in immunodeficient mice injected with MCF-7 cells. Investigation of miR-373 expression in clinical samples also indicated that miR-373 was upregulated in breast cancer metastasis.

Downregulation of tumor suppressor miRs may also aid breast cancer pathogenesis. For example, the let-7 family was reported as poorly expressed in breast cancer stem cells,

known as breast tumor-initiating cells (BT-IC) and was found to regulate self-renewal and differentiation of breast cancer cells<sup>218</sup>. Upregulation of let-7 reduced tumor formation *in vivo* in immunodeficient mice injected with a highly malignant breast cancer cell line enriched with BT-IC (Sk-3rd).

Downregulation of miR-132 may also play a role in breast cancer development. Reduced abundance of miR-132 was reported in human clinical samples of breast ductal carcinoma *in situ* (DCIS), an early stage of breast cancer, compared to paired samples of adjacent normal tissue<sup>219</sup>. Upregulation of miR-132 in MCF-7, MDA-MB-231 and BT549 breast cancer cell lines decreased cell viability and inhibited colony formation.

In summary, abnormal expression of miRs is implicated in breast cancer and targeting miR expression alters breast cancer development. The next section will discuss the role of miRs in regulating apoptosis in breast cancer cells.

#### **1.4.6. MiRs & apoptosis in breast cancer**

Impaired apoptosis is one of the hallmarks of cancer cells<sup>110,220</sup>. In breast cancer cells, abnormal miR expression can reduce susceptibility to apoptosis, thus contributing to increased survival of breast cancer cells<sup>17</sup>. MiRs exert their effects by regulating many proteins involved in cell death and survival pathways in cancer cells<sup>16</sup>. A number of miRs have been found to target the intrinsic mitochondrial apoptotic pathway, particularly at the level of the BCL-2 family, which in turn regulates mitochondrial membrane permeability<sup>17</sup>.

For example, miR-21 is a potent oncogene with antiapoptotic effects<sup>212</sup>. Inhibition of miR-21 in MCF-7 breast cancer cells as well as a MCF-7 derived xenograft carcinoma in

mice, suppressed growth of breast cancer cells due to decreased cell proliferation and increased apoptosis<sup>213</sup>. Interestingly, treatment of MCF-7 cells with a broad range caspase inhibitor, prevented the growth inhibitory effects of miR-21 knockdown, implicating caspases as effectors in miR-21-induced inhibition. Furthermore, inhibition of miR-21 in MCF-7 cells and MCF-7 derived breast tumors resulted in impaired expression of BCL-2, an anti-apoptotic protein, suggesting that miR-21 may exert its oncogenic effects through the death inhibitory functions of BCL-2.

Another miR generally upregulated in breast cancer tumors is miR-155, but in a cancer type specific manner<sup>198,199,221</sup>. MiR-155 expression has been found to regulate breast cancer cell survival and growth. In human invasive ductal breast carcinoma BT-474 cells, miR-155 was expressed at lower levels (compared to a number of other breast cancer cell lines) and upregulation of miR-155 expression in BT-474 cells promoted cell proliferation and suppressed apoptosis<sup>221</sup>. Conversely, fibroblast breast cancer HS578T cells had higher miR-155 expression, and knock down of miR-155 inhibited cell proliferation and induced apoptosis. MiR-155 directly targeted the pro-apoptotic transcription factor forkhead box O3a (FOXO3a) through translational inhibition. Reduced FOXO3 expression in turn inhibited the expression of its downstream targets Bim (a pro-apoptotic member of the BCL-2 family) and p27(Kip1, a cell cycle inhibitor) to prevent apoptosis. Expression of miR-155 also conferred resistance to apoptosis induced by multiple chemotherapeutic agents (i.e. doxorubicin, VP16, and paclitaxel).

Other studies also suggest that altered miR expression in breast cancer can provide resistance to chemotherapeutic drug-induced apoptosis. For example, the miR-221/222

cluster was found to be upregulated in ER- cell lines and breast tumors<sup>222</sup>. Furthermore, miR-221/222 were shown to directly negatively regulate ER and to confer resistance to tamoxifen treatment in vitro in MCF-7 and T47D cells<sup>222</sup>. Upregulation of miR-221/222 blocked tamoxifen-induced apoptosis in MCF-7 by targeting the cell cycle inhibitor p27(Kip1)<sup>223</sup>.

Increased expression of miR-125b provided resistance to paclitaxel (Taxol)-induced apoptosis in breast cancer MDA-MB-231 and MDA-MB-435 breast cancer cells<sup>224</sup>. MiR-125b upregulation delivered Taxol resistance by suppression of caspase-3 activity in MDA-MB-435 cells. Further investigation revealed that miR-125b exerted pro-survival effects by negatively regulating the pro-apoptotic protein BCL-2 antagonist killer 1 (BAK1) in multiple breast cancer cell lines, specifically MDA-MB-435, MDA-MB-231, MCF-7 and SkBr3 cells. BAK1 is a critical regulator of apoptosis as it induces pore formation in the mitochondria. Inhibition of BAK1 substantially restricted the ability of Taxol to induce apoptosis in breast cancer MDA-MB-435 and MDA-MB-231 cells. Also, increasing BAK1 expression in cells with upregulated miR-125b, resulted in restored sensitivity to Taxol treatment. Taken together, these findings indicate that miR-125b-mediated negative regulation of BAK1 provides an important mechanism for its resistance to Taxol-induced apoptosis.

Although the previous examples provide evidence of the anti-apoptotic effects of some highly expressed oncogenic miRs, downregulation of pro-apoptotic miRs may also contribute to breast cancer pathogenesis. In fact, globally the majority of miRs are

downregulated in cancers<sup>203</sup>, and impaired miR expression has been found to promote tumorigenesis<sup>210</sup>.

For example, invasive ductal breast carcinomas displayed low levels of miR-497 compared to paired normal breast tissues, and its expression was inversely correlated to lymphatic metastasis, tumor size and presence of HER-2<sup>225</sup>. Further investigation revealed that miR-497 inhibited cellular growth in MCF-7 breast cancer cells, by causing G0/G1 cell cycle arrest and inducing apoptosis. Upregulation of miR-497 suppressed the expression of Bcl-w, an anti-apoptotic member of the BCL-2 family.

In MCF-7 cells, miR-195, miR-24-2 and miR-365-2 were identified as negative regulators of the BCL-2 oncogene through a combination of computational predictions and experimental analysis<sup>226</sup>. Upregulation of these three miRs caused loss of mitochondrial membrane potential, release of cytochrome c, activation of caspase-9 and induction of apoptosis. Furthermore, overexpression of these miRs acted synergistically with the chemotherapeutic drug etoposide, to increase apoptosis in MCF-7 cells.

In summary, miRs targets include both pro- and anti-apoptotic proteins. Altered miR expression has been shown to regulate apoptosis and sensitivity to anticancer therapies in breast cancer cells. Therefore, targeting miRs could be a novel therapeutic strategy for treating breast cancer, as well as other cancers<sup>18</sup>.

### **1.5. Zinc and MiR Expression**

Regulation of miR expression by nutritional means, in particular by zinc status, is a newly emerging area of research with relatively few studies to date. Recently, the effects of low dietary zinc intake by young males on the serum miR profile was investigated, to determine if a molecular miR “signature” could be detected<sup>19</sup>. Following low zinc intake (10 d), serum zinc decreased and the miR expression profile was altered; of the 88 miRs tested, 20 had a greater than 1.5 magnitude fold change. After dietary zinc repletion, nine miRs responded in an opposite manner to zinc depletion, indicating that they may serve as useful biomarkers of zinc status.

Chronic zinc deficiency was investigated in a rat esophagus cancer model and shown to alter the miR profile in all tissues investigated, which were the esophagus, skin, lung, pancreas, liver, prostate and peripheral blood mononuclear cells<sup>20</sup>. In particular, two oncogenic miRs: miR-21 and miR-31 were the most commonly upregulated across the tissues profiled. Further research, using an esophageal cancer model in rats, revealed that miR-21 and miR-31 responded in a reversible manner to dietary zinc intake. Expression of these two miRs was upregulated in tumor bearing zinc deficient rats, but dietary zinc replenishment prevented cancer formation and reduced expression of miR-21 and miR-31, to levels similar to the control group.

*In vitro* studies also point to zinc as a regulator of miR expression. In human breast cancer MCF-7 cells, zinc supplementation plus Clioquinol, a zinc ionophore, increased intracellular zinc content to cytotoxic levels, which was associated with global downregulation of miR<sup>21</sup>. Zinc cytotoxicity suppressed Dicer and Ago2 protein expression,

which are used to produce and stabilize mature miR, respectively. Clioquinol plus zinc also increased assembly of processing bodies (P-bodies), which are small cytoplasmic granules where it is thought that RISC mediated regulation of mRNA may take place.

A recent study investigated the effects of zinc treatment on expression of some miRs in human prostate cancer 22Rv1, PC-3, and LNCaP cells and a non-tumorigenic human prostate PNT1A<sup>22</sup>. MiR-23a was elevated in all four cell lines following zinc treatment, while other miRs displayed cell-type specific trends.

Altered miR expression may play a role in zinc homeostasis in prostate cancer, which is associated with reduced zinc. The miR-183-96-182 cluster was overexpressed in prostate tumors and shown to regulate zinc homeostasis in primary prostatic epithelial (PrE) cells, as well as human embryonic kidney HEK-293 cells<sup>227</sup>. Overexpression of the miR-183-96-182 cluster lowered intracellular zinc content and decreased expression of six zinc transporters (Zip1, Zip3, Zip7, Zip9, ZnT1, and ZnT7) in PrE cells. Increased expression of the miR-183-96-182 cluster also decreased zinc uptake in HEK-293 cells. Therefore, dysregulation of miRs may contribute to altered zinc homeostasis.

Currently, there are no published studies on the role of miRs in zinc depletion-induced apoptosis. More research is still needed to determine the functional significance between zinc status and miR expression, especially in the context of cancer development and progression.

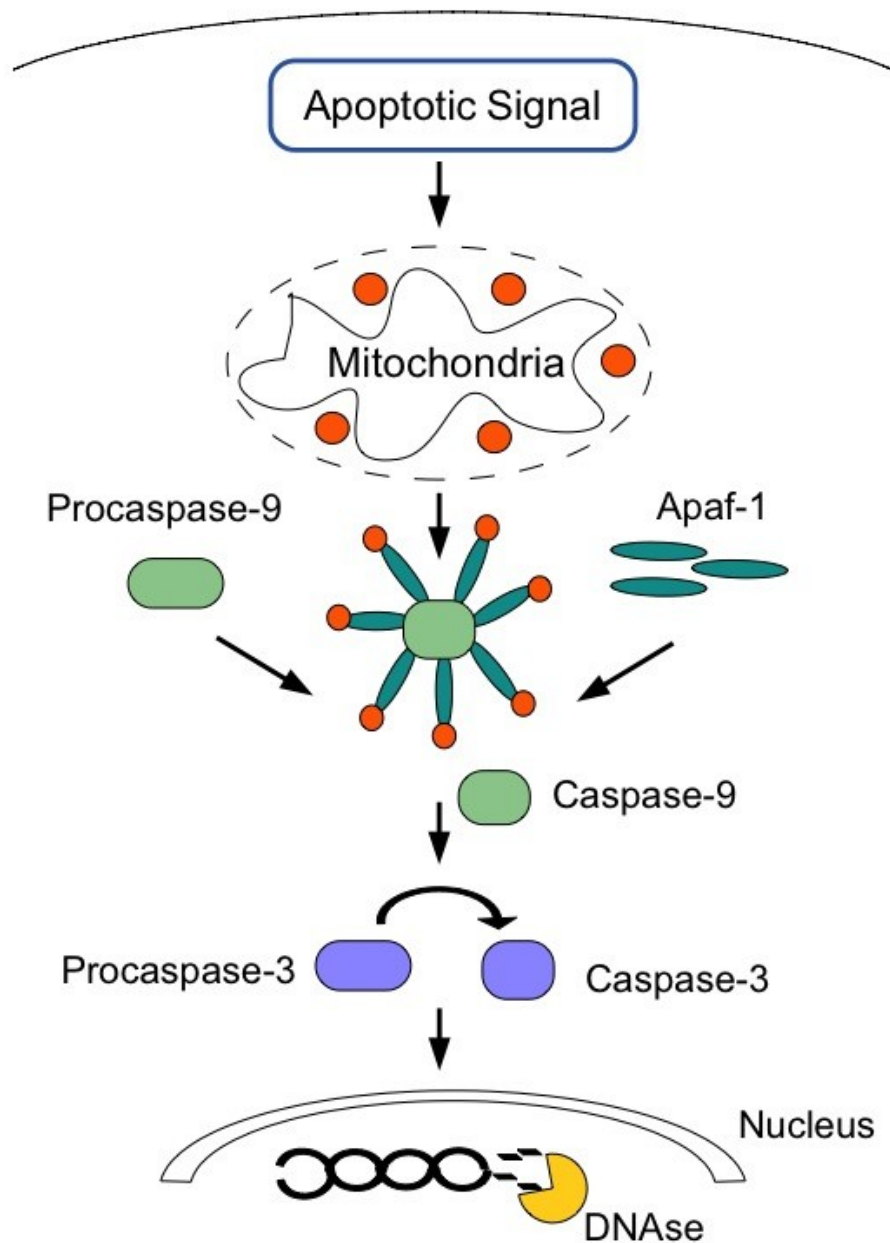


**Figure 1.1: Key elements of the intrinsic mitochondrial apoptotic pathway.**

An apoptotic signal induces permeabilization of the outer mitochondrial membrane (OMM), causing release of cytochrome c. In the cytosol, cytochrome c binds apoptotic protease activating factor (Apaf1), forming the apoptosome. The apoptosome activates caspase-9, which in turn activates caspase-3. Caspase-3 cleaves the inhibitor of caspase-activated deoxyribonuclease (ICAD), resulting in DNA fragmentation and apoptosis.<sup>13</sup>

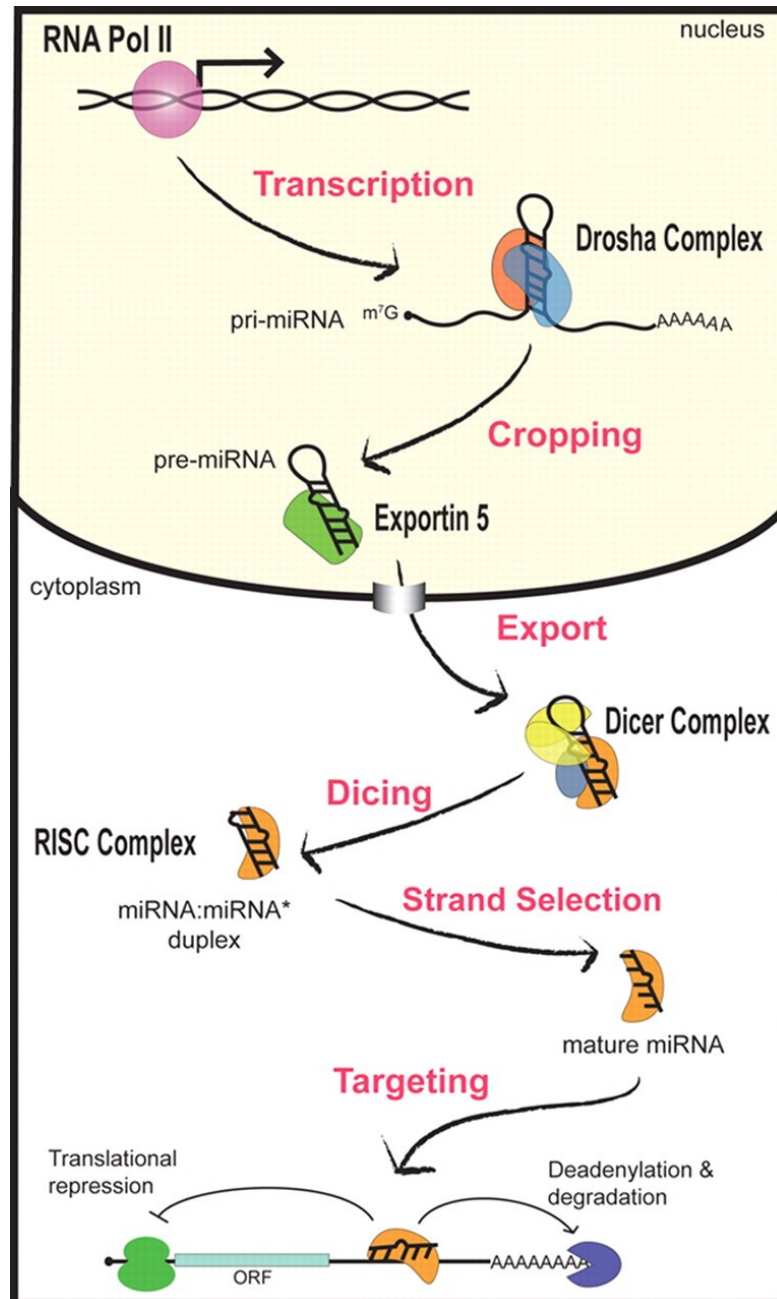


**Figure 1.2: General pathway for microRNA (miR / miRNA) biogenesis and function.** Primary (pri-) miRs are transcribed in the nucleus and undergo processing by Drosha into precursor (pre-) miRs, followed by Exportin-5 mediated nuclear export. In the cytoplasm, pre-miRs undergo an additional processing step by Dicer, producing double stranded mature miR. One of the strands of mature miR is loaded into the RNA-induced silencing complex (RISC) to mediate translational repression or degradation of target mRNA.<sup>202</sup>

## **1.6. Hypothesis**

Zinc depletion alters miR expression in human breast cancer MDA-MB-231 cells, which plays a role in mediating zinc depletion-induced apoptosis.

## **1.7. Overall Objective and Specific Aims**

The overall objective of this project was to determine the involvement of miRs in zinc depletion-induced apoptosis in MDA-MB-231 cells.

The specific aims of this research project were:

- 1) To determine if zinc depletion induced apoptosis in human breast cancer MDA-MB-231 cells, and
- 2) To profile the effects of zinc depletion on miR expression in human breast cancer MDA-MB-231 cells.

## **Chapter 2: Zinc depletion-induced apoptosis is associated with altered microRNA expression in human breast cancer MDA-MB-231 cells**

### **2.1. Materials and Methods**

#### **2.1.1. Cell culture system**

Human breast cancer MDA-MB-213 cells (American Type Culture Collection, Manassas, Virginia) were routinely cultured in Dulbecco's Modified Eagle's Medium (DMEM; Sigma, St Louis, Missouri) supplemented with fetal bovine serum (FBS, 10%; Gibco, Grand Island, New York), sodium pyruvate (1 mM; Gibco), penicillin-streptomycin (50 units/ml and 50 µg/ml, respectively; Gibco) at 37°C, 10% CO<sub>2</sub>. Through out the rest of this thesis, this medium is referred to as the 'regular medium'. The cells were cultured in 10 cm Petri dishes at an initial density of 5 x 10<sup>5</sup> cells / dish. Cells were harvested for passage when the plates reached 80 - 95 % of confluence. Cells with a passage number of 35-45 were used in this research project.

#### **2.1.2. Depletion of intracellular zinc**

N,N,N',N'-tetrakis(2-pyridylmethyl)ethylenediamine (TPEN; Sigma) stock solution was prepared by dissolving in dimethyl sulfoxide (DMSO; Sigma) with a concentration of 10 mM. The stock solution was stored at -20°C and thawed at room temperature prior to use.

Prior to zinc depletion, MDA-MB-231 cells were cultured in the regular medium for 3 days at 37°C, 10% CO<sub>2</sub> with an initial density of 2.5 x 10<sup>5</sup> cells per 6 cm dish. The regular

medium was replaced 2 days after initial seeding. At the end of the 3 day growth period, the cells were treated with TPEN, by adding the 10 mM stock TPEN solution to the regular medium (4  $\mu$ L; 0.1 % v/v) to a final concentration of 10  $\mu$ M. The control cells were treated with an equal volume of DMSO. The cells were then cultured at 37°C, 10% CO<sub>2</sub> for 0 - 72 h, depending on the experiment.

### **2.1.3. Apoptosis assay**

Apoptotic cells were measured by propidium iodide (PI; Sigma) flow cytometric assay<sup>228</sup>. PI binds to the DNA stoichiometrically, providing a measurement of the total cellular DNA content. In late-stage apoptotic cells, fragmented DNA leaves the cells resulting in lower DNA content. Apoptotic cells therefore are characterized by the presence of a sub-G<sub>1</sub> hypodiploid peak.

MDA-MB-231 cells were cultured in the growth medium with an initial density of 2.5 x 10<sup>5</sup> cells/well in a 6 cm plate. The growth medium was replaced after 2 days. At the end of the 3 day growth period, cells were treated with TPEN (10  $\mu$ M) or DMSO (control) for 0, 3, 6, 12, 24, 48, or 72 h. After the treatment period, the medium containing unattached cells was removed from both the control and TPEN plates and was transferred to a 15 ml conical tube. The cell culture plates containing adherent cells were rinsed once with warm phosphate buffered saline (PBS; 37°C). Adherent cells were harvested by addition of warm 0.25% trypsin-EDTA (ethylenediaminetetraacetic acid, Gibco; 37°C) and incubated (37°C, 10% CO<sub>2</sub>) for approximately 3 min or until cells had unattached, followed by addition of an equal volume of regular cold medium. The harvested cells were then placed into the same

tube used to collect the medium containing unattached cells. Cells were pelleted by centrifugation (300 g, 4°C, 5 min) and the supernatant was removed. The cells were washed once by resuspension in PBS (1 ml) by pipetting briefly, followed by centrifugation (300 g, 4°C, 5 min) and removal of the supernatant. The cells were fixed by slowly adding 100 µl cold PBS (4°C), followed by 900 µl of cold ethanol (-20°C; 70% EtOH in H<sub>2</sub>O, v/v) while gently vortexing, and then left at 4°C overnight. After fixation, the cells were pelleted by centrifugation (400 g, 5 min, 4°C), washed once with PBS (500 µl), re-pelleted by centrifugation (400 g, 5 min, 4°C) and the supernatant was removed. The cell pellet was then re-suspended in DNA staining solution [200 µg/ml ribonuclease A (Sigma) and 20 µg/ml PI (Sigma) in PBS; pH 7.4] at approximately 1 ml / 10<sup>6</sup> cells. Finally, the cell suspension was transferred to a 5 ml Falcon tube and incubated at room temperature and in the dark for 30 min. The presence of PI-stained cells was determined by flow cytometry (BD FACSCalibur Flow Cytometer and CellQuest Pro Software; BD Biosciences, San Jose, California). The excitation and emission wavelengths were 488 nm and 610 nm, respectively. A total of 25,000 events were counted for each sample. The percentage of cells with fragmented DNA content or apoptosis was determined using FlowJo Software (version 10.0.4; Tree Star, Ashland, OR).

#### **2.1.4. Total RNA isolation**

MDA-MB-231 cells were cultured under the same conditions described previously, and the cells were treated with TPEN (10 µM) or DMSO only (control) for 3, 12 or 24 h. At the end of the treatment period, total RNA was extracted using the mirVANA miR isolation kit (Ambion, Life Technologies Corporation, Burlington, Ontario) according to the

manufacturer's instructions. Briefly, the medium containing floating cells was collected by transferring to a 15 mL conical tube on ice and then pelleted by centrifugation (600 rpm, 4°C, 5 min). Both floating and adherent cells were rinsed with cold PBS and the denaturing lysis buffer was added in proportion to the amount of cells (100 – 600 µl). A spatula was used to dislodge adherent cells, which were then pipetted into a 2.0 mL microcentrifuge tube. The homogenate was added to both floating and adherent cells at 1/10<sup>th</sup> of the lysate volume and the mixture was vortexed briefly, followed by incubation for at least 10 min on ice. The lysate mixtures from the floating cells and adherent cells were combined into a single tube and then mixed with an equal volume of acid phenol-chloroform, followed by vigorous vortexing for two minutes. Samples were centrifuged (16,100 g, room temperature, 5 min) and the upper aqueous phase was carefully removed with minimal disturbance to the interface. Then 1.25 volumes of room temperature ethanol was added to the aqueous phase and mixed thoroughly by inversion. Subsequently, the samples were precipitated onto the filter cartridge provided in the RNA isolation kit. The RNA was purified using the provided wash solutions according to the manufacturer's instructions. Total RNA was collected by elution with 0.1 mM EDTA in nuclease-free water (100 µl) heated to 95°C.

RNA quality was assessed by both purity and integrity. RNA purity was measured using the Nanodrop spectrophotometer 260/280 and 260/230 ratios (Thermo Fisher Scientific, Wilmington, Delaware) and RNA integrity was visualized using gel electrophoresis (1% agarose gel). RNA samples having a 260/280 ratio of > 1.8 (1.99 – 2.49), a 260/230 ratio of > 1.0 (1.01 – 3.07) and being free of degradation were used for miR expression profiling. Intact RNA samples with 260/280 ratio > 1.8 (2.02 – 2.08) were used for real-time quantitative reverse transcription polymerase chain reaction (qRT-PCR) assay.

The majority of RNA samples used for qRT-PCR had a 260/230 ratio of > 1.0 (1.01 – 3.23), except for 2 samples with lower ratios (3hT: 0.88, 12hT: 0.57).

### **2.1.5. MiR microarray assay**

The genome-wide human (noted by the hsa prefix) miR profile was assessed through microarray profiling provided by LC Sciences (Houston, Texas; n = 3). Profiling was completed for all mature miRs included in the miRBase (a miR repository) release 19 (August 2012), containing 2019 mature human miRs. Starting with a total RNA sample (4–8 µg), RNAs were extended with a poly(A) tail and ligated to an oligonucleotide tag for later fluorescent dye staining. RNA samples were hybridized to detection probes overnight on a µParaflo microfluidic chip (Atactic Technologies, Houston, Texas)<sup>229,230</sup>. Each detection probe was composed of a chemically modified oligonucleotide, which was complementary to target miR (from miRBase) or other RNA (control), in addition to a polyethylene glycol spacer segment. The probes were prepared by *in situ* synthesis using photogenerated reagent chemistry and contained chemical modifications to balance the hybridization melting temperatures. Hybridization was performed at 34°C in 100 µL of 6x saline-sodium phosphate-EDTA (SSPE) buffer (0.90 M NaCl, 60 mM Na<sub>2</sub>HPO<sub>4</sub>, 6 mM EDTA, pH 6.8) containing 25% formamide. Each sample was analyzed on an individual chip containing four repeat probes per miR. Following hybridization, cyanine 3 dye was circulated through the chip for fluorescence staining. The microarrays were scanned with a GenePix 400B laser scanner (Molecular Devices, Sunnyvale, California) and image digitization was performed using Array-Pro image analysis software (Media Cybernetics, Rockville, Maryland). Following background subtraction, data was normalized using the cyclic LOWESS (locally

weighted scatterplot smoothing) method<sup>231</sup>. The normalized signal intensity was reported on a relative scale from 0 – 65,535. A minimum signal intensity of 32 for at least one individual sample was used as the cutoff for detectable miR expression.

#### **2.1.6. MiR heat maps**

MiR expression was clustered according to similarities in gene expression across sample groups. Clustered heat maps were generated using z-scores of log-transformed signal intensities for each individual miR at the time point(s) evaluated. The distance metric used to determine similarity in gene expression was Euclidean distance, which is the distance between two points. Hierarchical clustering was performed based on average linkage, where the similarity of two clusters was determined from the average distance of all pairwise comparisons. Multiexperiment Viewer software (TM4 MicroArray Software Suite) was used to perform cluster analysis.

#### **2.1.7. qRT-PCR miR assay**

Expression of some of the miRs most significantly affected by TPEN treatment (miR-132-3p, miR-1246, miR-1273g-3p, miR-4484, miR-4521 and miR-4787-5p) was subjected to validation using TaqMan qRT-PCR (n=6 with 2 technical replicates). The TaqMan miR assay is the gold standard for miR quantitation due to its high sensitivity and specificity over a wide range of miR expression levels<sup>232–234</sup>. Total RNA was quantified using a Qubit 2.0 Fluorometer (Life Technologies Inc., Burlington, ON). The starting amount of total RNA used in the RT reaction was 5 ng for miR-1246 and miR-1273g-3p, and 25 ng

for miR-132-3p, miR-4484, miR-4521 and miR-4787-5p. The RT and PCR reaction mixes were prepared according to the manufacturer's instructions (Taqman MicroRNA Reverse Transcription Kit and TaqMan MicroRNA Assays; Applied Biosystems, Life Technologies Corporation). Briefly, a RT master mix was prepared containing 0.15  $\mu$ l 100 mM dNTP (deoxyribonucleotide triphosphates) with dTTP (deoxythymidine triphosphate), 1  $\mu$ l Multiscribe Reverse Transcriptase (50 U/ $\mu$ l), 1.5  $\mu$ l Reverse Transcription Buffer (10x), 0.19  $\mu$ l RNase (ribonuclease) inhibitor (20 U/ $\mu$ l) and 4.16  $\mu$ l nuclease-free water. The RT reaction (15  $\mu$ l) was prepared with 7  $\mu$ l master mix, 5  $\mu$ l total RNA in nuclease-free water and 3  $\mu$ l RT Primer (5x). The RT reactions were run for 30 min at 16°C, 30 min at 42°C, and 5 min at 85°C, and then cooled down to 4°C in an Eppendorf Mastercycler Gradient (Eppendorf AG; Hamburg, Germany). If the PCR experiment was not performed immediately after, the RT reactions were stored at -20°C. Briefly, the PCR reactions (20  $\mu$ l) consisted of 1  $\mu$ l TaqMan Small RNA Assay, 1.33  $\mu$ l cDNA, 10  $\mu$ l TaqMan Universal PCR Master Mix II (2x no UNG), and 7.67  $\mu$ l nuclease-free water. The PCR reactions were run with a 10 min incubation at 95°C followed by 40 PCR cycles of 95°C for 15 seconds and 60°C for 60 seconds in an Applied Biosystems 7500 Real-Time PCR System (Applied Biosystems, Foster City, CA). Relative quantification was determined according to the Delta Delta CT method<sup>235</sup>.

MiR-16-5p was chosen as an endogenous control from 3 candidate endogenous controls screened. The microarray results indicated that miR-16-5p was highly expressed and that there were no significant differences with treatment, treatment duration and interaction ( $p < 0.05$ , Figure A.1, Table A.1). Expression of miR-16-5p was also subjected to validation by qRT-PCR. Relative quantification of miR-16-5p was determined according to the Delta

CT method<sup>235</sup>. Although the individual qRT-PCR runs showed some differences in miR-16-5p abundance, the differences were relatively small and did not indicate any consistent alterations in miR-16-5p expression at the different treatments or time points examined (Figure A.2-5). Overall, miR-16-5p was highly and consistently expressed, making it a suitable endogenous control. Furthermore, miR-16-5p has also been reported as a suitable endogenous control for malignant, benign and normal breast tissues in the literature<sup>236</sup>.

### 2.1.8. Statistics

**MicroArray statistics.** The z-scores of log-transformed signal intensities were used for all statistical analyses. Data was analyzed for treatment effect at each time point using an error-weighted T-test. The effects of treatment, treatment duration, and their interactions among multiple time-points were analyzed using 2-way analysis of variance (ANOVA) ( $p < 0.05$ ). The fold change standard deviation (SD) was calculated by propagation of error using the following formula<sup>237</sup>:

$$S_y = \frac{1}{G1} \sqrt{\left(\frac{G2}{G1}\right)^2 S_{G1}^2 + S_{G2}^2}$$

$y = f(G1, G2) = G2/G1$ , where G1 and G2 are average values of group 1 and group 2 signal intensities

$S_y$ ,  $S_{G1}$ , and  $S_{G2}$  are the standard deviations of  $y$ , group 1 and group 2

**qRT-PCR statistics.** The effects of treatment, treatment duration, and their interactions on abundance of miR-16 (endogenous control) were analyzed by 2-way ANOVA, followed by post-hoc Tukey's Honestly Significant Difference (HSD) test.

Student's t-test ( $p < 0.05$ ) was used to assess significant differences between miR abundance in the control and TPEN groups at each time point. Welch's t-test was applied when the variances between the control and TPEN groups were unequal ( $p < 0.05$ ). One-way ANOVA was used to test the treatment-duration effects followed by Tukey's HSD test for the significant difference among the 3 time points ( $p < 0.05$ ). Outliers, which exceeded 3 standard deviations from the mean, were omitted from data analyses.

## **2.2. Results**

### **2.2.1. Zinc depletion-induced apoptosis**

The time-course of zinc depletion-induced apoptosis in MDA-MB-231 cells is shown in Figure as well as Figure A.6-12. The control group exhibited < 1% of apoptotic cells at all time points examined. At 0 h, 0.79 % of cells were apoptotic, indicating a low basal level of apoptosis in cultured cells. TPEN treatment (10  $\mu$ M) resulted in negligible levels of apoptosis after 3 and 6 h, which were comparable to the control group (0.5% vs. 0.4% at 3 h and 0.5% vs. 0.6% at 6 h for the control and TPEN groups, respectively). After 12 h TPEN treatment, only 1.2 % of cells had fragmented DNA, compared to 0.6% in the control group. By 24 h, the proportion of apoptotic cells increased slightly to 4.5%, versus 0.6% apoptosis in the control group. The longer TPEN treatment durations of 48 and 72 h substantially increased the proportion of apoptotic cells to 24.4 and 28.0% respectively, compared to 1.0 and 0.7 % in their corresponding controls.

In summary, TPEN-induced depletion of intracellular zinc in MDA-MB-231 cells resulted in a time-dependent induction of apoptosis. After 24-h TPEN treatment, just under 5% of MDA-MB-231 cells were apoptotic, while TPEN treatment for 48 and 72 h substantially increased the proportion of apoptotic cells.

### 2.2.2. Zinc depletion altered miR expression

The time-points chosen to investigate the effects of the early stages of zinc depletion-induced apoptosis on global miR expression were 3, 12 and 24 h, due to the low level of apoptosis (<5% cells with fragmented DNA) observed following up to 24 h TPEN treatment. The miR microarray detected 397 of 2019 unique mature human miRs in at least one of the samples (Table A.1), indicating that a subset of the human microRNA genome (miRNome) was expressed in control and TPEN-treated MDA-MB-231 cells.

The global miR expression profile remained largely unchanged following three hours of TPEN treatment. The expression of just 8 miRs was significantly affected compared to the control group, with 6 miRs increased and 2 miRs decreased (Figure ). The signal intensity of miRs significantly affected after 3 hours TPEN treatment were generally low (< 500), with only one miR (182-5p) just exceeding a signal intensity of greater than 500 for at least one individual sample, which is the minimum signal required for validation by RT-qPCR. The expression of miR-182-5p was decreased by 1.3 times in the TPEN treated group compared to the control group (Table 2.1, Table A.1).

Following 12 h TPEN treatment, the miR expression profile was largely affected with almost one-quarter of detected miRs significantly altered (90 / 397; Figure ). The expression of majority of differentially expressed miRs was increased (51 / 90). Of those miRs significantly affected, 10 miRs had a greater than two-fold change in expression and also met the minimum signal intensity cutoff of 500 for at least one individual sample (Table 2.2). Interestingly, the expression of all 10 of these miRs (miR-3127-5p, -5194, -4485, -132-3p, -

4734, -1273g-3pg-3p, -5096, -4484, -1973 and -4690-5p) was increased. Among these 10 miRs, miR-3127-5p and miR-5194 showed the greatest fold increase in the TPEN treated groups compared to their corresponding controls. However, the expression of miR-3127-5p and miR-5194 in the control groups was negligible, as the signal intensities were below the cutoff of 32 for detectable expression (average signal intensities: 1, 4, respectively, Table A.1). In the TPEN treated groups, there was a small increase in the signal intensities of miR-3127-5p and miR-5194 (average signal intensities: 490, 403 respectively). Therefore, the abundance of miR-3127-5p and miR-5194 was low in both the control and TPEN treated groups. The expression of miR-4485 and miR-132-3p was also very low in the control group (average signal intensities: 35, 38, respectively) and was significantly increased by TPEN treatment (average signal intensities: 1,217, 630, respectively), with a 34.5 and 16.4 fold increase, respectively. The remainder of the miRs displayed approximately 2-3 fold increases in their expression following 12 h TPEN treatment.

After 24-h TPEN treatment, approximately one-quarter of miRs (94 / 397) were significantly affected, and the majority of differentially expressed miRs had increased expression (74 / 94; Figure ). Among those miRs having signal intensities greater than 500 for at least one individual sample and a fold change greater than two, the expression of 22 miRs was increased and 2 miRs was decreased (Table 2.3). The expression of 5 miRs (miR-132-3p, -1273g-3pg-3p, -1973, -4484 and -4485) was increased by more than two-fold after both 12 and 24 h TPEN treatment.

There were numerous miRs significantly altered by zinc depletion, duration of zinc depletion, and their interactions. In total, 285 unique miRs were significantly affected by zinc

depletion, duration of zinc depletion and their interactions, making up 72% of expressed miRs, while less than 1/3 of expressed miRs (112/397) remained unaffected by treatment, treatment duration and their interactions. Of the significantly affected miRs, approximately 50% (149/285) were significant for an interaction effect between zinc depletion and duration of zinc depletion. The number of miRs significant for zinc depletion only, duration of zinc depletion only or both zinc depletion and duration was 56, 48 and 32, respectively.

### **2.2.3. Zinc depletion altered abundance of miR-132-3p, miR-1246, miR-1273g-3p, miR-4484, miR-4521 and miR-4787-5p**

Expression of selected miRs was validated after 3, 12 and 24 h TPEN treatment using qRT-PCR. The miRs investigated were miR-132-3p, miR-1246, miR-1273g-3p, miR-4484, miR-4521 and miR-4787-5p.

MiR-132-3p was found to be the most responsive to zinc depletion, out of the six miRs examined by qRT-PCR. After just 3 h of TPEN treatment, the abundance of miR-132-3p was significantly increased (2.2 folds), and further increased by 17.7 and 28.5 folds after 12 and 24 h, respectively, compared to their respective control groups (Figure ). TPEN treatment resulted in a time-dependent increase in the abundance of miR-132-3p while its abundance remained the same in the control groups at 3, 12 and 24 h.

Another miR substantially affected by TPEN treatment was miR-1246, which was significantly increased in a time-dependent manner. At 3 h the abundance of miR-1246 was the same between TPEN and control groups. However, TPEN treatment increased the abundance of miR-1246 by 3.8 and 18.4 folds at 12 and 24 h, respectively, compared to their

respective control group (Figure ). In contrast, in the control groups the abundance of miR-1246 was significantly decreased by 1.8 and 1.7 folds at 12 and 24 h, respectively, compared to that at 3 h.

Zinc depletion significantly increased the abundance of miR-4484 in a time-dependent manner (Figure ). While miR-4484 was significantly elevated at all 3 time points investigated, the peak increase in abundance occurred at 12 h TPEN treatment, with a 5.5 fold increase compared to the 12 h control group. At 3 h TPEN treatment miR-4484 abundance increased by 1.4 fold and, at 24 h TPEN treatment, by 3.5 fold compared to the respective control groups. Abundance of miR-448 in the control groups was also increased over time.

The abundance of miR-4787-5p was significantly elevated by 1.6 and 4.0 folds at 3 and 24 h TPEN treatment, respectively, compared to their respective control groups, but the abundance of miR-4787-5p was unaffected by TPEN treatment at 12 h (Figure ). The abundance of miR-4787-5p remained the same from 3 to 12 h of TPEN treatment; but was increased by 3.6 folds after 24 h of TPEN treatment compared to the 3 h TPEN treatment durations. The abundance of miR-4787-5p in the control group varied, with 1.6 and 1.4 fold increases at 12 and 24 h, respectively, compared to that at 3 h.

The abundance of miR-1273g-3p was decreased by 2.4 folds in the 3-h TPEN-treated group compared to the 3-h control, but was increased by 2.2 and 3.4 folds after 12 and 24 h of TPEN treatment, respectively, compared to their respective controls (Figure ). TPEN treatment significantly increased in the abundance of miR-1273g-3p in a time-dependent manner. In contrast, the abundance of miR-1273g-3p was decreased by 2.9 and 3.2 folds in

the 12 and 24-h control groups, respectively compared to the 3-h control group. Therefore, miR-1273 exhibited opposite patterns with decreased abundance over time in the control groups and increased abundance in the TPEN treated groups.

Zinc depletion resulted in 1.4 and 1.3 fold increases in the abundance of miR-4521 in the 3 and 12-h TPEN groups compared to their respective control groups, respectively; Figure ). However, after 24 h TPEN treatment, abundance of miR-4521 decreased by 5.1 folds compared to its control group. Treatment duration-dependent decrease in miR-4521 abundance was observed in both the control and TPEN treated groups, but to a larger extent in the TPEN treated groups. In the control groups, miR-4521 abundance decreased by 1.4 and 2.0 fold at 12 and 24 h, respectively, compared to the 3 h control group. The 12 and 24 h TPEN treatments decreased miR-4521 by 1.6 and 14.4 folds, respectively, compared to the 3 h control group.

In summary, we observed that the longer TPEN treatment duration (24 h) typically led to the largest changes in the abundance of miRs; however, the abundance of miR-4484 was observed at the highest level after 12 h TPEN treatment. Abundance of miR-132-3p, miR-1246, miR-4484, miR-4787-5p and miR-1273g-3p were significantly increased by 24 h TPEN treatment compared to their respective controls. Of the miRs assessed, the largest increase in abundance was observed for miR-132-3p, with a 28 folds increase in the 24h TPEN group, followed by miR-1246, which was increased by 18 folds in the 24 h TPEN group. MiR-4521 was the only miR among the 6 miRs assessed which decreased in abundance after 24 h TPEN treatment.

### **2.3. Discussion**

Zinc depletion was shown to induce apoptosis in a time-dependent manner in MDA-MB-231 breast cancer cells, similarly to previous findings from our laboratory<sup>13,238</sup>. The apoptotic effects of reduced zinc from TPEN treatment have been demonstrated in many other cell lines including thymocytes<sup>135</sup>, lymphocytes<sup>136,137</sup>, malignant airway epithelial cells<sup>138</sup>, leukemia cells<sup>139</sup>, retinal pigment epithelial cells<sup>140</sup>, melanoma cells<sup>141</sup>, keratinocytes<sup>142</sup>, pancreatic cancer cells<sup>143</sup> and cervical cancer cells<sup>132</sup>. Dietary zinc deficiency also induces apoptosis *in vivo* in rats in multiple tissues<sup>123</sup>. While much progress has been made towards elucidating the mechanisms of zinc depletion-induced apoptosis, particularly on the central role of the intrinsic mitochondrial apoptotic pathway<sup>13,14,137,148,149</sup>, the molecular pathways involved are still poorly understood. This research provided novel information on miR expression during apoptosis arising from zinc depletion.

The effect of zinc depletion on the miR expression profile of MDA-MB-231 cells was measured after just 3, 12 or 24 h of TPEN treatment (10  $\mu$ M), while the majority of cells still had intact DNA, indicating that they had not yet reached late-stage apoptosis. Expression of numerous miRs was altered after 12 and 24 h TPEN treatment, indicating possible involvement of these miRs in mediating zinc depletion-induced apoptosis. Overall, the majority of differentially expressed miRs were upregulated by zinc depletion.

Cellular zinc status may regulate post-transcriptional miR processing, as treatment of MCF-7 breast cancer cells with a chemotherapeutic agent (Clioquinol) which raised intracellular zinc to cytotoxic levels suppressed expression of Dicer as well as Ago2, and was also associated with global downregulation of miR, presumably through decreased miR

biogenesis and stability<sup>21</sup>. It is conceivable that in our study zinc depletion altered the miR profile by modulating miR biogenesis; however, this hypothesis requires validation with further research.

The earliest miR that was significantly affected by zinc depletion was miR-182-5p, with a modest 1.3 fold decrease in its expression after just 3 h of zinc depletion. MiR-182-5p has been reported as upregulated in breast cancer, as well as in many other types of cancer, including colorectal, prostate and lung cancer<sup>239</sup>. Additionally, a recent study found that expression of miR-182-5p was significantly higher in triple negative breast cancers as well as in triple negative MDA-MB-231 breast cancer cells compared to normal breast tissue<sup>240</sup>. MiR-182-5p has been reported to act as an oncogene in a number of studies, including reported anti-apoptotic roles<sup>239</sup>. For example, inhibition of miR-182-5p expression in MDA-MB-231 cells inhibited cellular proliferation and invasion, and induced apoptosis<sup>240</sup>. In MCF-7 breast cancer cells, miR-182-5p negatively regulated FOXO1, a pro-apoptotic transcription factor, to increase cell viability<sup>241</sup>. MiR-182-5p targets include other pro-apoptotic genes including p27(Kip1) in MDA-MB-231 and HEK-293 cells, as well as the Bcl-2 family members BAK and BAX in HEK-293T cells<sup>242</sup>.

Interestingly, a role for miR-182 in the regulation of zinc homeostasis has also been reported. In PrE cells, overexpression of miR-182 with a pre-miR-182 mimic negatively regulated Zip1, which transports zinc into the cytoplasm from the extracellular space or organelles, through 2 binding sites in its 3'UTR resulting in Zip1 mRNA degradation<sup>227</sup>. Additionally, miR-182 upregulation decreased mRNA of 5 other zinc transporters (Zip3, Zip7, Zip9, ZnT1 and ZnT7). The overall effect of miR-182 overexpression on zinc

homeostasis was to lower intracellular zinc in PrE, possibly through reduced cellular zinc uptake as observed in HEK-293 cells.

Based on these findings, the decrease in miR-182-5p expression that we observed after 3 h of zinc depletion may have served to increase zinc uptake in response to intracellular zinc depletion. However, the miR microarray indicated that miR-182-5p was poorly expressed in the control group (average signal intensity: 465.1) and the 3 h TPEN treatment only induced a modest decrease in overall expression (average signal intensity: 356.2 TPEN, 1.3 fold decrease). Furthermore, no significant changes in miR-182-5p expression were observed after 12 or 24 h TPEN treatment. Due to its role in zinc homeostasis and apoptosis, miR-182-5p could possibly provide an early connection between zinc depletion and subsequent induction of apoptosis; however, more research is required to validate its expression as well as functional significance in zinc depletion-induced apoptosis in MDA-MB-231 cells.

The expression of miR-132-3p, -1246, -1273g-3p, -4484, -4521 and -4787-5p were shown to be substantially altered by zinc depletion using the microarray profiling assay and these observations were validated using qRT-PCR. Of these validated miRs, miR-132-3p displayed the greatest induction following zinc depletion. The abundance of miR-132-3p doubled after just 3 h of TPEN treatment and continued to increase to 28 times of the control group after 24 h of TPEN treatment.

Decreased expression of miR-132-3p has been previously reported in cancer and it has been found to have tumor suppressive roles<sup>219,243</sup>. For example, miR-132-3p was reported as significantly downregulated in breast DCIS, an early stage of breast cancer, compared to

paired samples of adjacent normal breast tissue<sup>219</sup>. Transfection of MCF-7, MDA-MB-231 and BT-549 breast cancer cell lines with pre-miR-132 mimics decreased cell viability in all three cell lines 96 h post-transfection. Furthermore, transfection of MDA-MB-231 and MCF-7 cells with miR-132 mimics for 24 h inhibited colony formation after 2-weeks, indicating that miR-132 negatively regulated anchorage-independent growth. Therefore, miR-132 appears to exert an inhibitory role in the survival of breast cancer cells.

In prostate cancer samples, expression of miR-132-3p was also significantly downregulated due to DNA methylation<sup>243</sup>. Decreased miR-132-3p expression correlated with metastasis and lymph node invasion as well as an increased likelihood of tumor recurrence. Transfection of PC-3 prostate cancer cells with a pre-miR-132 mimic caused cells to develop a rounded phenotype and become unattached from the plates at 72 h, followed by increased apoptosis at 96 h. Additionally, miR-132 upregulation dramatically reduced cellular migration and invasion of PC-3 cells. MiR-132 was found to negatively regulate talin 2, a protein that plays a role in the assembly of actin filaments, and inhibition of talin 2 was linked to decreased cellular adherence and migration.

MiR-132-3p has previously been reported to play an important role in response to nutritional stress. In response to serum deprivation, miR-132-3p was shown to rapidly increase in human preadipocytes and *in vitro* differentiated adipocytes<sup>244</sup>. Furthermore, miR-132 overexpression directly repressed silent information regulator 1 (SirT1) expression in preadipocytes. SirT1 inhibits activation of nuclear-factor- $\kappa$ B (NF- $\kappa$ B) by deacetylation. As a result, miR-132 upregulation inhibited SirT1-mediated deacetylation of NF- $\kappa$ B, ultimately resulting in NF- $\kappa$ B activation and translocation from the cytosol to the nucleus. Interestingly,

activation of NF- $\kappa$ B has also been reported to mediate zinc depletion-induced apoptosis in leukemia cells<sup>154</sup>. In this study it is unknown whether induction of miR-132-3p following nutritional stress was due in part to zinc depletion or solely to other nutritional deficiencies.

In accordance with these findings, our research study also found that zinc depletion, a form of nutritional stress, induced miR-132-3p expression. Since miR-132-3p was reported to have pro-apoptotic effects in prostate cancer cells<sup>243</sup> and to decrease viability in breast cancer cells<sup>219</sup>, it may potentially serve a critical link between zinc depletion and induction of apoptosis; however, further research is required to affirm its role in zinc depletion-induced apoptosis in MDA-MB-231 breast cancer cells.

Abundance of miR-1246 was also largely elevated after 12 and 24 h of TPEN treatment. The mechanisms by which zinc depletion altered miR-1246 expression in our study are currently unknown. Reduced abundance of miR-1246 in malignant cells may occur as a result of increased cellular export. Malignant breast cancer cell lines (e.g. MDA-MB-231, MCF-7, Sk-Br3) selectively released miR-1246 into exosomes, while human breast epithelial MCF-10A cells and human lung fibroblasts IMR90 cells retained a higher amount of miR-1246<sup>245</sup>.

MiR-1246 has been reported to exert a pro-apoptotic effect. In human lung carcinoma A-549 cells, overexpression of a pre-miR-1246 mimic promoted apoptosis<sup>246</sup>. Further investigation revealed that miR-1246 negatively regulated the amount of protein kinase DYRK1A (dual specificity tyrosine-phosphorylation-regulated kinase 1A) in human lung cancer H1299 cells and human osteosarcoma U2OS cells, and was shown to directly target the 3'UTR derived from DYRK1A mRNA in human colon cancer HCT-116 cells<sup>246</sup>.

DYRK1A is an anti-apoptotic protein that has been found to negatively regulate caspase-9 in retina cells<sup>247</sup>.

These observations collectively suggest that miR-1246 plays a role in apoptosis. Therefore, the increased abundance of miR-1246 observed in this research may have been involved in initiating zinc depletion-induced apoptosis in MDA-MB-231 cells; however, more research is needed to verify its role in this model system.

The microarray results also indicated that zinc depletion resulted in downregulation of miR-181b-5p by greater than 2 fold after 24 hours of treatment (Table 2.3). Overexpression of miR-181b-5p occurs frequently in human breast cancer, and its expression levels are correlated with increased breast tumor aggressiveness and shorter disease free survival<sup>248-251</sup>. Increased expression of miR-181b may be induced by a variety of oncogenic pathways implicated in breast tumorigenesis involving hypoxia<sup>252</sup> as well as transforming growth factor  $\beta$ <sup>253,254</sup>, signal transducer and activation of transcription 3<sup>255</sup>, and high mobility group A1 proteins<sup>250</sup>.

Expression of miR-181b has been shown to play an important role during tumorigenesis, as inhibition of miR-181b-1 (precursor for miR-181b-5p) reduced tumor colony formation in multiple cancer cell lines including breast cancer cells (transformed MCF-10A ER-Src) as well as colon (HT-29, HCT-116), lung (A-549) and liver (Hep-3B) cancer cells<sup>255</sup>. Treatment of transformed MCF-10A ER-Src cells with anti-miR-181b-1 also inhibited cellular invasion. Furthermore, anti-miR-181b-1 inhibited tumor growth *in vivo* in multiple types of mouse xenografts (derived from MCF-10A ER-Src, HT-29 and HCT-116 cells). Increased expression (> 100 fold increase) of miR-181b by transfection with pre-miR-

181b in MDA-MB-435s breast cancer cells promoted cell proliferation and reduced apoptosis<sup>250</sup>. Additionally, miR-181b-5p has been found to regulate tamoxifen resistance in mice. Treatment of mice with tamoxifen as well as anti-miR-181b-5p, reduced tumor growth of tamoxifen-resistant xenografts (derived from MCF-7 cells), compared to just treating with tamoxifen and a negative control<sup>256</sup>. In another study, miR-181b-5p was identified as inhibiting the DNA damage response in breast cancer, by negatively regulates ataxia telangiectasia mutated, which is involved in repairing double stranded DNA breaks<sup>248</sup>. These studies suggest that downregulation of oncogenic miR-181b-5p could play a role in regulating cellular growth and survival in response to zinc depletion, however, more research is needed.

Many of the miRs identified as significantly altered by zinc depletion in this research, have only been recently discovered and their biological functions are largely unknown. For example, miR-1273g-3p was discovered in 2008 by deep sequencing of human embryonic stem cells<sup>257</sup>. MiR-4484 and miR-4521 were identified in 2010 by deep sequencing of normal and malignant B-cells<sup>258</sup>. MiR-4484 was also identified as encoded in the mitochondrial genome of HEK-293 and HeLa cells in 2012<sup>259</sup>. MiR-4787-5p was identified in 2011 by sequencing of normal and tumor breast tissue<sup>260</sup>. In the absence of knowledge in biological functions of these miRs, the significance of an increased abundance of these miRs in zinc depletion-induced apoptosis in MDA-MB-231 cells remains to be elucidated.

In summary, zinc depletion induced apoptosis in a time-dependent manner in MDA-MB-231 cells. Zinc depletion altered the abundance of numerous miRs in MDA-MB-231 cells, and differentially expressed miRs were mainly increased by zinc depletion. Notably,

the abundance of miR-132-3p and miR-1246 were substantially increased by zinc depletion. Based on the previously demonstrated role of miR-132-3p and miR-1246 in promoting apoptosis<sup>243,246</sup>, these two miRs may be involved in mediating zinc depletion-induced apoptosis. Furthermore, a considerable number of miRs identified as altered by zinc depletion have only been discovered in recent years and have yet unknown biological functions. An altered abundance of these miRs in zinc depletion-induced apoptosis indicates an association between these miRs and zinc depletion-induced apoptosis. Taken together, for the first time, this research provided evidence of an association between miRs and zinc depletion-induced apoptosis in human breast cancer MDA-MB-231 cells; however, their specific roles in the induction and regulation of zinc depletion-induced apoptosis in human breast cancer MDA-MB-231 cells remains to be elucidated.

**Table 2.1: Differential expression of miR-182-5p induced by 3-h TPEN treatment.** MDA-MB-231 cells were treated with DMSO (control) or TPEN (10  $\mu$ M in DMSO) for 3 h (n=3). The values are mean  $\pm$  SD. Cutoff criteria was set at signal intensity > 500 for at least one individual sample and  $p < 0.05$ .

<b>MiR</b>	<b>Fold Change</b>	<b><i>p</i>-value</b>
hsa-miR-182-5p	-1.3 $\pm$ 1.1E-01	4.7E-02

**Table 2.2: Differential expression of miRs induced by 12-h TPEN treatment.**

MDA-MB-231 cells were treated with DMSO (control) or TPEN (10  $\mu$ M in DMSO) for 12 h (n=3). The values are mean  $\pm$  SD. Cutoff criteria was set at magnitude fold change  $> 2$ ; signal intensity  $> 500$  for at least one individual sample, and  $p < 0.05$ .

<b>MiR</b>	<b>Fold Change</b>	<b><i>p</i>-value</b>
hsa-miR-3127-5p	374.1 $\pm$ 3.1E+02	6.7E-03
hsa-miR-5194	113.2 $\pm$ 6.8E+01	1.2E-03
hsa-miR-4485	34.5 $\pm$ 1.5E+01	8.4E-04
hsa-miR-132-3p	16.4 $\pm$ 2.9E+00	1.4E-03
hsa-miR-4734	3.3 $\pm$ 1.8E+00	2.8E-02
hsa-miR-1273g-3p	3.2 $\pm$ 1.3E+00	4.4E-02
hsa-miR-5096	2.5 $\pm$ 8.7E-01	1.7E-02
hsa-miR-4484	2.5 $\pm$ 5.5E-01	5.2E-03
hsa-miR-1973	2.2 $\pm$ 7.1E-01	5.0E-02
hsa-miR-4690-5p	2.2 $\pm$ 6.3E-01	1.5E-02

**Table 2.3: Differential expression of miRs induced by 24-h TPEN treatment.**

MDA-MB-231 cells were treated with DMSO (control) or TPEN (10  $\mu$ M in DMSO) for 24 h (n=3). The values are mean  $\pm$  SD. Cutoff criteria was set at magnitude fold change  $> 2$ ; signal intensity  $> 500$  for at least one individual sample, and  $p < 0.05$ .

MiR	Fold Change		<i>p</i> -value
hsa-miR-30c-1-3p	15.5	$\pm$ 2.2E+00	5.7E-05
hsa-miR-132-3p	14.0	$\pm$ 5.1E+00	6.4E-03
hsa-miR-4484	11.3	$\pm$ 1.7E+00	1.4E-03
hsa-miR-4485	10.8	$\pm$ 8.6E+00	4.2E-02
hsa-miR-1246	5.5	$\pm$ 2.1E+00	2.4E-02
hsa-miR-4530	5.4	$\pm$ 2.6E+00	8.1E-03
hsa-miR-6126	5.1	$\pm$ 1.4E+00	2.1E-03
hsa-miR-4787-5p	4.5	$\pm$ 6.6E-01	4.2E-04
hsa-miR-1273g-3p	3.7	$\pm$ 1.3E+00	1.0E-02
hsa-miR-3196	3.4	$\pm$ 9.8E-01	5.7E-03
hsa-miR-4516	3.3	$\pm$ 9.9E-01	6.5E-03
hsa-miR-3960	3.1	$\pm$ 1.0E+00	2.3E-02
hsa-miR-638	3.1	$\pm$ 3.0E-01	2.5E-04
hsa-miR-4454	3.0	$\pm$ 1.3E+00	4.3E-02
hsa-miR-6125	2.9	$\pm$ 7.3E-01	5.2E-03
hsa-miR-3665	2.8	$\pm$ 6.1E-01	3.8E-03
hsa-miR-1234-5p	2.8	$\pm$ 7.7E-01	2.5E-02
hsa-miR-1973	2.7	$\pm$ 8.1E-01	2.7E-02
hsa-miR-6087	2.7	$\pm$ 5.3E-01	1.3E-02
hsa-miR-4508	2.6	$\pm$ 1.2E+00	3.5E-02
hsa-miR-1260b	2.2	$\pm$ 8.5E-01	3.9E-02
hsa-miR-4497	2.1	$\pm$ 5.4E-01	1.4E-02
hsa-miR-181b-5p	-2.2	$\pm$ 1.1E-01	3.4E-02
hsa-miR-4521	-10.6	$\pm$ 3.6E-02	1.9E-03

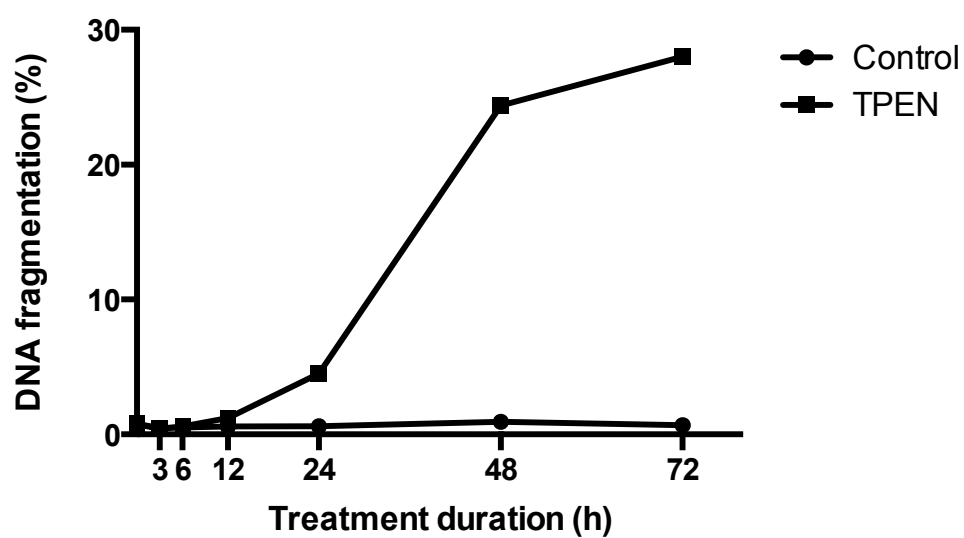


**Figure 2.1: Zinc depletion-induced apoptosis in MDA-MB-231 cells.**

MDA-MB-231 cells were treated with DMSO only (control) or TPEN (10  $\mu$ M in DMSO) for 0, 3, 6, 12, 24, 48 or 72 h. Apoptosis was assessed by PI-staining flow cytometry.

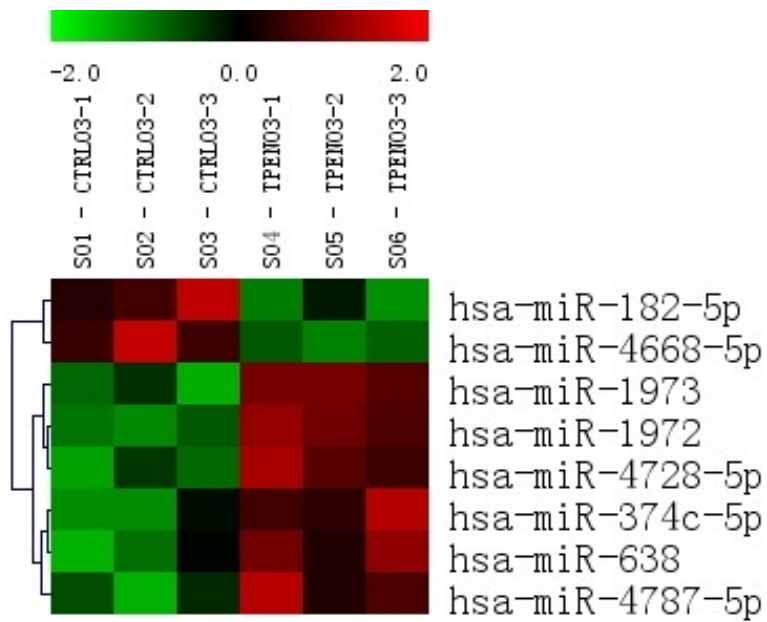


**Figure 2.2: 3-h TPEN treatment altered expression of several miRNAs.**

MDA-MB-231 cells were treated with DMSO (control) or TPEN (10  $\mu$ M in DMSO) for 3 h. Red indicates upregulation, black indicates no change and green indicates downregulation ( $p < 0.05$ ).

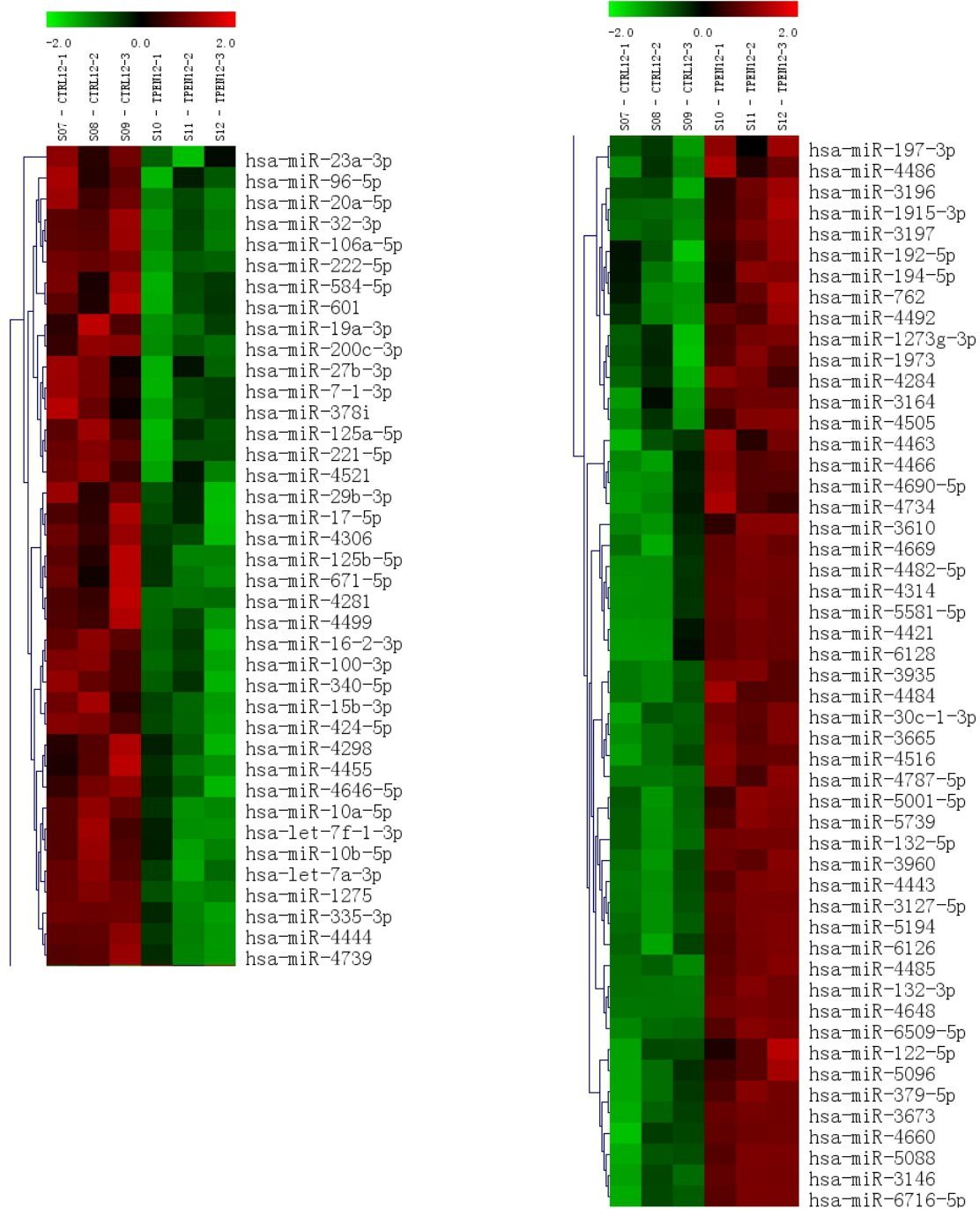


**Figure 2.3: 12-h TPEN treatment altered expression of many miRs.**

MDA-MB-231 cells were treated with DMSO (control) or TPEN (10  $\mu$ M in DMSO) for 12 h. Red indicates upregulation, black indicates no change and green indicates downregulation ( $p < 0.05$ ).

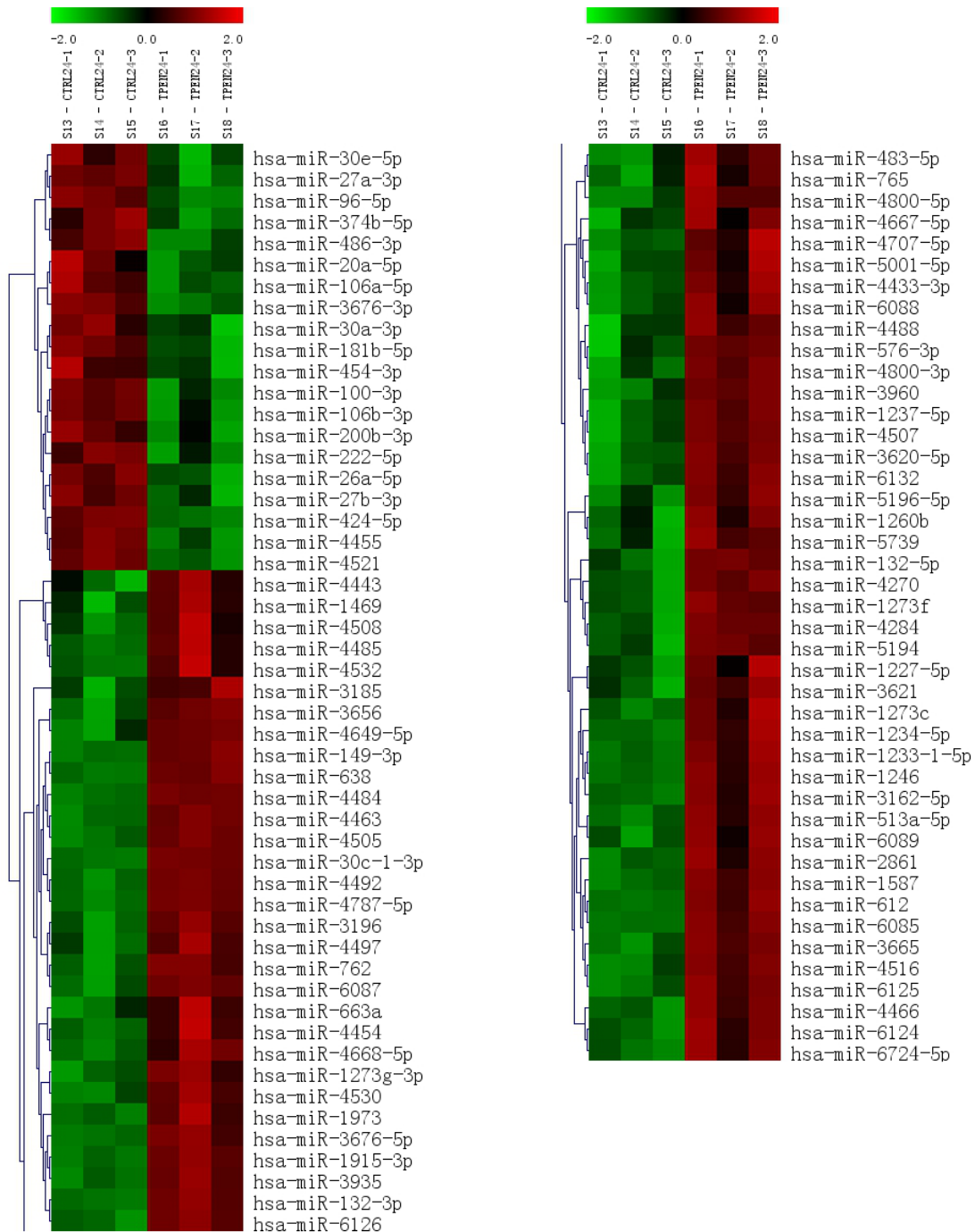


**Figure 2.4: 24-h TPEN treatment altered expression of many miRNs.**

MDA-MB-231 cells were treated with DMSO (control) or TPEN (10 μM in DMSO) for 24 h. Red indicates upregulation, black indicates no change and green indicates downregulation ( $p < 0.05$ ).

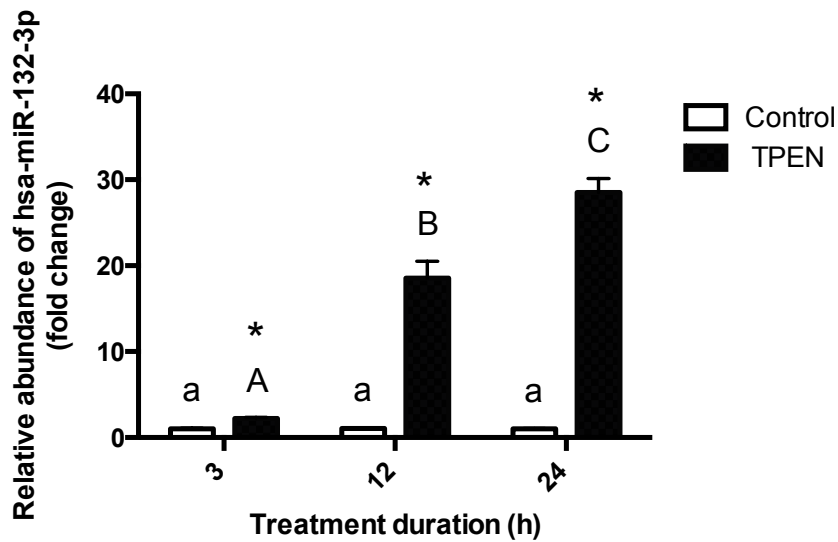


**Figure 2.5: Zinc depletion promoted a time-dependent increase in hsa-miR-132-3p expression.**

MDA-MB-231 cells were treated with DMSO (control) or TPEN (10  $\mu$ M in DMSO) for 3, 12 or 24 h. Values are mean  $\pm$  SD (n = 6). Expression is reported as relative to the control at 3 h. Lower case letters indicate the significance among the control groups while upper case letters indicate the significance among the TPEN treated groups. Different letters indicate significant differences among the means within the same treatment group. Asterisks indicate significant differences between the control and TPEN-treated groups at the same time point ( $p < 0.05$ ).

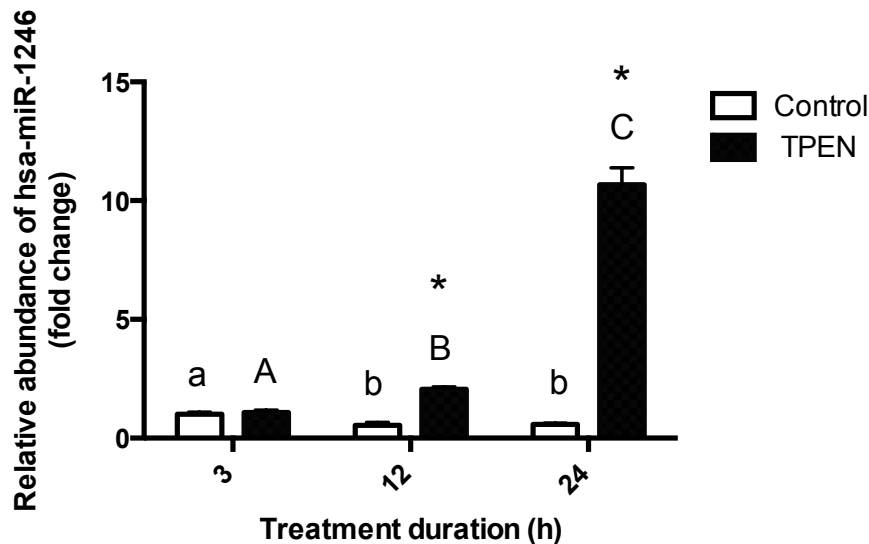


**Figure 2.6: Zinc depletion increased expression of hsa-miR-1246 after 12 and 24 h TPEN treatment.**

MDA-MB-231 cells were treated with control (DMSO) or TPEN (10  $\mu$  M in DMSO) for 3, 12 and 24 h. Values are mean  $\pm$  SD (n = 6 except TPEN at 12 h where n = 5 due to removal of an outlier). Expression is reported relative to the control sample at 3 h. Lower case letters indicate the control groups while upper case letters indicate the TPEN treated groups. Different letters indicate significant differences between means within a treatment group. Asterisks indicate significant differences between control and TPEN-treated groups at a single time point (n=6, except 12h TPEN group, where n=5 due to removal of an outlier ( $p < 0.05$ )).

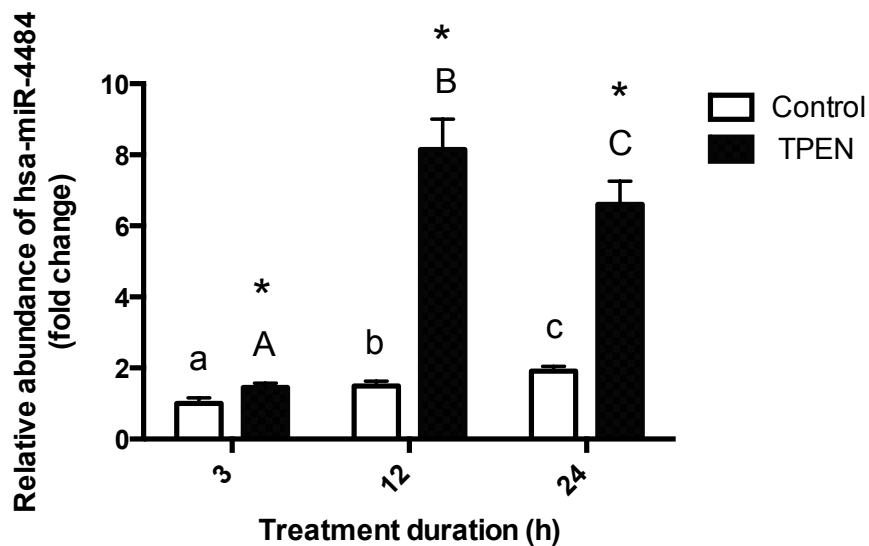


**Figure 2.7: Zinc depletion-induced time-dependent upregulation of hsa-miR-4484.**

MDA-MB-231 cells were treated with control (DMSO) or TPEN (10  $\mu$ M in DMSO) for 3, 12 and 24 h. Values are mean  $\pm$  SD (n = 6 except TPEN at 3 h and Control at 24 h, where n = 5 due to removal of outliers). Expression is reported relative to the control sample at 3 h. Lower case letters indicate the control groups while upper case letters indicate the TPEN treated groups. Different letters indicate significant differences between means within a treatment group. Asterisks indicate significant differences between control and TPEN-treated groups at a single time point ( $p < 0.05$ ).

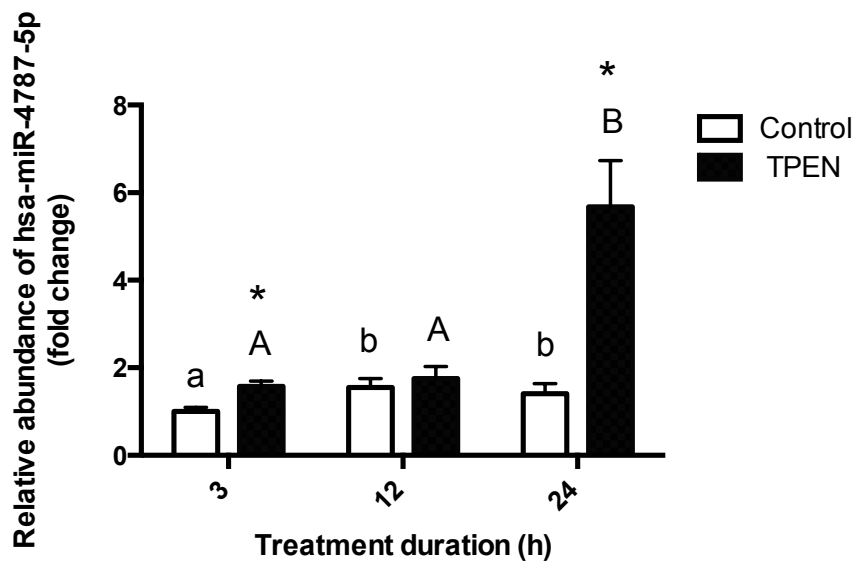


**Figure 2.8: Zinc depletion increased hsa-miR-4787-5p expression at 3 and 12 h.**

MDA-MB-231 cells were treated with control (DMSO) or TPEN ( $10 \mu\text{M}$  in DMSO) for 3, 12 and 24 h. Values are mean  $\pm$  SD ( $n = 6$  except TPEN at 3 h and 12 h, where  $n = 5$  due to removal of outliers). Expression is reported relative to the control sample at 3 h. Lower case letters indicate the control groups while upper case letters indicate the TPEN treated groups. Different letters indicate significant differences between means within a treatment group. Asterisks indicate significant differences between control and TPEN-treated groups at a single time point ( $p < 0.05$ ).

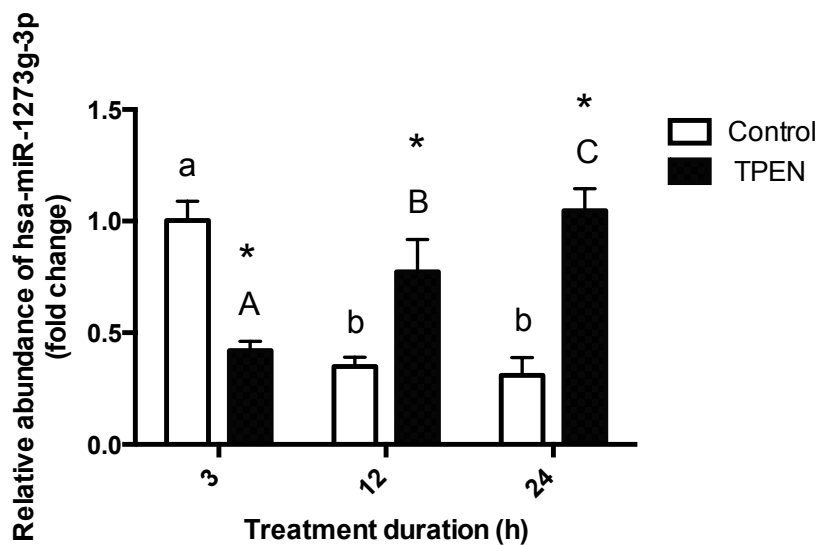


**Figure 2.9: Zinc depletion promoted expression of a-miR-1273g-3p in a time-dependent manner.**

MDA-MB-231 cells were treated with control (DMSO) or TPEN (10  $\mu$  M in DMSO) for 3, 12 and 24 h. Values are mean  $\pm$  SD (n = 6 except TPEN at 24 h, where n = 5 due to removal of an outlier). Expression is reported relative to the control sample at 3 h. Lower case letters indicate the control groups while upper case letters indicate the TPEN treated groups. Different letters indicate significant differences between means within a treatment group. Asterisks indicate significant differences between control and TPEN-treated groups at a single time point ( $p < 0.05$ ).

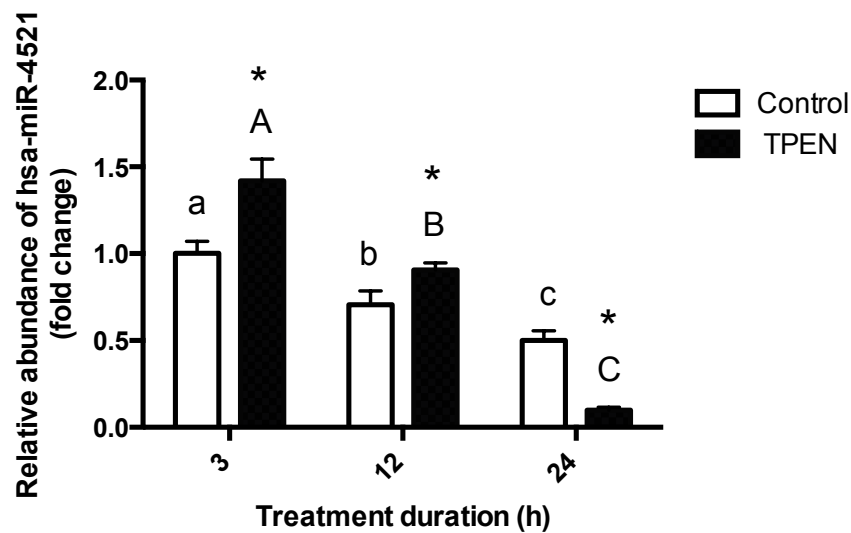


**Figure 2.10: Zinc depletion inhibited has-miR-4521 expression in a time-dependent manner.**

MDA-MB-231 cells were treated with control (DMSO) or TPEN (10  $\mu$  M in DMSO) for 3, 12 and 24 h. Values are mean  $\pm$  SD (n = 6). Expression is reported relative to the control sample at 3 h. Lower case letters indicate the control groups while upper case letters indicate the TPEN treated groups. Different letters indicate significant differences between means within a treatment group. Asterisks indicate significant differences between control and TPEN-treated groups at a single time point ( $p < 0.05$ ).

## Chapter 3: Conclusions, Limitations, and Future Directions

### 3.1. Conclusions

The effect of zinc depletion on the human global microRNA expression profile (>2000 miRs) in human breast cancer MDA-MB-231 cells was investigated in this study. Although it has been previously shown that acute zinc deficiency altered serum miR expression profile in young human males<sup>19</sup> and chronic zinc deficiency altered tissue miR expression profile in rats<sup>20</sup>, the effect of TPEN-induced zinc depletion on the miR expression profile in vitro was unknown and this was the first study to investigate the topic.

In this study, zinc depletion altered expression of many miRs in a time-dependent manner. After just 3 h of zinc depletion using TPEN (10  $\mu$ M), the miR expression profile was largely unaffected, one exception being miR-182-5p, which was significantly downregulated. In contrast, after 12 and 24 h of zinc depletion, approximately one-quarter of the expressed miRs were differentially affected with the majority being upregulated. In total, almost 75% of the expressed miRs were significantly affected by zinc depletion, treatment-duration and their interactions, providing evidence of a broad ranging effect of zinc depletion on the miR expression profile in human breast cancer MDA-MB-231 cells.

Zinc is known to exert diverse physiological functions as it is required for growth, reproduction, neurological development, immune function, etc.<sup>1</sup> but the molecular basis for zinc's wide-ranging physiological functions are not well understood. This research provided novel evidence that cellular zinc status greatly impacted the miR expression profile. The extent of gene-regulation by miRs is broad ranging and complex; with more than 60% of

protein-coding genes predicted as miR targets<sup>168</sup>, and these collective miR-target interactions drive cellular functions. Evidence obtained from this study, together with published evidence, provides a foundation for a new mode of zinc-mediated cellular regulation at the level of miR expression, which could help explain the diverse effects of zinc deficiency. However, the functional significance of zinc depletion-induced changes to miR expression needs to be validated in further research studies.

### **3.2. Limitations**

There are several limitations associated with this research. One such limitation was the use on an in vitro system with a single breast cancer cell line. The MDA-MB-231 cell line employed has a high invasive potential compared to other breast cancer cell lines (e.g. non-invasive MCF-7)<sup>261</sup>. MDA-MB-231 cells are also triple negative (ER-, PR- and HER2-) and express mutated p53. MiR expression has been reported to vary between breast cancer cell lines, with decreased expression of two-thirds of miRs investigated in triple negative human breast cancer MDA-MB-231 and BT-549 cells compared to ER+ human breast cancer MCF-7 and T47D cells<sup>209</sup>. In breast tumors, the overall global miR expression level was also found to be lower in more aggressive ER- tumors<sup>201</sup> and also decreased with higher tumor grade<sup>204</sup>. On average, breast cancer cell lines had lower global miR expression compared to breast tumors<sup>204</sup>. Reduced expression of miRs in more aggressive cancers may be due to differences in miR biogenesis and stability<sup>201,204,209</sup>. Therefore, the effects of zinc depletion might influence miR expression in a cell type specific manner. Investigation into the effects of zinc depletion-induced apoptosis on miR expression in other breast cancer cell lines and in

vivo (e.g. rodent experimental model) would provide a better understanding of the influence of zinc status on miR expression.

Another limitation is that the microarray profiling data showed a significant increase in the expression of miR-30c-1-3p and miR-638 in response to zinc depletion; however these effects of zinc were unable to be validated by qRT-PCR. MiR-30c-1-3p could not be validated by qRT-PCR due to extremely low expression (cycle threshold > 35 for 100 ng starting RNA, data not shown). MiR-638 also showed inconsistent expression in a dose curve study so it was not examined further.

Generally, the qRT-PCR results were consistent with the results obtained using microarray profiling assay, although the magnitude of change varied somewhat. For example, microarray assay and qRT-PCR assay showed a 14.0 and 28.5 fold increase, respectively, in the expression of miR-132-3p after 24 h of TPEN treatment (Table 2.3, Figure ). The results after 12 h TPEN treatment were more consistent with the microarray assay and qRT-PCR assay indicating a 16.4 and 17.7 fold increases, respectively, in expression of miR-132-3p (Table 2.2, Figure ). Additionally, qRT-PCR assay detected a 2.2 fold increase in the abundance of miR-132-3p after 3 h of TPEN treatment, while the microarray profiling assay showed that TPEN treatment had no effect on the expression of miR-132-3p (Figure , Figure ). These discrepancies may be due to biological and experimental variations, as well as differences between these two platforms. In a study comparing miR expression as measured by TaqMan qRT-PCR-array to miRNA microarray analysis by LC Sciences (the same company that performed the miR microarray profiling assay reported in this thesis), a low correlation was observed ( $r=-0.443$ ) indicating large

variability between the two platforms<sup>262</sup>. The variation between these two methods was inversely proportional to the level of miR expression, with the largest variation for miRs with low abundance. The sensitivity of TaqMan qRT-PCR is greater than microarray, and has a dynamic range of 7 logs<sup>232</sup> compared to a >3.5 log dynamic range reported by LC sciences<sup>263</sup>, which may account for some of the variation observed for poorly expressed miRs. The LC Sciences microarray was also found to have a higher false positive rate between technical replicates (13%) compared to the TaqMan qPCR-array (1%). Therefore, qRT-PCR has been used as a “gold standard” due to its high sensitivity and specificity<sup>234</sup>.

Despite these differences that we observed between the microarray and qRT-PCR platforms, the microarray still served as a valuable cost-effective and rapid screening tool for identifying differentially expressed miRs. The microarray analysis indicated many changes in zinc depletion-induced alterations in miR expression, of which the abundance of 6 miRs was confirmed by qRT-PCR. Overall, the qRT-PCR results tend to be in line with the microarray findings that numerous miRs were altered by zinc depletion-induced apoptosis; however, changes in expression of individual miRs should be validated using qRT-PCR.

### **3.3. Future Directions**

The microarray profiling results indicated that many miRs were significantly altered by zinc depletion and only a handful of these miRs were validated by qRT-PCR in this research. There are future opportunities to validate expression of other miRs significantly affected by zinc depletion using qRT-PCR.

Further research is required to establish the role of miR up/down regulation on zinc depletion-induced apoptosis in breast cancer cells. Some of the miRs identified as significantly altered by zinc depletion in our research have been implicated in apoptosis in other types of cells; however the functional significance in our model system is still unknown. For example, it would be interesting to examine the role of miR-132-3p upregulation in zinc depletion-induced apoptosis, since miR-132-3p overexpression has been associated with decreased viability of breast cancer cells including MDA-MB-231 cells<sup>219</sup>, and induction of apoptosis in PC-3 cells<sup>243</sup>. MiR-1246, which was also substantially upregulated during zinc depletion-induced apoptosis, promoted apoptosis in human lung carcinoma A549 cells<sup>246</sup>. Additionally, our work identified some miRs (miR-1273, -4484, -4521 and -4787-5p) as significantly affected by zinc depletion, but they have no reported role in apoptosis at the time of this work. Currently, work is underway in the Xu laboratory to establish stable miR transfected cell lines using a PiggyBac transposon vector system, in order to investigate the functional significance of some of these miRs in zinc depletion-induced apoptosis.

Finally, it would be interesting to examine the pathways involved in altered miR expression during zinc depletion-induced apoptosis. It has been previously reported that increased intracellular zinc at cytotoxic levels reduced expression of proteins involved in miR biogenesis and stability (Dicer and Ago2), however the mechanisms involved here are unknown<sup>14</sup>. Further research is required to assess the pathways underlying changes in miR expression during zinc depletion and whether or not this involves changes to miR processing and stability.

In summary, this work provides novel evidence that zinc depletion regulates miR expression, opening the door for research opportunities into the mechanisms of zinc depletion-induced alterations in miR expression as well as the functional significance of zinc-regulated miRs.

## References

1. Maret, W. & Sandstead, H. H. Zinc requirements and the risks and benefits of zinc supplementation. *J. Trace. Elem. Med. Biol.* **20**, 3–18 (2006).
2. Alam, S. & Kelleher, S. L. Cellular mechanisms of zinc dysregulation: a perspective on zinc homeostasis as an etiological factor in the development and progression of breast cancer. *Nutrients* **4**, 875–903 (2012).
3. Manning, D. L. *et al.* Oestrogen-regulated genes in breast cancer: association of pLIV1 with lymph node involvement. *Eur. J. Cancer* **30A**, 675–678 (1994).
4. Taylor, K. M. *et al.* ZIP7-mediated intracellular zinc transport contributes to aberrant growth factor signaling in antihormone-resistant breast cancer cells. *Endocrinology* **149**, 4912–4920 (2008).
5. Kagara, N., Tanaka, N., Noguchi, S. & Hirano, T. Zinc and its transporter ZIP10 are involved in invasive behavior of breast cancer cells. *Cancer Sci.* **98**, 692–697 (2007).
6. Lopez, V., Foolad, F. & Kelleher, S. L. ZnT2-overexpression represses the cytotoxic effects of zinc hyper-accumulation in malignant metallothionein-null T47D breast tumor cells. *Cancer Lett.* **304**, 41–51 (2011).
7. Pedersen, M. Ø., Larsen, A., Stoltenberg, M. & Penkowa, M. The role of metallothionein in oncogenesis and cancer prognosis. *Prog. Histochem. Cytochem.* **44**, 29–64 (2009).
8. Abdel-Mageed, A. & Agrawal, K. C. Antisense down-regulation of metallothionein induces growth arrest and apoptosis in human breast carcinoma cells. *Cancer Gene Ther.* **4**, 199–207 (1997).
9. Lim, D., Jocelyn, K. M.-X., Yip, G. W.-C. & Bay, B.-H. Silencing the Metallothionein-2A gene inhibits cell cycle progression from G1- to S-phase involving ATM and cdc25A signaling in breast cancer cells. *Cancer Lett.* **276**, 109–117 (2009).
10. Kim, H. G. *et al.* Metallothionein-2A overexpression increases the expression of matrix metalloproteinase-9 and invasion of breast cancer cells. *FEBS Lett.* **585**, 421–428 (2011).
11. Truong-Tran, A. Q., Ho, L. H., Chai, F. & Zalewski, P. D. Cellular zinc fluxes and the regulation of apoptosis/gene-directed cell death. *J. Nutr.* **130**, 1459S–1466S (2000).
12. Fraker, P. J. Roles for cell death in zinc deficiency. *J. Nutr.* **135**, 359–362 (2005).
13. Lin, Y.-H. Zinc depletion induced apoptosis through Ca<sup>2+</sup>-dependent mitochondrial apoptotic pathway in human breast cancer MDA-MB-231 cells. (2012). at <<https://circle.ubc.ca/handle/2429/43500>>

14. Hashemi, M., Ghavami, S., Eshraghi, M., Booy, E. P. & Los, M. Cytotoxic effects of intra and extracellular zinc chelation on human breast cancer cells. *Eur. J. Pharmacol.* **557**, 9–19 (2007).
15. Cai, Y., Yu, X., Hu, S. & Yu, J. A brief review on the mechanisms of miRNA regulation. *Genomics Proteomics Bioinformatics* **7**, 147–154 (2009).
16. Lima, R. T. *et al.* MicroRNA regulation of core apoptosis pathways in cancer. *Eur. J. Cancer* **47**, 163–174 (2011).
17. Cawley, K. MicroRNA regulation of apoptosis in breast cancer. *Cancer Rep.* **2**, 1–8 (2012).
18. Garzon, R., Marcucci, G. & Croce, C. M. Targeting microRNAs in cancer: rationale, strategies and challenges. *Nat. Rev. Drug Discov.* **9**, 775–789 (2010).
19. Ryu, M.-S., Langkamp-Henken, B., Chang, S.-M., Shankar, M. N. & Cousins, R. J. Genomic analysis, cytokine expression, and microRNA profiling reveal biomarkers of human dietary zinc depletion and homeostasis. *Proc. Nat. Acad. Sci. USA* **108**, 20970–20975 (2011).
20. Alder, H. *et al.* Dysregulation of miR-31 and miR-21 induced by zinc deficiency promotes esophageal cancer. *Carcinogenesis* **33**, 1736–1744 (2012).
21. Zheng, J., Zhang, X.-X., Yu, H., Taggart, J. E. & Ding, W.-Q. Zinc at cytotoxic concentrations affects posttranscriptional events of gene expression in cancer cells. *Cell. Physiol. Biochem.* **29**, 181–188 (2012).
22. Hlavna, M. *et al.* MicroRNAs and zinc metabolism-related gene expression in prostate cancer cell lines treated with zinc(II) ions. *Int. J. Oncol.* **41**, 2237–2244 (2012).
23. Wastney, M. E., Aamodt, R. L., Rumble, W. F. & Henkin, R. I. Kinetic analysis of zinc metabolism and its regulation in normal humans. *Am. J. Physiol.* **251**, R398–R408 (1986).
24. Vallee, B. L. & Falchuk, K. H. The biochemical basis of zinc physiology. *Physiol. Rev.* **73**, 79–118 (1993).
25. Wang, X. & Zhou, B. Dietary zinc absorption: a play of Zips and ZnTs in the gut. *IUBMB Life* **62**, 176–182 (2010).
26. Beyersmann, D. & Haase, H. Functions of zinc in signaling, proliferation and differentiation of mammalian cells. *Biometals* **14**, 331–341 (2001).
27. MacDonald, R. S. The role of zinc in growth and cell proliferation. *J. Nutr.* **130**, 1500S–8S (2000).
28. Andreini, C., Banci, L., Bertini, I. & Rosato, A. Counting the zinc-proteins encoded in the human genome. *J. Proteome Res.* **5**, 196–201 (2011).

29. Berg, J. M. & Shi, Y. The galvanization of biology: a growing appreciation for the roles of zinc. *Science* **271**, 1081–1085 (1996).
30. Yamasaki, S. *et al.* Zinc is a novel intracellular second messenger. *J. Cell Biol.* **177**, 637–645 (2007).
31. Government of Canada, H. C. Nutrient Data - Food and Nutrition - Health Canada. (2010). at <<http://www.hc-sc.gc.ca/fn-an/nutrition/fiche-nutri-data/index-eng.php>>
32. Gropper, S. S. & Smith, J. L. *Advanced Nutrition and Human Metabolism, 6th ed.* Belmont: Wadsworth Cengage Learning (2012).
33. Lo, G. S., Settle, S. L., Steinke, F. H. & Hopkins, D. T. Effect of phytate:zinc molar ratio and isolated soybean protein on zinc bioavailability. *J. Nutr.* **111**, 2223–2235 (1981).
34. Reinhold, J. G., Nasr, K., Lahimgarzadeh, A. & Hedayati, H. Effects of purified phytate and phytate-rich bread upon metabolism of zinc, calcium, phosphorus, and nitrogen in man. *Lancet* **1**, 283–288 (1973).
35. Sandstroem, B. A., Almgren, A., Kivisto, B. C. & Cederblad, A. Effect of protein level and protein source on zinc absorption in humans. *J. Nutr.* **119:1**, (1989).
36. Sandström, B. & Cederblad, A. Zinc absorption from composite meals. II. Influence of the main protein source. *Am. J. Clin. Nutr.* **33**, 1778–1783 (1980).
37. King, J. C., Shames, D. M. & Woodhouse, L. R. Zinc homeostasis in humans. *J. Nutr.* **130**, 1360S–1366S (2000).
38. Krebs, N. F. Overview of zinc absorption and excretion in the human gastrointestinal tract. *J. Nutr.* **130**, 1374S–1377S (2000).
39. Lee, H. H., Prasad, A. S., Brewer, G. J. & Owyang, C. Zinc absorption in human small intestine. *Am. J. Physiol.* **256**, G87–G91 (1989).
40. Hunt, J. R., Beiseigel, J. M. & Johnson, L. K. Adaptation in human zinc absorption as influenced by dietary zinc and bioavailability. *Am. J. Clin. Nutr.* **87**, 1336–1345 (2008).
41. Lichten, L. A. & Cousins, R. J. Mammalian zinc transporters: nutritional and physiologic regulation. *Annu. Rev. Nutr.* **29**, 153–176 (2009).
42. Wang, K., Zhou, B., Kuo, Y.-M., Zemansky, J. & Gitschier, J. A novel member of a zinc transporter family is defective in acrodermatitis enteropathica. *Am. J. Hum. Genet.* **71**, 66–73 (2002).
43. Küry, S. *et al.* Identification of SLC39A4, a gene involved in acrodermatitis enteropathica. *Nat. Genet.* **31**, 239–240 (2002).

44. Dufner-Beattie, J. *et al.* The acrodermatitis enteropathica gene ZIP4 encodes a tissue-specific, zinc-regulated zinc transporter in mice. *J. Biol. Chem.* **278**, 33474–33481 (2003).
45. Liuzzi, J. P., Bobo, J. A., Lichten, L. A., Samuelson, D. A. & Cousins, R. J. Responsive transporter genes within the murine intestinal-pancreatic axis form a basis of zinc homeostasis. *Proc. Natl. Acad. Sci. USA* **101**, 14355–14360 (2004).
46. Valentine, R. A. *et al.* ZnT5 variant B is a bidirectional zinc transporter and mediates zinc uptake in human intestinal Caco-2 cells. *J. Biol. Chem.* **282**, 14389–14393 (2007).
46. Rink, L. *Zinc in Human Health*. Amsterdam: IOS Press (2011).
48. Lee, D. Y., Prasad, A. S., Hydrick-Adair, C., Brewer, G. & Johnson, P. E. Homeostasis of zinc in marginal human zinc deficiency: role of absorption and endogenous excretion of zinc. *J. Lab. Clin. Med.* **122**, 549–556 (1993).
49. Sian, L. *et al.* Zinc absorption and intestinal losses of endogenous zinc in young Chinese women with marginal zinc intakes. *Am. J. Clin. Nutr.* **63**, 348–353 (1996).
50. McMahan, R. J. & Cousins, R. J. Regulation of the zinc transporter ZnT-1 by dietary zinc. *PNAS* **95**, 4841–4846 (1998).
51. Yu, Y. Y., Kirschke, C. P. & Huang, L. Immunohistochemical analysis of ZnT1, 4, 5, 6, and 7 in the mouse gastrointestinal tract. *J. Histochem. Cytochem.* **55**, 223–234 (2007).
52. Palmiter, R. D. & Findley, S. D. Cloning and functional characterization of a mammalian zinc transporter that confers resistance to zinc. *EMBO J.* **14**, 639–649 (1995).
53. Roohani, N., Hurrell, R., Kelishadi, R. & Schulin, R. Zinc and its importance for human health: An integrative review. *J. Res. Med. Sci.* **18**, (2013).
54. King, J. C. Zinc: an essential but elusive nutrient. *Am. J. Clin. Nutr.* **94**, 679S–84S (2011).
55. Johnson, P. E., Hunt, C. D., Milne, D. B. & Mullen, L. K. Homeostatic control of zinc metabolism in men: zinc excretion and balance in men fed diets low in zinc. *Am. J. Clin. Nutr.* **57**, 557–565 (1993).
56. Krężel, A. & Maret, W. Zinc-buffering capacity of a eukaryotic cell at physiological pZn. *J. Biol. Inorg. Chem.* **11**, 1049–1062 (2006).
57. Maret, W. Zinc biochemistry: from a single zinc enzyme to a key element of life. *Adv. Nutr.* **4**, 82–91 (2013).
58. Maret, W. Metals on the move: zinc ions in cellular regulation and in the coordination dynamics of zinc proteins. *Biometals* **24**, 411–418 (2011).

59. Liuzzi, J. P. & Cousins, R. J. Mammalian zinc transporters. *Annu. Rev. Nutr.* **24**, 151–172 (2004).
60. Krizkova, S. *et al.* Metallothioneins and zinc in cancer diagnosis and therapy. *Drug Metab. Rev.* **44**, 287–301 (2012).
61. Krężel, A. & Maret, W. Dual nanomolar and picomolar Zn(II) binding properties of metallothionein. *J. Am. Chem. Soc.* **129**, 10911–10921 (2007).
62. Tapiero, H. & Tew, K. D. Trace elements in human physiology and pathology: zinc and metallothioneins. *Biomed. Pharmacother.* **57**, 399–411 (2003).
63. Laity, J. H. & Andrews, G. K. Understanding the mechanisms of zinc-sensing by metal-response element binding transcription factor-1 (MTF-1). *Arch. Biochem. Biophys.* **463**, 201–210 (2007).
64. Günther, V., Lindert, U. & Schaffner, W. The taste of heavy metals: gene regulation by MTF-1. *Biochim. Biophys. Acta.* **1823**, 1416–1425 (2012).
65. Smirnova, I. V., Bittel, D. C., Ravindra, R., Jiang, H. & Andrews, G. K. Zinc and cadmium can promote rapid nuclear translocation of metal response element-binding transcription factor-1. *J. Biol. Chem.* **275**, 9377–9384 (2000).
66. Radtke, F. *et al.* Cloned transcription factor MTF-1 activates the mouse metallothionein I promoter. *EMBO J.* **12**, 1355–1362 (1993).
67. Heuchel, R. *et al.* The transcription factor MTF-1 is essential for basal and heavy metal-induced metallothionein gene expression. *EMBO J.* **13**, 2870–2875 (1994).
68. Koizumi, S., Suzuki, K., Ogra, Y., Yamada, H. & Otsuka, F. Transcriptional activity and regulatory protein binding of metal-responsive elements of the human metallothionein-IIA gene. *Eur. J. Biochem.* **259**, 635–642 (1999).
69. Langmade, S. J., Ravindra, R., Daniels, P. J. & Andrews, G. K. The transcription factor MTF-1 mediates metal regulation of the mouse ZnT1 gene. *J. Biol. Chem.* **275**, 34803–34809 (2000).
70. Devirgiliis, C., Zalewski, P. D., Perozzi, G. & Murgia, C. Zinc fluxes and zinc transporter genes in chronic diseases. *Mutat. Res.* **622**, 84–93 (2007).
71. Hogstrand, C., Kille, P., Nicholson, R. I. & Taylor, K. M. Zinc transporters and cancer: a potential role for ZIP7 as a hub for tyrosine kinase activation. *Trends Mol. Med.* **15**, 101–111 (2009).
72. Franklin, R. B. & Costello, L. C. The important role of the apoptotic effects of zinc in the development of cancers. *J. Cell Biochem.* **106**, 750–757 (2009).

73. Woo, W. & Xu, Z. Body zinc distribution profile during N-methyl-N-nitrosourea-induced mammary tumorigenesis in rats at various levels of dietary zinc intake. *Biol. Trace Elem. Res.* **87**, 157–169 (2002).
74. Clegg, M. S., Hanna, L. A., Niles, B. J., Momma, T. Y. & Keen, C. L. Zinc deficiency-induced cell death. *IUBMB Life* **57**, 661–669 (2005).
75. McQuitty, J. T. *et al.* Inhibition of tumor growth by dietary zinc deficiency. *Cancer Res.* **30**, 1387–1390 (1970).
76. DeWys, W. & Pories, W. Inhibition of a spectrum of animal tumors by dietary zinc deficiency. *J. Natl. Cancer Inst.* **48**, 375–381 (1972).
77. Minkel, D. T., Dolhun, P. J., Calhoun, B. L., Saryan, L. A. & Petering, D. H. Zinc deficiency and growth of ehrlich ascites tumor. *Cancer Res.* **39**, 2451–2456 (1979).
78. Mills, B. J., Broghamer, W. L., Higgins, P. J. & Lindeman, R. D. A specific dietary zinc requirement for the growth of Walker 256/M1 tumor in the rat. *Am. J. Clin. Nutr.* **34**, 1661–1669 (1981).
79. Takeda, A., Goto, K. & Okada, S. Zinc depletion suppresses tumor growth in mice. *Biol. Trace Elem. Res.* **59**, 23–29 (1997).
80. Mills, B. J., Broghamer, W. L., Higgins, P. J. & Lindeman, R. D. Inhibition of tumor growth by zinc depletion of rats. *J. Nutr.* **114**, 746–752 (1984).
81. Lee, S., Simpson, M., Nimmo, M. & Xu, Z. Low zinc intake suppressed N-methyl-N-nitrosourea-induced mammary tumorigenesis in Sprague-Dawley rats. *Carcinogenesis* **25**, 1879–1885 (2004).
82. Sun, D. *et al.* Regulation of zinc transporters by dietary zinc supplement in breast cancer. *Mol. Biol. Rep.* **34**, 241–247 (2007).
83. Drake, E. N. & Sky-Peck, H. H. Discriminant analysis of trace element distribution in normal and malignant human tissues. *Cancer Res.* **49**, 4210–4215 (1989).
84. Ng, K. H., Bradley, D. A. & Looi, L. M. Elevated trace element concentrations in malignant breast tissues. *Br. J. Radiol.* **70**, 375–382 (1997).
85. Kuo, H. W., Chen, S. F., Wu, C. C., Chen, D. R. & Lee, J. H. Serum and tissue trace elements in patients with breast cancer in Taiwan. *Biol. Trace Elem. Res.* **89**, 1–11 (2002).
86. Geraki, K., Farquharson, M. J. & Bradley, D. A. Concentrations of Fe, Cu and Zn in breast tissue: a synchrotron XRF study. *Phys. Med. Biol.* **47**, 2327–2339 (2002).
87. Geraki, K., Farquharson, M. J. & Bradley, D. A. X-ray fluorescence and energy dispersive x-ray diffraction for the quantification of elemental concentrations in breast tissue. *Phys. Med. Biol.* **49**, 99–110 (2004).

88. Raju, G. J. N. *et al.* Trace elemental correlation study in malignant and normal breast tissue by PIXE technique. *Nucl. Instrum. Meth. B* **247**, 361–367 (2006).
89. Siddiqui, M. K. J. *et al.* Comparison of some trace elements concentration in blood, tumor free breast and tumor tissues of women with benign and malignant breast lesions: an Indian study. *Environ. Int.* **32**, 630–637 (2006).
90. Ebrahim, A. M. *et al.* Study of selected trace elements in cancerous and non-cancerous human breast tissues from Sudanese subjects using instrumental neutron activation analysis. *Sci. Total Environ.* **383**, 52–58 (2007).
91. Millos, J., Costas-Rodríguez, M., Lavilla, I. & Bendicho, C. Multielemental determination in breast cancerous and non-cancerous biopsies by inductively coupled plasma-mass spectrometry following small volume microwave-assisted digestion. *Anal. Chim. Acta.* **622**, 77–84 (2008).
92. Silva, M. P., Tomal, A., Pérez, C. A., Ribeiro-Silva, A. & Poletti, M. E. Determination of Ca, Fe, Cu and Zn and their correlations in breast cancer and normal adjacent tissues. *X Ray Spectrom.* **38**, 103–111 (2009).
93. Piacenti da Silva, M., Zucchi, O. L. A. D., Ribeiro-Silva, A. & Poletti, M. E. Discriminant analysis of trace elements in normal, benign and malignant breast tissues measured by total reflection X-ray fluorescence. *Spectrochim. Acta. B* **64**, 587–592 (2009).
94. Al-Ebraheem, A., Farquharson, M. J. & Ryan, E. The evaluation of biologically important trace metals in liver, kidney and breast tissue. *Appl. Radiat. Isot.* **67**, 470–474 (2009).
95. Silva, M. P., Soave, D. F., Ribeiro-Silva, A. & Poletti, M. E. Trace elements as tumor biomarkers and prognostic factors in breast cancer: a study through energy dispersive x-ray fluorescence. *BMC Res. Notes* **5**, 194 (2012).
96. Farquharson, M. J., Al-Ebraheem, A., Geraki, K., Leek, R. & Harris, A. L. Zinc presence in invasive ductal carcinoma of the breast and its correlation with oestrogen receptor status. *Phys. Med. Biol.* **54**, 4213–4223 (2009).
97. Cui, Y., Vogt, S., Olson, N., Glass, A. G. & Rohan, T. E. Levels of zinc, selenium, calcium, and iron in benign breast tissue and risk of subsequent breast cancer. *Cancer Epidemiol. Biomarkers Prev.* **16**, 1682–1685 (2007).
98. Lee, R. *et al.* Zinc accumulation in N-methyl-N-nitrosourea-induced rat mammary tumors is accompanied by an altered expression of ZnT-1 and metallothionein. *Exp. Biol. Med.* **228**, 689–696 (2003).
99. Manning, D. L. *et al.* Differential expression of oestrogen regulated genes in breast cancer. *Acta. Oncol.* **34**, 641–646 (1995).

100. Taylor, K. M. *et al.* The emerging role of the LIV-1 subfamily of zinc transporters in breast cancer. *Mol. Med.* **13**, 396–406 (2007).
101. Hogstrand, C., Kille, P., Ackland, M., Hiscox, S. & Taylor, K. A Mechanism for Epithelial-Mesenchymal Transition and Anoikis Resistance in Breast Cancer Triggered by Zinc Channel ZIP6 and Signal Transducer and Activator of Transcription 3 (STAT3). *Biochem. J.* (2013).
102. Manning, D. L. *et al.* The role of four oestrogen-responsive genes, pLIV1, pS2, pSYD3 and pSYD8, in predicting responsiveness to endocrine therapy in primary breast cancer. *Eur. J. Cancer* **29**, 1462–1468 (1993).
103. Kasper, G. *et al.* Expression levels of the putative zinc transporter LIV-1 are associated with a better outcome of breast cancer patients. *Int. J. Cancer* **117**, 961–973 (2005).
104. Hogstrand, C., Kille, P., Ackland, M. L., Hiscox, S. & Taylor, K. M. A mechanism for epithelial-mesenchymal transition and anoikis resistance in breast cancer triggered by zinc channel ZIP6 and signal transducer and activator of transcription 3 (STAT3). *Biochem. J.* (2013). doi:10.1042/BJ20130483
105. Lopez, V. & Kelleher, S. L. Zip6-attenuation promotes epithelial-to-mesenchymal transition in ductal breast tumor (T47D) cells. *Exp. Cell Res.* **316**, 366–375 (2010).
106. Taylor, K. M., Morgan, H. E., Johnson, A. & Nicholson, R. I. Structure-function analysis of HKE4, a member of the new LIV-1 subfamily of zinc transporters. *Biochem. J.* **377**, 131–139 (2004).
107. Palmiter, R. D., Cole, T. B. & Findley, S. D. ZnT-2, a mammalian protein that confers resistance to zinc by facilitating vesicular sequestration. *EMBO J.* **15**, 1784–1791 (1996).
108. Shi, Y. *et al.* The metal-responsive transcription factor-1 protein is elevated in human tumors. *Cancer Biol. Ther.* **9**, 469–476 (2010).
109. Truong-Tran, A. Q., Carter, J., Ruffin, R. E. & Zalewski, P. D. The role of zinc in caspase activation and apoptotic cell death. *Biometals* **14**, 315–330 (2001).
110. Hanahan, D. & Weinberg, R. A. The hallmarks of cancer. *Cell* **100**, 57–70 (2000).
111. Antonsson, B. Mitochondria and the Bcl-2 family proteins in apoptosis signaling pathways. *Mol. Cell. Biochem.* **256-257**, 141–155 (2004).
112. Wong, R. S. Apoptosis in cancer: from pathogenesis to treatment. *J. Exp. Clin. Cancer Res.* **30**, 87 (2011).
113. Orrenius, S., Zhivotovsky, B. & Nicotera, P. Regulation of cell death: the calcium–apoptosis link. *Nat. Rev. Mol. Cell Biol.* **4**, 552–565 (2003).

114. Liu, X., Kim, C. N., Yang, J., Jemmerson, R. & Wang, X. Induction of apoptotic program in cell-free extracts: requirement for dATP and cytochrome c. *Cell* **86**, 147–157 (1996).
115. Zou, H., Li, Y., Liu, X. & Wang, X. An APAF-1·cytochrome c multimeric complex is a functional apoptosome that activates procaspase-9. *J. Biol. Chem.* **274**, 11549–11556 (1999).
116. Vaux, D. L. Apoptogenic factors released from mitochondria. *Biochim. Biophys. Acta.* **1813**, 546–550 (2011).
117. Norberg, E., Orrenius, S. & Zhivotovsky, B. Mitochondrial regulation of cell death: processing of apoptosis-inducing factor (AIF). *Biochem. Biophys. Res. Commun.* **396**, 95–100 (2010).
118. Taylor, R. C., Cullen, S. P. & Martin, S. J. Apoptosis: controlled demolition at the cellular level. *Nat. Rev. Mol. Cell Biol.* **9**, 231–241 (2008).
119. Wyllie, A. H. ‘Where, O death, is thy sting?’ A brief review of apoptosis biology. *Mol. Neurobiol.* **42**, 4–9 (2010).
120. Elmes, M. E. Apoptosis in the small intestine of zinc deficient and fasted rats. *J Pathol.* **123**, 219–223 (1977).
121. Wang, X., Fosmire, G. J., Gay, C. V. & Leach, R. M. Short-term zinc deficiency inhibits chondrocyte proliferation and induces cell apoptosis in the epiphyseal growth plate of young chickens. *J. Nutr.* **132**, 665–673 (2002).
122. Allen-Redpath, K. *et al.* Marginal dietary zinc deficiency in vivo induces vascular smooth muscle cell apoptosis in large arteries. *Cardiovasc. Res.* **99**, 525–534 (2013).
123. Nodera, M., Yanagisawa, H. & Wada, O. Increased apoptosis in a variety of tissues of zinc-deficient rats. *Life Sci.* **69**, 1639–1649 (2001).
124. King, L. E., Osati-Ashtiani, F. & Fraker, P. J. Apoptosis plays a distinct role in the loss of precursor lymphocytes during zinc deficiency in mice. *J. Nutr.* **132**, 974–979 (2002).
125. Rogers, J. M. *et al.* Zinc deficiency causes apoptosis but not cell cycle alterations in organogenesis-stage rat embryos: Effect of varying duration of deficiency. *Teratology* **52**, 149–159 (1995).
126. Jankowski-Hennig, M. A., Clegg, M. S., Daston, G. P., Rogers, J. M. & Keen, C. L. Zinc-deficient rat embryos have increased caspase 3-like activity and apoptosis. *Biochem. Biophys. Res. Commun.* **271**, 250–256 (2000).
127. Hanna, L. A. *et al.* Zinc influences the in vitro development of peri-implantation mouse embryos. *Birth Defects Res. Part A Clin. Mol. Teratol.* **67**, 414–420 (2003).

128. Martin, S. J., Mazdai, G., Strain, J. J., Cotter, T. G. & Hannigan, B. M. Programmed cell death (apoptosis) in lymphoid and myeloid cell lines during zinc deficiency. *Clin. Exp. Immunol.* **83**, 338–343 (1991).
129. Duffy, J. Y. *et al.* A decrease in intracellular zinc level precedes the detection of early indicators of apoptosis in HL-60 cells. *Apoptosis* **6**, 161–172 (2001).
130. Verstraeten, S. V., Zago, M. P., MacKenzie, G. G., Keen, C. L. & Oteiza, P. I. Influence of zinc deficiency on cell-membrane fluidity in Jurkat, 3T3 and IMR-32 cells. *Biochem. J.* **378**, 579–587 (2004).
131. Arslan, P., Virgilio, F. D., Beltrame, M., Tsien, R. Y. & Pozzan, T. Cytosolic Ca<sup>2+</sup> homeostasis in Ehrlich and Yoshida carcinomas. A new, membrane-permeant chelator of heavy metals reveals that these ascites tumor cell lines have normal cytosolic free Ca<sup>2+</sup>. *J. Biol. Chem.* **260**, 2719–2727 (1985).
132. Chimienti, F., Seve, M., Richard, S., Mathieu, J. & Favier, A. Role of cellular zinc in programmed cell death: temporal relationship between zinc depletion, activation of caspases, and cleavage of Sp family transcription factors. *Biochem. Pharmacol.* **62**, 51–62 (2001).
133. Wu, B. W. N,N,N,N-tetrakis (2-pyridylmethyl) ethylenediamine-induced depletion of the labile intracellular pool of zinc suppressed the growth of human breast cancer cells. (2003). at <<https://circle.ubc.ca/handle/2429/14283>>
134. Rana, U. *et al.* Zinc binding ligands and cellular zinc trafficking: apo-metallothionein, glutathione, TPEN, proteomic zinc, and Zn-Sp1. *J. Inorg. Biochem.* **102**, 489–499 (2008).
135. McCabe, M. J., Jr, Jiang, S. A. & Orrenius, S. Chelation of intracellular zinc triggers apoptosis in mature thymocytes. *Lab. Invest.* **69**, 101–110 (1993).
136. Treves, S., Trentini, P. L., Ascanelli, M., Bucci, G. & Di Virgilio, F. Apoptosis is dependent on intracellular zinc and independent of intracellular calcium in lymphocytes. *Exp. Cell Res.* **211**, 339–343 (1994).
137. Kolenko, V. M. *et al.* Mechanism of apoptosis induced by zinc deficiency in peripheral blood T lymphocytes. *Apoptosis* **6**, 419–429 (2001).
138. Truong-Tran, A. Q., Ruffin, R. E. & Zalewski, P. D. Visualization of labile zinc and its role in apoptosis of primary airway epithelial cells and cell lines. *Am. J. Physiol. Lung Cell Mol. Physiol.* **279**, L1172–L1183 (2000).
139. Cao, J., Bobo, J. A., Liuzzi, J. P. & Cousins, R. J. Effects of intracellular zinc depletion on metallothionein and ZIP2 transporter expression and apoptosis. *J. Leukoc. Biol.* **70**, 559–566 (2001).
140. Hyun, H. J. *et al.* Depletion of intracellular zinc and copper with TPEN results in apoptosis of cultured human retinal pigment epithelial cells. *Invest. Ophthalmol. Vis. Sci.* **42**, 460–465 (2001).

141. Rudolf, E. & Cervinka, M. Depletion of endogenous zinc stores induces oxidative stress and cell death in human melanoma cells. *Acta Medica. (Hradec Kralove)* **47**, 91–96 (2004).
142. Wilson, D., Varigos, G. & Ackland, M. L. Apoptosis may underlie the pathology of zinc-deficient skin. *Immunol. Cell Biol.* **84**, 28–37 (2006).
143. Donadelli, M. *et al.* Zinc depletion efficiently inhibits pancreatic cancer cell growth by increasing the ratio of antiproliferative/proliferative genes. *J. Cell Biochem.* **104**, 202–212 (2008).
144. Zalewski, P. D., Forbes, I. J. & Betts, W. H. Correlation of apoptosis with change in intracellular labile Zn(II) using zinquin [(2-methyl-8-p-toluenesulphonamido-6-quinolyloxy)acetic acid], a new specific fluorescent probe for Zn(II). *Biochem. J.* **296**, 403–408 (1993).
145. Meerarani, P. *et al.* Zinc protects against apoptosis of endothelial cells induced by linoleic acid and tumor necrosis factor  $\alpha$ . *Am. J. Clin. Nutr.* **71**, 81–87 (2000).
146. Thambiayya, K., Wasserloos, K., Kagan, V. E., Stoyanovsky, D. & Pitt, B. R. A critical role for increased labile zinc in reducing sensitivity of cultured sheep pulmonary artery endothelial cells to LPS-induced apoptosis. *Am. J. Physiol. Lung Cell Mol. Physiol.* **302**, L1287–L1295 (2012).
147. Telford, W. G. & Fraker, P. J. Preferential induction of apoptosis in mouse CD4+CD8+ alpha beta TCRloCD3 epsilon lo thymocytes by zinc. *J. Cell. Physiol.* **164**, 259–270 (1995).
148. Adamo, A. M. *et al.* The role of zinc in the modulation of neuronal proliferation and apoptosis. *Neurotox. Res.* **17**, 1–14 (2010).
149. Guo, B. *et al.* Cell apoptosis induced by zinc deficiency in osteoblastic MC3T3-E1 cells via a mitochondrial-mediated pathway. *Mol. Cell Biochem.* **361**, 209–216 (2012).
150. Chai, F., Truong- Tran, A. Q., Evdokiou, A., Young, G. P. & Zalewski, P. D. Intracellular zinc depletion induces caspase activation and p21<sup>Waf1/Cip1</sup> cleavage in human epithelial cell lines. *J. Infect. Dis.* **182**, S85–S92 (2000).
150. Purtzki, M. & Xu, Z. Zinc depletion-induced apoptosis in human breast cancer MDA-MB-231 cells is calcium-dependent. *Experimental Biology*. Washington, DC. (2010).
152. Deveraux, Q. L. *et al.* Cleavage of human inhibitor of apoptosis protein XIAP results in fragments with distinct specificities for caspases. *EMBO J.* **18**, 5242–5251 (1999).
153. Zuo, J. *et al.* Novel Polypyridyl chelators deplete cellular zinc and destabilize the X-linked inhibitor of apoptosis protein (XIAP) prior to induction of apoptosis in human prostate and breast cancer cells. *J. Cell Biochem.* **113**, 2567–2575 (2012).
154. Mendivil-Perez, M., Velez-Pardo, C. & Jimenez-Del-Rio, M. TPEN induces apoptosis independently of zinc chelator activity in a model of acute lymphoblastic leukemia and ex

vivo acute leukemia cells through oxidative stress and mitochondria caspase-3- and AIF-dependent pathways. *Oxid. Med. Cell Longev.* (2012). doi:10.1155/2012/313275

155. Eide, D. J. The oxidative stress of zinc deficiency. *Metallomics* **3**, 1124–1129 (2011).

156. Cui, L. *et al.* Nitric oxide synthase inhibitor attenuates intestinal damage induced by zinc deficiency in rats. *J. Nutr.* **129**, 792–798 (1999).

157. Cui, L., Takagi, Y., Sando, K., Wasa, M. & Okada, A. Nitric oxide synthase inhibitor attenuates inflammatory lesions in the skin of zinc-deficient rats. *Nutrition* **16**, 34–41 (2000).

158. Nakatani, T., Tawaramoto, M., Opare Kennedy, D., Kojima, A. & Matsui-Yuasa, I. Apoptosis induced by chelation of intracellular zinc is associated with depletion of cellular reduced glutathione level in rat hepatocytes. *Chem. Biol. Interact.* **125**, 151–163 (2000).

158. Purtzki, M. & Xu, Zhaoming. Reactive nitrogen species-mediated DNA damage is involved in zinc-depletion-induced apoptosis in human breast cancer MDA-MB-231 cells. *Canadian Nutrition Society Annual Meeting*. Guelph, ON. (2011).

160. Lee, R. C., Feinbaum, R. L. & Ambros, V. The *C. elegans* heterochronic gene *lin-4* encodes small RNAs with antisense complementarity to *lin-14*. *Cell* **75**, 843–854 (1993).

161. Wightman, B., Ha, I. & Ruvkun, G. Posttranscriptional regulation of the heterochronic gene *lin-14* by *lin-4* mediates temporal pattern formation in *C. elegans*. *Cell* **75**, 855–862 (1993).

162. Chen, C.-Z., Li, L., Lodish, H. F. & Bartel, D. P. MicroRNAs modulate hematopoietic lineage differentiation. *Science* **303**, 83–86 (2004).

162. miRBase v20. (2013). at <<http://www.mirbase.org/cgi-bin/query.pl?terms=hsa>>

164. Ameres, S. L. & Zamore, P. D. Diversifying microRNA sequence and function. *Nat. Rev. Mol. Cell Biol.* **14**, 475–488 (2013).

165. Chang, T.-C. & Mendell, J. T. MicroRNAs in vertebrate physiology and human disease. *Annu. Rev. Genomics Hum. Genet.* **8**, 215–239 (2007).

166. Taganov, K. D., Boldin, M. P. & Baltimore, D. MicroRNAs and Immunity: Tiny Players in a Big Field. *Immunity* **26**, 133–137 (2007).

167. Krek, A. *et al.* Combinatorial microRNA target predictions. *Nat. Genet.* **37**, 495–500 (2005).

168. Friedman, R. C., Farh, K. K.-H., Burge, C. B. & Bartel, D. P. Most mammalian mRNAs are conserved targets of microRNAs. *Genome Res.* **19**, 92–105 (2009).

169. Kim, V. N. MicroRNA biogenesis: coordinated cropping and dicing. *Nat. Rev. Mol. Cell Biol.* **6**, 376–385 (2005).

170. Huntzinger, E. & Izaurralde, E. Gene silencing by microRNAs: contributions of translational repression and mRNA decay. *Nat. Rev. Genet.* **12**, 99–110 (2011).
171. Kim, V. N. & Nam, J.-W. Genomics of microRNA. *Trends Genet.* **22**, 165–173 (2006).
172. Lee, Y. *et al.* MicroRNA genes are transcribed by RNA polymerase II. *EMBO J.* **23**, 4051–4060 (2004).
173. Saini, H. K., Griffiths-Jones, S. & Enright, A. J. Genomic analysis of human microRNA transcripts. *Proc. Natl. Acad. Sci. U.S.A.* **104**, 17719–17724 (2007).
174. Denli, A. M., Tops, B. B. J., Plasterk, R. H. A., Ketting, R. F. & Hannon, G. J. Processing of primary microRNAs by the Microprocessor complex. *Nature* **432**, 231–235 (2004).
175. Gregory, R. I. *et al.* The Microprocessor complex mediates the genesis of microRNAs. *Nature* **432**, 235–240 (2004).
176. Han, J. *et al.* The Drosha-DGCR8 complex in primary microRNA processing. *Genes Dev.* **18**, 3016–3027 (2004).
177. Landthaler, M., Yalcin, A. & Tuschl, T. The human DiGeorge syndrome critical region gene 8 and Its D. melanogaster homolog are required for miRNA biogenesis. *Curr. Biol.* **14**, 2162–2167 (2004).
178. Lee, Y. *et al.* The nuclear RNase III Drosha initiates microRNA processing. *Nature* **425**, 415–419 (2003).
179. Lee, Y., Jeon, K., Lee, J.-T., Kim, S. & Kim, V. N. MicroRNA maturation: stepwise processing and subcellular localization. *EMBO J.* **21**, 4663–4670 (2002).
180. Yi, R., Qin, Y., Macara, I. G. & Cullen, B. R. Exportin-5 mediates the nuclear export of pre-microRNAs and short hairpin RNAs. *Genes Dev.* **17**, 3011–3016 (2003).
181. Bohnsack, M. T., Czaplinski, K. & Gorlich, D. Exportin 5 is a RanGTP-dependent dsRNA-binding protein that mediates nuclear export of pre-miRNAs. *RNA* **10**, 185–191 (2004).
182. Lund, E., Güttinger, S., Calado, A., Dahlberg, J. E. & Kutay, U. Nuclear export of microRNA precursors. *Science* **303**, 95–98 (2004).
183. Bernstein, E., Caudy, A. A., Hammond, S. M. & Hannon, G. J. Role for a bidentate ribonuclease in the initiation step of RNA interference. *Nature* **409**, 363–366 (2001).
184. Finnegan, E. F. & Pasquinelli, A. E. MicroRNA biogenesis: regulating the regulators. *Crit. Rev. Biochem. Mol. Biol.* **48**, 51–68 (2013).

185. Winter, J., Jung, S., Keller, S., Gregory, R. I. & Diederichs, S. Many roads to maturity: microRNA biogenesis pathways and their regulation. *Nat. Cell Biol.* **11**, 228–234 (2009).
186. Czech, B. & Hannon, G. J. Small RNA sorting: matchmaking for Argonautes. *Nat. Rev. Genet.* **12**, 19–31 (2011).
187. Iwasaki, S. *et al.* Hsc70/Hsp90 chaperone machinery mediates ATP-dependent RISC loading of small RNA duplexes. *Mol. Cell* **39**, 292–299 (2010).
188. Schwarz, D. S. *et al.* Asymmetry in the assembly of the RNAi enzyme complex. *Cell* **115**, 199–208 (2003).
189. Khvorova, A., Reynolds, A. & Jayasena, S. D. Functional siRNAs and miRNAs exhibit strand bias. *Cell* **115**, 209–216 (2003).
190. Fabian, M. R., Sonenberg, N. & Filipowicz, W. Regulation of mRNA translation and stability by microRNAs. *Annu. Rev. Biochem.* **79**, 351–379 (2010).
191. Vasudevan, S., Tong, Y. & Steitz, J. A. Switching from repression to activation: microRNAs can up-regulate translation. *Science* **318**, 1931–1934 (2007).
192. Ørom, U. A., Nielsen, F. C. & Lund, A. H. MicroRNA-10a binds the 5'UTR of ribosomal protein mRNAs and enhances their translation. *Mol. Cell* **30**, 460–471 (2008).
193. Zhang, Z., Qin, Y.-W., Brewer, G. & Jing, Q. MicroRNA degradation and turnover: regulating the regulators. *Wiley Interdiscip. Rev. RNA* **3**, 593–600 (2012).
194. Rügger, S. & Großhans, H. MicroRNA turnover: when, how, and why. *Trends Biochem. Sci.* **37**, 436–446 (2012).
195. Bail, S. *et al.* Differential regulation of microRNA stability. *RNA* **16**, 1032–1039 (2010).
196. Gantier, M. P. *et al.* Analysis of microRNA turnover in mammalian cells following Dicer1 ablation. *Nucl. Acids Res.* **39**, 5692–5703 (2011).
197. Garofalo, M. & Croce, C. M. MicroRNAs: master regulators as potential therapeutics in cancer. *Annu. Rev. Pharmacol. Toxicol.* **51**, 25–43 (2011).
198. Iorio, M. V. *et al.* MicroRNA gene expression deregulation in human breast cancer. *Cancer Res.* **65**, 7065–7070 (2005).
199. Volinia, S. *et al.* A microRNA expression signature of human solid tumors defines cancer gene targets. *Proc. Natl. Acad. Sci. USA* **103**, 2257–2261 (2006).
200. Calin, G. A. & Croce, C. M. MicroRNA signatures in human cancers. *Nat. Rev. Cancer* **6**, 857–866 (2006).

201. Blenkinson, C. *et al.* MicroRNA expression profiling of human breast cancer identifies new markers of tumor subtype. *Genome Biol.* **8**, R214 (2007).
203. Figure 2 from © Davis-Dusenbery, B. N. & Hata, A. MicroRNA in cancer: the involvement of aberrant microRNA biogenesis regulatory pathways. *Genes Cancer* **1**, 1100–1114. Page 1101. (2010). By permission from SAGE Publications.
203. Lu, J. *et al.* MicroRNA expression profiles classify human cancers. *Nature* **435**, 834–838 (2005).
204. Dvinge, H. *et al.* The shaping and functional consequences of the microRNA landscape in breast cancer. *Nature* **497**, 378–382 (2013).
205. Thomson, J. M. *et al.* Extensive post-transcriptional regulation of microRNAs and its implications for cancer. *Genes Dev.* **20**, 2202–2207 (2006).
206. Lee, E. J. *et al.* Systematic evaluation of microRNA processing patterns in tissues, cell lines, and tumors. *RNA* **14**, 35–42 (2008).
207. Dedes, K. J. *et al.* Down-regulation of the miRNA master regulators Drosha and Dicer is associated with specific subgroups of breast cancer. *Eur. J. Cancer* **47**, 138–150 (2011).
208. Grelier, G. *et al.* Prognostic value of Dicer expression in human breast cancers and association with the mesenchymal phenotype. *Br. J. Cancer* **101**, 673–683 (2009).
209. Cochrane, D. R. *et al.* MicroRNAs link estrogen receptor alpha status and Dicer levels in breast cancer. *Horm. Cancer* **1**, 306–319 (2010).
210. Kumar, M. S., Lu, J., Mercer, K. L., Golub, T. R. & Jacks, T. Impaired microRNA processing enhances cellular transformation and tumorigenesis. *Nat. Genet.* **39**, 673–677 (2007).
211. Liu, H. MicroRNAs in breast cancer initiation and progression. *Cell. Mol. Life Sci.* **69**, 3587–3599 (2012).
212. Wang, Y. & Lee, C. G. L. MicroRNA and cancer – focus on apoptosis. *J. Cell Mol. Med.* **13**, 12–23 (2008).
213. Si, M.-L. *et al.* MiR-21-mediated tumor growth. *Oncogene* **26**, 2799–2803 (2007).
214. Frankel, L. B. *et al.* Programmed cell death 4 (PDCD4) is an important functional target of the microRNA miR-21 in breast cancer cells. *J. Biol. Chem.* **283**, 1026–1033 (2008).
215. Lu, Z. *et al.* MicroRNA-21 promotes cell transformation by targeting the programmed cell death 4 gene. *Oncogene* **27**, 4373–4379 (2008).
216. Zhu, S., Si, M.-L., Wu, H. & Mo, Y.-Y. MicroRNA-21 targets the tumor suppressor gene tropomyosin 1 (TPM1). *J. Biol. Chem.* **282**, 14328–14336 (2007).

217. Huang, Q. *et al.* The microRNAs miR-373 and miR-520c promote tumour invasion and metastasis. *Nat. Cell Biol.* **10**, 202–210 (2008).
218. Yu, F. *et al.* let-7 regulates self renewal and tumorigenicity of breast cancer cells. *Cell* **131**, 1109–1123 (2007).
219. Li, S. *et al.* MicroRNA-132 is frequently down-regulated in ductal carcinoma in situ (DCIS) of breast and acts as a tumor suppressor by inhibiting cell proliferation. *Pathol. Res. Pract.* **209**, 179–183 (2013).
220. Kelly, G. L. & Strasser, A. The essential role of evasion from cell death in cancer. *Adv. Cancer Res.* **111**, 39–96 (2011).
221. Kong, W. *et al.* MicroRNA-155 regulates cell survival, growth, and chemosensitivity by targeting FOXO3a in breast cancer. *J. Biol. Chem.* **285**, 17869–17879 (2010).
222. Zhao, J.-J. *et al.* MicroRNA-221/222 negatively regulates estrogen receptor alpha and is associated with tamoxifen resistance in breast cancer. *J. Biol. Chem.* **283**, 31079–31086 (2008).
223. Miller, T. E. *et al.* MicroRNA-221/222 confers tamoxifen resistance in breast cancer by targeting p27Kip1. *J. Biol. Chem.* **283**, 29897–29903 (2008).
224. Zhou, M. *et al.* MicroRNA-125b confers the resistance of breast cancer cells to paclitaxel through suppression of pro-apoptotic Bcl-2 antagonist killer 1 (Bak1) expression. *J. Biol. Chem.* **285**, 21496–21507 (2010).
225. Shen, L. *et al.* MiR-497 induces apoptosis of breast cancer cells by targeting Bcl-w. *Exp. Ther. Med.* **3**, 475–480 (2012).
226. Singh, R. & Saini, N. Downregulation of BCL2 by miRNAs augments drug-induced apoptosis – a combined computational and experimental approach. *J. Cell Sci.* **125**, 1568–1578 (2012).
227. Mihelich, B. L. *et al.* MiR-183-96-182 cluster is overexpressed in prostate tissue and regulates zinc homeostasis in prostate cells. *J. Biol. Chem.* **286**, 44503–44511 (2011).
228. Riccardi, C. & Nicoletti, I. Analysis of apoptosis by propidium iodide staining and flow cytometry. *Nat. Protocols* **1**, 1458–1461 (2006).
229. Gao, X., Gulari, E. & Zhou, X. In situ synthesis of oligonucleotide microarrays. *Biopolymers* **73**, 579–596 (2004).
230. Zhu, Q. *et al.* microParaflo biochip for nucleic acid and protein analysis. *Methods Mol. Biol.* **382**, 287–312 (2007).

231. Bolstad, B. M., Irizarry, R. A., Astrand, M. & Speed, T. P. A comparison of normalization methods for high density oligonucleotide array data based on variance and bias. *Bioinformatics* **19**, 185–193 (2003).
232. Chen, C. *et al.* Real-time quantification of microRNAs by stem–loop RT–PCR. *Nucl. Acids Res.* **33**, e179–e179 (2005).
233. Schmittgen, T. D. *et al.* Real-time PCR quantification of precursor and mature microRNA. *Methods* **44**, 31–38 (2008).
234. Chen, C., Tan, R., Wong, L., Fekete, R. & Halsey, J. Quantitation of microRNAs by real-time RT-qPCR. *Methods Mol. Biol.* **687**, 113–134 (2011).
235. Livak, K. J. & Schmittgen, T. D. Analysis of relative gene expression data using real-time quantitative PCR and the 2(-Delta Delta C(T)) Method. *Methods* **25**, 402–408 (2001).
236. Davoren, P., McNeill, R., Lowery, A., Kerin, M. & Miller, N. Identification of suitable endogenous control genes for microRNA gene expression analysis in human breast cancer. *BMC Mol. Biol.* **9**, 76 (2008).
237. Ku, H. H. Notes on the use of propagation of error formulas. *Journal of Research of the National Bureau of Standards* **70C**, 263–273 (1966).
231. Purtzki, M & Xu, Z. Zinc depletion-induced apoptosis is associated with an altered expression of apoptotic regulatory genes in MDA-MB-231 breast cancer cells. *Canadian Nutrition Society Annual Meeting*. Edmonton, AB. (2010).
239. Zhang, Q.-H. *et al.* Meta-analysis of microRNA-183 family expression in human cancer studies comparing cancer tissues with noncancerous tissues. *Gene* **527**, 26–32 (2013).
240. Liu, H. *et al.* Expression and regulatory function of miRNA-182 in triple-negative breast cancer cells through its targeting of profilin 1. *Tumour Biol.* **34**, 1713–1722 (2013).
241. Guttilla, I. K. & White, B. A. Coordinate regulation of FOXO1 by miR-27a, miR-96, and miR-182 in breast cancer cells. *J. Biol. Chem.* **284**, 23204–23216 (2009).
242. Krishnan, K. *et al.* MicroRNA-182-5p targets a network of genes involved in DNA repair. *RNA* **19**, 230–242 (2013).
243. Formosa, A. *et al.* DNA methylation silences miR-132 in prostate cancer. *Oncogene* **32**, 127–134 (2013).
244. Strum, J. C. *et al.* MicroRNA 132 regulates nutritional stress-induced chemokine production through repression of SirT1. *Mol. Endocrinol.* **23**, 1876–1884 (2009).
245. Pigati, L. *et al.* Selective release of microRNA species from normal and malignant mammary epithelial cells. *PLoS ONE* **5**, e13515 (2010).

246. Zhang, Y., Liao, J.-M., Zeng, S. X. & Lu, H. p53 downregulates Down syndrome-associated DYRK1A through miR-1246. *EMBO Rep.* **12**, 811–817 (2011).
247. Laguna, A. *et al.* The protein kinase DYRK1A regulates caspase-9-mediated apoptosis during retina development. *Dev. Cell* **15**, 841–853 (2008).
248. Bisso, A. *et al.* Oncogenic miR-181a/b affect the DNA damage response in aggressive breast cancer. *Cell Cycle* **12**, 1679–1687 (2013).
249. Rothé, F. *et al.* Global microRNA expression profiling identifies MiR-210 associated with tumor proliferation, invasion and poor clinical outcome in breast cancer. *PLoS ONE* **6**, e20980 (2011).
250. Mansueto, G. *et al.* Identification of a new pathway for tumor progression: microRNA-181b up-regulation and CBX7 down-regulation by HMGA1 protein. *Genes Cancer* **1**, 210–224 (2010).
251. Yan, L.-X. *et al.* MicroRNA miR-21 overexpression in human breast cancer is associated with advanced clinical stage, lymph node metastasis and patient poor prognosis. *RNA* **14**, 2348–2360 (2008).
252. Kulshreshtha, R. *et al.* A microRNA signature of hypoxia. *Mol. Cell. Biol.* **27**, 1859–1867 (2007).
253. Neel, J.-C. & Lebrun, J.-J. Activin and TGF $\beta$  regulate expression of the microRNA-181 family to promote cell migration and invasion in breast cancer cells. *Cell. Signal.* **25**, 1556–1566 (2013).
254. Wang, Y. *et al.* Transforming growth factor- $\beta$  regulates the sphere-initiating stem cell-like feature in breast cancer through miRNA-181 and ATM. *Oncogene* **30**, 1470–1480 (2011).
255. Iliopoulos, D., Jaeger, S. A., Hirsch, H. A., Bulyk, M. L. & Struhl, K. STAT3 activation of miR-21 and miR-181b-1 via PTEN and CYLD are part of the epigenetic switch linking inflammation to cancer. *Mol. Cell* **39**, 493–506 (2010).
256. Lu, Y. *et al.* Anti-microRNA-222 (anti-miR-222) and -181B suppress growth of tamoxifen-resistant xenografts in mouse by targeting TIMP3 protein and modulating mitogenic signal. *J. Biol. Chem.* **286**, 42292–42302 (2011).
257. Morin, R. D. *et al.* Application of massively parallel sequencing to microRNA profiling and discovery in human embryonic stem cells. *Genome Res.* **18**, 610–621 (2008).
258. Jima, D. D. *et al.* Deep sequencing of the small RNA transcriptome of normal and malignant human B cells identifies hundreds of novel microRNAs. *Blood* **116**, e118–127 (2010).

259. Sripada, L. *et al.* Systematic analysis of small RNAs associated with human mitochondria by deep sequencing: detailed analysis of mitochondrial associated miRNA. *PLoS ONE* **7**, e44873 (2012).
260. Persson, H. *et al.* Identification of new microRNAs in paired normal and tumor breast tissue suggests a dual role for the ERBB2/Her2 gene. *Cancer Res.* **71**, 78–86 (2011).
261. Liu, Z., Brattain, M. G. & Appert, H. Differential display of reticulocalbin in the highly invasive cell line, MDA-MB-435, versus the poorly invasive cell line, MCF-7. *Biochem. Biophys. Res. Commun.* **231**, 283–289 (1997).
262. Chen, Y., Gelfond, J. A., McManus, L. M. & Shireman, P. K. Reproducibility of quantitative RT-PCR array in miRNA expression profiling and comparison with microarray analysis. *BMC Genomics* **10**, 407 (2009).
263. MicroRNA Microarray - LC Sciences. (2012). at <http://www.lcsciences.com/applications/transcriptomics/mirna-profiling/mirna/?gclid=CMWykKO3pawCFSYaQgodidVhEg>

## Appendices

**Table A.1: MiR expression in control and TPEN-treated MDA-MB-231 cells.**

MDA-MB-231 cells were treated with DMSO (control) or TPEN (10  $\mu$ M in DMSO) for 3, 12 and 24 h (n=3). The values are mean signal intensity  $\pm$  SD.

MiR	3 H CONTROL	3 H TPEN	12 H CONTROL	12 H TPEN	24 H CONTROL	24 H TPEN
hsa-let-7a-2-3p	29 $\pm$ 4	30 $\pm$ 4	27 $\pm$ 7	14 $\pm$ 7	28 $\pm$ 9	9 $\pm$ 6
hsa-let-7a-3p	16 $\pm$ 6	20 $\pm$ 2	29 $\pm$ 4	10 $\pm$ 2	33 $\pm$ 23	32 $\pm$ 8
hsa-let-7a-5p	12,488 $\pm$ 1,406	11,499 $\pm$ 550	14,485 $\pm$ 4,324	14,231 $\pm$ 1,978	10,416 $\pm$ 1,458	11,937 $\pm$ 2,151
hsa-let-7b-3p	14 $\pm$ 2	16 $\pm$ 3	24 $\pm$ 8	14 $\pm$ 3	24 $\pm$ 6	15 $\pm$ 5
hsa-let-7b-5p	2,509 $\pm$ 319	2,446 $\pm$ 964	3,802 $\pm$ 2,168	2,461 $\pm$ 2,107	1,350 $\pm$ 328	2,909 $\pm$ 1,806
hsa-let-7c	8,789 $\pm$ 757	7,963 $\pm$ 826	10,001 $\pm$ 3,477	8,075 $\pm$ 3,189	5,635 $\pm$ 1,597	6,713 $\pm$ 2,035
hsa-let-7d-3p	57 $\pm$ 8	71 $\pm$ 13	86 $\pm$ 20	81 $\pm$ 11	72 $\pm$ 23	41 $\pm$ 20
hsa-let-7d-5p	10,046 $\pm$ 919	9,678 $\pm$ 720	11,610 $\pm$ 3,473	11,658 $\pm$ 982	8,363 $\pm$ 1,606	9,189 $\pm$ 690
hsa-let-7e-5p	8,682 $\pm$ 622	7,067 $\pm$ 1,495	10,290 $\pm$ 3,616	8,586 $\pm$ 2,885	5,438 $\pm$ 1,470	6,171 $\pm$ 2,472
hsa-let-7f-1-3p	21 $\pm$ 6	22 $\pm$ 2	28 $\pm$ 6	12 $\pm$ 3	23 $\pm$ 5	14 $\pm$ 6
hsa-let-7f-5p	11,794 $\pm$ 2,631	11,942 $\pm$ 547	14,362 $\pm$ 3,580	14,663 $\pm$ 1,605	11,409 $\pm$ 1,441	12,250 $\pm$ 1,545
hsa-let-7g-5p	3,495 $\pm$ 226	3,209 $\pm$ 106	3,847 $\pm$ 1,035	3,188 $\pm$ 838	2,911 $\pm$ 342	3,135 $\pm$ 923
hsa-let-7i-5p	3,063 $\pm$ 158	2,781 $\pm$ 125	2,611 $\pm$ 452	3,218 $\pm$ 535	2,848 $\pm$ 543	2,808 $\pm$ 164
hsa-miR-7-1-3p	63 $\pm$ 9	52 $\pm$ 6	65 $\pm$ 14	30 $\pm$ 7	60 $\pm$ 7	30 $\pm$ 12
hsa-miR-7-5p	1,082 $\pm$ 295	1,016 $\pm$ 118	1,435 $\pm$ 197	1,127 $\pm$ 81	788 $\pm$ 104	831 $\pm$ 144
hsa-miR-10a-5p	189 $\pm$ 32	185 $\pm$ 23	177 $\pm$ 10	120 $\pm$ 11	157 $\pm$ 26	182 $\pm$ 38
hsa-miR-10b-5p	119 $\pm$ 36	131 $\pm$ 28	136 $\pm$ 16	75 $\pm$ 15	109 $\pm$ 24	79 $\pm$ 22
hsa-miR-15a-5p	323 $\pm$ 40	326 $\pm$ 2	318 $\pm$ 62	235 $\pm$ 32	463 $\pm$ 45	211 $\pm$ 104
hsa-miR-15b-3p	45 $\pm$ 7	23 $\pm$ 11	46 $\pm$ 10	20 $\pm$ 3	35 $\pm$ 11	23 $\pm$ 3
hsa-miR-15b-5p	3,942 $\pm$ 535	3,717 $\pm$ 659	3,341 $\pm$ 765	3,209 $\pm$ 454	5,753 $\pm$ 629	2,816 $\pm$ 1,213
hsa-miR-16-2-3p	33 $\pm$ 12	36 $\pm$ 8	47 $\pm$ 4	25 $\pm$ 4	38 $\pm$ 14	25 $\pm$ 7
hsa-miR-16-5p	5,332 $\pm$ 1,526	5,272 $\pm$ 326	4,392 $\pm$ 875	5,035 $\pm$ 475	6,085 $\pm$ 640	4,507 $\pm$ 1,053
hsa-miR-17-5p	1,011 $\pm$ 75	950 $\pm$ 127	1,245 $\pm$ 121	929 $\pm$ 106	778 $\pm$ 150	512 $\pm$ 60
hsa-miR-18a-5p	40 $\pm$ 8	38 $\pm$ 3	42 $\pm$ 8	31 $\pm$ 6	45 $\pm$ 13	30 $\pm$ 20

<b>MiR</b>	<b>3 H CONTROL</b>	<b>3 H TPEN</b>	<b>12 H CONTROL</b>	<b>12 H TPEN</b>	<b>24 H CONTROL</b>	<b>24 H TPEN</b>
hsa-miR-18b-5p	18 ± 4	16 ± 6	23 ± 1	12 ± 2	25 ± 10	14 ± 12
hsa-miR-19a-3p	36 ± 18	43 ± 9	47 ± 10	26 ± 3	43 ± 8	21 ± 8
hsa-miR-19b-3p	426 ± 107	690 ± 346	276 ± 61	382 ± 87	190 ± 24	123 ± 54
hsa-miR-20a-5p	1,138 ± 369	1,053 ± 159	1,396 ± 78	1,060 ± 44	949 ± 210	562 ± 65
hsa-miR-20b-5p	391 ± 44	457 ± 32	639 ± 149	373 ± 188	257 ± 51	218 ± 118
hsa-miR-21-5p	9,473 ± 1,659	9,190 ± 619	10,598 ± 693	8,626 ± 827	11,333 ± 1,764	10,488 ± 1,501
hsa-miR-22-3p	746 ± 33	753 ± 17	645 ± 115	585 ± 77	809 ± 147	580 ± 229
hsa-miR-22-5p	55 ± 19	92 ± 32	84 ± 7	68 ± 14	98 ± 13	67 ± 29
hsa-miR-23a-3p	6,494 ± 1,374	6,638 ± 471	7,032 ± 246	6,147 ± 379	6,966 ± 216	6,888 ± 505
hsa-miR-23b-3p	6,762 ± 507	7,315 ± 273	6,585 ± 510	6,308 ± 235	6,859 ± 648	6,696 ± 214
hsa-miR-23c	1,623 ± 332	1,663 ± 454	1,813 ± 32	1,249 ± 282	1,165 ± 486	1,351 ± 590
hsa-miR-24-1-5p	14 ± 17	1 ± 1	3 ± 0	1 ± 1	4 ± 2	2 ± 1
hsa-miR-24-2-5p	30 ± 8	28 ± 3	34 ± 10	17 ± 6	47 ± 15	19 ± 12
hsa-miR-24-3p	4,868 ± 236	5,203 ± 465	4,349 ± 300	4,319 ± 374	4,801 ± 634	4,517 ± 780
hsa-miR-25-3p	1,184 ± 34	1,103 ± 313	1,416 ± 167	1,121 ± 284	1,070 ± 92	1,077 ± 50
hsa-miR-26a-5p	6,129 ± 850	5,594 ± 568	5,246 ± 164	4,402 ± 353	6,703 ± 465	3,967 ± 501
hsa-miR-26b-5p	1,358 ± 116	1,104 ± 261	1,671 ± 365	979 ± 399	1,154 ± 246	1,270 ± 502
hsa-miR-27a-3p	1,328 ± 57	1,457 ± 156	1,315 ± 179	1,029 ± 50	1,456 ± 32	1,012 ± 107
hsa-miR-27b-3p	815 ± 153	793 ± 62	721 ± 73	547 ± 60	1,094 ± 94	625 ± 116
hsa-miR-28-3p	94 ± 29	90 ± 6	112 ± 9	95 ± 22	107 ± 3	73 ± 42
hsa-miR-28-5p	176 ± 33	186 ± 11	146 ± 8	122 ± 29	137 ± 44	136 ± 34
hsa-miR-29a-3p	2,734 ± 1,056	3,072 ± 232	3,312 ± 639	3,056 ± 448	2,963 ± 192	3,144 ± 376
hsa-miR-29a-5p	44 ± 6	37 ± 4	31 ± 6	25 ± 9	28 ± 13	13 ± 1
hsa-miR-29b-1-5p	38 ± 1	19 ± 9	37 ± 13	18 ± 10	27 ± 11	5 ± 4
hsa-miR-29b-3p	3,071 ± 552	2,710 ± 392	3,650 ± 410	2,426 ± 376	3,178 ± 347	1,701 ± 511
hsa-miR-29c-3p	549 ± 150	603 ± 15	818 ± 186	444 ± 390	309 ± 125	1,040 ± 811
hsa-miR-30a-3p	632 ± 87	660 ± 92	593 ± 72	521 ± 16	548 ± 51	386 ± 52

<b>MiR</b>	<b>3 H CONTROL</b>	<b>3 H TPEN</b>	<b>12 H CONTROL</b>	<b>12 H TPEN</b>	<b>24 H CONTROL</b>	<b>24 H TPEN</b>
hsa-miR-30a-5p	8,651 ± 831	8,699 ± 824	7,119 ± 1,125	9,065 ± 794	8,994 ± 894	7,488 ± 1,614
hsa-miR-30b-3p	23 ± 5	26 ± 0	33 ± 7	26 ± 4	48 ± 12	61 ± 10
hsa-miR-30b-5p	8,888 ± 808	8,423 ± 1,091	7,992 ± 1,045	8,639 ± 2,040	8,573 ± 607	8,954 ± 1,887
hsa-miR-30c-1-3p	37 ± 5	47 ± 5	42 ± 5	86 ± 4	84 ± 9	1,307 ± 117
hsa-miR-30c-2-3p	19 ± 4	25 ± 4	20 ± 1	14 ± 1	24 ± 2	72 ± 30
hsa-miR-30c-5p	9,767 ± 2,202	9,799 ± 178	8,408 ± 1,539	10,549 ± 599	10,691 ± 944	8,909 ± 464
hsa-miR-30d-5p	5,773 ± 571	6,226 ± 365	4,750 ± 637	5,655 ± 443	5,441 ± 678	4,152 ± 549
hsa-miR-30e-3p	437 ± 133	468 ± 39	479 ± 47	322 ± 103	369 ± 62	293 ± 51
hsa-miR-30e-5p	6,652 ± 1,489	7,371 ± 549	5,872 ± 946	6,213 ± 689	6,566 ± 236	5,715 ± 253
hsa-miR-32-3p	57 ± 5	45 ± 10	85 ± 18	29 ± 6	52 ± 3	23 ± 10
hsa-miR-34b-3p	22 ± 9	22 ± 1	27 ± 5	20 ± 3	36 ± 10	13 ± 7
hsa-miR-34c-3p	76 ± 14	90 ± 5	67 ± 15	50 ± 2	84 ± 16	41 ± 16
hsa-miR-34c-5p	32 ± 5	27 ± 3	26 ± 3	15 ± 7	37 ± 8	14 ± 9
hsa-miR-92a-3p	1,357 ± 242	1,593 ± 244	1,552 ± 112	1,639 ± 360	1,499 ± 504	975 ± 324
hsa-miR-92b-3p	755 ± 35	708 ± 119	635 ± 79	659 ± 187	730 ± 166	311 ± 136
hsa-miR-93-5p	392 ± 160	415 ± 17	463 ± 51	417 ± 72	438 ± 52	333 ± 65
hsa-miR-96-5p	55 ± 18	66 ± 11	76 ± 16	39 ± 10	101 ± 10	44 ± 6
hsa-miR-98-5p	2,123 ± 314	2,547 ± 229	3,871 ± 2,149	2,624 ± 1,923	1,368 ± 383	3,151 ± 1,874
hsa-miR-99a-5p	3,495 ± 956	4,207 ± 640	4,126 ± 392	3,080 ± 1,027	3,058 ± 837	3,692 ± 1,674
hsa-miR-99b-5p	921 ± 38	614 ± 449	652 ± 149	683 ± 222	1,002 ± 190	550 ± 178
hsa-miR-100-3p	76 ± 26	68 ± 31	82 ± 22	13 ± 5	94 ± 18	11 ± 8
hsa-miR-100-5p	8,821 ± 925	8,692 ± 615	8,458 ± 969	8,987 ± 1,264	7,178 ± 1,081	8,565 ± 1,021
hsa-miR-101-3p	5 ± 3	8 ± 1	8 ± 1	5 ± 5	19 ± 14	6 ± 3
hsa-miR-103a-3p	2,081 ± 185	2,068 ± 81	1,863 ± 118	1,993 ± 225	1,945 ± 495	1,193 ± 351
hsa-miR-106a-5p	874 ± 363	892 ± 163	1,203 ± 57	910 ± 44	755 ± 94	481 ± 39
hsa-miR-106b-3p	64 ± 5	67 ± 1	57 ± 11	58 ± 4	67 ± 4	34 ± 9
hsa-miR-106b-5p	667 ± 71	559 ± 272	568 ± 14	510 ± 95	473 ± 164	206 ± 73

<b>MiR</b>	<b>3 H CONTROL</b>	<b>3 H TPEN</b>	<b>12 H CONTROL</b>	<b>12 H TPEN</b>	<b>24 H CONTROL</b>	<b>24 H TPEN</b>
hsa-miR-107	1,901 ± 129	1,972 ± 9	1,887 ± 181	1,923 ± 202	1,965 ± 479	1,230 ± 356
hsa-miR-122-5p	20 ± 2	20 ± 1	7 ± 2	29 ± 15	9 ± 9	34 ± 14
hsa-miR-125a-5p	1,875 ± 645	2,101 ± 223	2,078 ± 47	1,877 ± 64	1,823 ± 138	1,282 ± 203
hsa-miR-125b-5p	4,161 ± 359	4,420 ± 556	5,489 ± 333	4,622 ± 179	3,770 ± 268	3,833 ± 421
hsa-miR-126-3p	98 ± 19	90 ± 19	80 ± 21	54 ± 15	110 ± 9	40 ± 24
hsa-miR-128	116 ± 6	104 ± 8	86 ± 33	68 ± 29	140 ± 55	60 ± 54
hsa-miR-130a-3p	1,519 ± 278	1,346 ± 80	1,251 ± 102	1,048 ± 90	1,767 ± 348	940 ± 278
hsa-miR-130b-3p	285 ± 76	236 ± 41	278 ± 17	237 ± 22	310 ± 74	218 ± 80
hsa-miR-130b-5p	28 ± 4	28 ± 6	32 ± 2	30 ± 3	28 ± 11	20 ± 9
hsa-miR-132-3p	49 ± 7	61 ± 6	38 ± 2	630 ± 110	47 ± 4	663 ± 234
hsa-miR-132-5p	4 ± 2	7 ± 1	2 ± 1	92 ± 5	6 ± 4	109 ± 16
hsa-miR-138-1-3p	46 ± 5	38 ± 7	32 ± 4	30 ± 8	73 ± 12	30 ± 14
hsa-miR-138-5p	301 ± 118	322 ± 13	252 ± 40	253 ± 59	438 ± 79	255 ± 133
hsa-miR-139-5p	48 ± 17	54 ± 7	42 ± 7	38 ± 12	62 ± 11	24 ± 15
hsa-miR-140-3p	532 ± 73	546 ± 36	369 ± 99	575 ± 200	793 ± 162	390 ± 326
hsa-miR-146a-5p	2,196 ± 404	1,690 ± 358	1,563 ± 359	1,429 ± 305	2,010 ± 352	919 ± 413
hsa-miR-146b-5p	188 ± 84	220 ± 59	236 ± 74	118 ± 96	134 ± 31	167 ± 85
hsa-miR-148b-3p	264 ± 82	311 ± 23	251 ± 82	233 ± 38	373 ± 140	256 ± 145
hsa-miR-149-3p	47 ± 18	47 ± 10	54 ± 13	71 ± 33	41 ± 3	188 ± 25
hsa-miR-151a-3p	266 ± 36	251 ± 43	251 ± 35	240 ± 49	299 ± 68	183 ± 108
hsa-miR-151a-5p	1,970 ± 381	1,806 ± 100	1,447 ± 308	1,822 ± 214	1,915 ± 419	1,197 ± 602
hsa-miR-151b	1,940 ± 443	1,890 ± 169	1,391 ± 361	1,814 ± 271	1,891 ± 260	1,108 ± 600
hsa-miR-152	71 ± 8	68 ± 5	64 ± 15	43 ± 13	89 ± 20	32 ± 24
hsa-miR-181a-2-3p	25 ± 2	25 ± 21	25 ± 5	18 ± 8	26 ± 9	17 ± 6
hsa-miR-181a-5p	2,391 ± 1,092	2,668 ± 381	2,227 ± 564	3,001 ± 558	3,237 ± 308	2,456 ± 1,020
hsa-miR-181b-5p	1,202 ± 435	845 ± 85	1,025 ± 137	770 ± 24	867 ± 103	392 ± 86
hsa-miR-181c-5p	548 ± 230	766 ± 113	451 ± 138	419 ± 84	509 ± 237	314 ± 84

<b>MiR</b>	<b>3 H CONTROL</b>	<b>3 H TPEN</b>	<b>12 H CONTROL</b>	<b>12 H TPEN</b>	<b>24 H CONTROL</b>	<b>24 H TPEN</b>
hsa-miR-181d	565 ± 202	548 ± 168	586 ± 70	352 ± 138	393 ± 66	201 ± 83
hsa-miR-182-5p	465 ± 52	356 ± 32	532 ± 47	478 ± 20	580 ± 76	323 ± 85
hsa-miR-183-5p	177 ± 27	151 ± 17	147 ± 40	136 ± 12	169 ± 24	106 ± 62
hsa-miR-185-5p	72 ± 5	54 ± 15	73 ± 17	53 ± 6	93 ± 18	41 ± 27
hsa-miR-186-5p	266 ± 72	227 ± 71	241 ± 69	194 ± 43	313 ± 40	123 ± 74
hsa-miR-191-5p	2,583 ± 938	3,801 ± 188	2,897 ± 637	3,681 ± 494	3,803 ± 411	3,177 ± 1,430
hsa-miR-192-5p	40 ± 4	39 ± 11	38 ± 8	60 ± 7	42 ± 11	67 ± 24
hsa-miR-193a-3p	31 ± 25	35 ± 4	29 ± 8	20 ± 5	61 ± 26	27 ± 11
hsa-miR-193b-3p	32 ± 16	37 ± 8	22 ± 6	18 ± 3	43 ± 33	22 ± 5
hsa-miR-194-5p	22 ± 1	30 ± 10	27 ± 6	49 ± 8	45 ± 5	57 ± 46
hsa-miR-195-5p	146 ± 64	176 ± 26	170 ± 31	117 ± 62	131 ± 30	210 ± 133
hsa-miR-197-3p	72 ± 36	67 ± 17	81 ± 9	128 ± 24	93 ± 27	73 ± 22
hsa-miR-197-5p	20 ± 6	24 ± 13	24 ± 11	28 ± 15	10 ± 8	39 ± 26
hsa-miR-200b-3p	42 ± 12	44 ± 2	62 ± 7	25 ± 9	67 ± 8	40 ± 9
hsa-miR-200c-3p	23 ± 1	29 ± 5	35 ± 3	24 ± 1	33 ± 7	31 ± 6
hsa-miR-206	7 ± 3	6 ± 3	24 ± 10	79 ± 33	2 ± 2	11 ± 3
hsa-miR-210	59 ± 13	57 ± 4	54 ± 12	51 ± 22	113 ± 32	55 ± 38
hsa-miR-214-3p	14 ± 7	16 ± 4	14 ± 3	20 ± 13	15 ± 4	12 ± 2
hsa-miR-215	24 ± 9	28 ± 7	32 ± 2	38 ± 8	24 ± 12	46 ± 5
hsa-miR-221-3p	10,377 ± 1,583	8,811 ± 1,408	9,506 ± 1,427	9,690 ± 695	9,460 ± 389	10,390 ± 549
hsa-miR-221-5p	290 ± 42	266 ± 9	291 ± 19	149 ± 25	308 ± 29	131 ± 55
hsa-miR-222-3p	8,961 ± 3,729	11,374 ± 259	11,335 ± 703	11,734 ± 869	11,496 ± 343	11,038 ± 158
hsa-miR-222-5p	100 ± 25	84 ± 17	133 ± 18	12 ± 4	67 ± 20	13 ± 8
hsa-miR-224-5p	245 ± 64	203 ± 61	184 ± 18	132 ± 21	221 ± 28	129 ± 30
hsa-miR-301a-3p	93 ± 28	73 ± 5	75 ± 17	39 ± 16	119 ± 30	28 ± 19
hsa-miR-320a	730 ± 93	638 ± 99	875 ± 147	939 ± 140	841 ± 73	675 ± 307
hsa-miR-320b	633 ± 157	616 ± 46	732 ± 109	864 ± 143	658 ± 88	483 ± 193

<b>MiR</b>	<b>3 H CONTROL</b>		<b>3 H TPEN</b>		<b>12 H CONTROL</b>		<b>12 H TPEN</b>		<b>24 H CONTROL</b>		<b>24 H TPEN</b>	
hsa-miR-320c	649	± 116	644	± 13	783	± 167	900	± 146	664	± 81	532	± 210
hsa-miR-320d	559	± 44	542	± 66	726	± 147	828	± 120	624	± 111	480	± 177
hsa-miR-320e	601	± 122	553	± 33	617	± 63	717	± 69	560	± 80	428	± 139
hsa-miR-324-5p	70	± 32	55	± 13	66	± 3	61	± 14	81	± 21	45	± 25
hsa-miR-328	2	± 1	4	± 4	23	± 10	12	± 6	1	± 1	2	± 1
hsa-miR-330-3p	17	± 3	20	± 4	14	± 7	9	± 5	26	± 10	11	± 8
hsa-miR-331-3p	71	± 4	78	± 11	76	± 14	47	± 12	82	± 12	38	± 14
hsa-miR-335-3p	54	± 7	64	± 6	85	± 1	30	± 10	46	± 21	29	± 7
hsa-miR-335-5p	392	± 33	365	± 51	363	± 86	269	± 41	531	± 83	238	± 77
hsa-miR-340-5p	56	± 9	60	± 9	67	± 7	38	± 7	81	± 5	36	± 14
hsa-miR-342-3p	76	± 25	95	± 8	76	± 14	64	± 11	79	± 7	82	± 53
hsa-miR-345-5p	31	± 5	26	± 4	28	± 4	13	± 2	37	± 2	16	± 8
hsa-miR-346	3	± 2	3	± 1	19	± 15	8	± 6	1	± 1	2	± 1
hsa-miR-361-5p	291	± 67	221	± 8	244	± 44	158	± 51	363	± 129	131	± 68
hsa-miR-362-5p	30	± 8	25	± 2	23	± 6	27	± 11	27	± 6	10	± 8
hsa-miR-365a-3p	93	± 47	141	± 34	172	± 18	76	± 44	128	± 26	103	± 50
hsa-miR-374a-5p	129	± 60	151	± 25	210	± 39	89	± 51	147	± 42	142	± 84
hsa-miR-374b-5p	336	± 37	285	± 55	370	± 77	231	± 35	389	± 42	263	± 24
hsa-miR-374c-5p	187	± 13	225	± 16	248	± 66	167	± 5	226	± 82	186	± 10
hsa-miR-378a-3p	132	± 17	129	± 14	100	± 28	78	± 25	119	± 28	58	± 45
hsa-miR-378c	34	± 11	29	± 21	26	± 15	18	± 5	33	± 10	17	± 14
hsa-miR-378d	70	± 9	70	± 7	55	± 10	41	± 11	76	± 21	37	± 32
hsa-miR-378e	167	± 19	159	± 13	145	± 21	97	± 31	168	± 27	79	± 45
hsa-miR-378f	42	± 2	46	± 7	42	± 9	24	± 10	40	± 8	21	± 11
hsa-miR-378g	86	± 5	74	± 21	60	± 13	38	± 16	83	± 15	35	± 30
hsa-miR-378i	84	± 8	72	± 2	58	± 8	41	± 4	69	± 7	33	± 24
hsa-miR-379-5p	1	± 1	0	± 1	1	± 1	26	± 10	2	± 1	4	± 1

<b>MiR</b>	<b>3 H CONTROL</b>	<b>3 H TPEN</b>	<b>12 H CONTROL</b>	<b>12 H TPEN</b>	<b>24 H CONTROL</b>	<b>24 H TPEN</b>
hsa-miR-381-5p	5 ± 3	13 ± 7	3 ± 2	8 ± 6	18 ± 12	22 ± 12
hsa-miR-421	65 ± 18	46 ± 6	60 ± 6	35 ± 16	76 ± 3	36 ± 22
hsa-miR-422a	26 ± 8	26 ± 5	18 ± 6	7 ± 3	9 ± 5	12 ± 6
hsa-miR-423-5p	317 ± 28	371 ± 11	283 ± 63	281 ± 83	476 ± 98	242 ± 121
hsa-miR-424-3p	25 ± 12	18 ± 2	15 ± 3	7 ± 5	30 ± 10	7 ± 5
hsa-miR-424-5p	559 ± 47	491 ± 71	552 ± 45	305 ± 37	796 ± 48	406 ± 20
hsa-miR-425-3p	32 ± 3	30 ± 1	31 ± 8	25 ± 1	34 ± 13	19 ± 8
hsa-miR-425-5p	732 ± 105	597 ± 242	547 ± 152	650 ± 144	1,029 ± 156	630 ± 434
hsa-miR-454-3p	594 ± 141	518 ± 92	631 ± 28	467 ± 63	537 ± 107	311 ± 58
hsa-miR-455-3p	153 ± 21	123 ± 16	120 ± 27	123 ± 40	140 ± 35	75 ± 30
hsa-miR-466	1,389 ± 552	1,257 ± 551	907 ± 492	1,076 ± 311	1,170 ± 95	1,758 ± 407
hsa-miR-483-3p	3 ± 1	6 ± 5	27 ± 17	17 ± 13	5 ± 2	2 ± 1
hsa-miR-483-5p	204 ± 24	192 ± 14	167 ± 44	94 ± 40	90 ± 24	195 ± 41
hsa-miR-484	84 ± 39	53 ± 15	46 ± 8	38 ± 8	62 ± 18	19 ± 12
hsa-miR-486-3p	26 ± 9	16 ± 6	2 ± 2	14 ± 5	50 ± 10	14 ± 4
hsa-miR-486-5p	36 ± 7	28 ± 5	21 ± 3	16 ± 3	34 ± 12	12 ± 6
hsa-miR-489	15 ± 6	22 ± 4	16 ± 1	11 ± 6	36 ± 5	13 ± 8
hsa-miR-494	456 ± 124	451 ± 77	351 ± 32	239 ± 75	268 ± 111	568 ± 188
hsa-miR-503-5p	48 ± 7	45 ± 23	41 ± 12	18 ± 5	87 ± 9	29 ± 21
hsa-miR-505-3p	23 ± 9	33 ± 4	27 ± 4	16 ± 5	32 ± 9	16 ± 2
hsa-miR-513a-5p	9 ± 2	5 ± 2	11 ± 5	9 ± 3	18 ± 5	173 ± 83
hsa-miR-532-3p	5 ± 2	4 ± 2	3 ± 1	13 ± 20	2 ± 3	3 ± 1
hsa-miR-568	86 ± 34	111 ± 5	63 ± 15	52 ± 5	52 ± 21	57 ± 35
hsa-miR-574-3p	1,128 ± 409	1,446 ± 402	382 ± 264	563 ± 173	1,020 ± 121	804 ± 252
hsa-miR-574-5p	228 ± 48	208 ± 37	124 ± 36	169 ± 53	248 ± 16	141 ± 52
hsa-miR-576-3p	1 ± 0	4 ± 2	3 ± 3	211 ± 72	2 ± 2	30 ± 4
hsa-miR-584-5p	68 ± 17	80 ± 3	110 ± 23	57 ± 11	105 ± 19	55 ± 25

<b>MiR</b>	<b>3 H CONTROL</b>	<b>3 H TPEN</b>	<b>12 H CONTROL</b>	<b>12 H TPEN</b>	<b>24 H CONTROL</b>	<b>24 H TPEN</b>
hsa-miR-601	25 ± 4	23 ± 2	42 ± 26	7 ± 3	11 ± 9	7 ± 4
hsa-miR-603	15 ± 12	34 ± 22	12 ± 4	6 ± 2	19 ± 6	24 ± 9
hsa-miR-612	5 ± 2	5 ± 4	4 ± 3	5 ± 3	6 ± 0	38 ± 13
hsa-miR-625-3p	42 ± 7	37 ± 4	33 ± 4	20 ± 5	43 ± 10	19 ± 8
hsa-miR-625-5p	69 ± 6	73 ± 4	70 ± 6	51 ± 16	109 ± 23	55 ± 37
hsa-miR-629-5p	23 ± 12	25 ± 8	33 ± 3	22 ± 4	33 ± 3	24 ± 7
hsa-miR-638	199 ± 30	276 ± 27	197 ± 34	282 ± 40	190 ± 10	582 ± 47
hsa-miR-641	5 ± 1	14 ± 16	5 ± 3	8 ± 4	11 ± 2	8 ± 5
hsa-miR-663a	29 ± 23	44 ± 7	30 ± 8	44 ± 12	45 ± 13	117 ± 44
hsa-miR-664b-3p	23 ± 2	17 ± 8	15 ± 3	15 ± 2	24 ± 4	18 ± 16
hsa-miR-668	15 ± 21	40 ± 8	11 ± 3	17 ± 1	52 ± 32	58 ± 54
hsa-miR-671-5p	61 ± 14	55 ± 12	86 ± 21	46 ± 6	45 ± 7	40 ± 21
hsa-miR-744-5p	75 ± 22	67 ± 16	75 ± 18	51 ± 18	107 ± 30	37 ± 30
hsa-miR-762	153 ± 43	135 ± 20	98 ± 26	211 ± 46	151 ± 23	359 ± 45
hsa-miR-765	154 ± 56	238 ± 33	200 ± 44	203 ± 63	99 ± 15	158 ± 28
hsa-miR-877-5p	86 ± 29	58 ± 10	58 ± 13	59 ± 25	64 ± 6	30 ± 20
hsa-miR-885-5p	2 ± 2	3 ± 2	23 ± 13	9 ± 9	3 ± 2	2 ± 1
hsa-miR-936	13 ± 4	19 ± 7	8 ± 2	17 ± 5	6 ± 5	33 ± 21
hsa-miR-937-3p	6 ± 4	4 ± 3	30 ± 19	16 ± 6	3 ± 1	4 ± 1
hsa-miR-937-5p	40 ± 13	49 ± 16	103 ± 51	136 ± 60	24 ± 5	102 ± 78
hsa-miR-1180	14 ± 2	16 ± 7	38 ± 11	45 ± 7	18 ± 3	9 ± 5
hsa-miR-1183	5 ± 5	6 ± 3	32 ± 9	34 ± 11	5 ± 4	4 ± 0
hsa-miR-1227-5p	27 ± 5	32 ± 3	29 ± 10	51 ± 10	17 ± 5	57 ± 27
hsa-miR-1228-3p	5 ± 4	5 ± 7	15 ± 13	21 ± 17	7 ± 4	4 ± 1
hsa-miR-1228-5p	50 ± 6	46 ± 5	44 ± 7	41 ± 2	19 ± 1	19 ± 7
hsa-miR-1229-5p	9 ± 6	10 ± 5	13 ± 7	6 ± 1	8 ± 6	20 ± 15
hsa-miR-1233-1-5p	26 ± 13	41 ± 14	30 ± 9	48 ± 15	24 ± 2	79 ± 23

<b>MiR</b>	<b>3 H CONTROL</b>		<b>3 H TPEN</b>		<b>12 H CONTROL</b>		<b>12 H TPEN</b>		<b>24 H CONTROL</b>		<b>24 H TPEN</b>	
hsa-miR-1234-5p	392	± 39	444	± 40	413	± 40	384	± 35	276	± 18	770	± 208
hsa-miR-1236-3p	0	± 1	3	± 3	32	± 18	8	± 8	1	± 1	1	± 0
hsa-miR-1237-5p	39	± 33	68	± 6	44	± 16	59	± 12	45	± 17	219	± 41
hsa-miR-1246	897	± 104	824	± 107	876	± 77	1,385	± 680	929	± 71	5,073	± 1,939
hsa-miR-1260a	10	± 10	17	± 10	22	± 4	18	± 14	12	± 7	30	± 14
hsa-miR-1260b	386	± 224	423	± 51	433	± 127	728	± 68	744	± 231	1,645	± 371
hsa-miR-1268a	27	± 9	25	± 9	90	± 24	107	± 33	11	± 6	16	± 2
hsa-miR-1268b	46	± 9	56	± 16	140	± 43	147	± 64	70	± 12	71	± 26
hsa-miR-1273c	6	± 6	11	± 2	4	± 3	6	± 5	4	± 1	26	± 13
hsa-miR-1273f	16	± 3	14	± 0	9	± 3	13	± 1	14	± 4	60	± 12
hsa-miR-1273g-3p	920	± 234	870	± 556	797	± 313	2,510	± 346	1,153	± 253	4,219	± 1,209
hsa-miR-1275	214	± 35	216	± 20	207	± 5	142	± 7	260	± 8	817	± 314
hsa-miR-1281	5	± 3	7	± 3	28	± 8	29	± 15	6	± 7	4	± 1
hsa-miR-1305	15	± 20	4	± 3	4	± 3	12	± 6	3	± 4	5	± 2
hsa-miR-1306-3p	9	± 4	5	± 1	24	± 9	25	± 5	3	± 1	3	± 1
hsa-miR-1307-3p	96	± 31	79	± 16	116	± 15	141	± 8	117	± 32	66	± 13
hsa-miR-1469	124	± 27	81	± 17	107	± 29	137	± 40	89	± 17	152	± 27
hsa-miR-1538	6	± 5	8	± 4	4	± 1	15	± 21	4	± 1	12	± 4
hsa-miR-1587	25	± 8	25	± 9	82	± 37	121	± 76	25	± 3	120	± 30
hsa-miR-1825	4	± 4	6	± 6	20	± 5	15	± 18	6	± 4	1	± 1
hsa-miR-1908	7	± 4	7	± 4	3	± 2	17	± 20	7	± 4	4	± 2
hsa-miR-1915-3p	24	± 8	35	± 2	16	± 1	47	± 13	28	± 3	122	± 23
hsa-miR-1972	6	± 1	49	± 15	6	± 2	28	± 3	8	± 6	7	± 1
hsa-miR-1973	208	± 38	386	± 23	226	± 68	507	± 52	293	± 23	799	± 229
hsa-miR-2392	18	± 5	12	± 2	17	± 4	26	± 4	7	± 6	87	± 69
hsa-miR-2861	22	± 14	19	± 5	22	± 6	22	± 4	9	± 1	37	± 13
hsa-miR-3064-3p	14	± 13	23	± 8	19	± 6	15	± 6	24	± 8	18	± 4

<b>MiR</b>	<b>3 H CONTROL</b>	<b>3 H TPEN</b>	<b>12 H CONTROL</b>	<b>12 H TPEN</b>	<b>24 H CONTROL</b>	<b>24 H TPEN</b>
hsa-miR-3065-5p	12 ± 3	15 ± 5	11 ± 2	21 ± 2	12 ± 6	22 ± 10
hsa-miR-3127-5p	6 ± 5	4 ± 2	1 ± 1	490 ± 142	4 ± 3	63 ± 17
hsa-miR-3141	280 ± 43	245 ± 25	260 ± 89	166 ± 59	109 ± 25	114 ± 42
hsa-miR-3145-3p	2 ± 2	3 ± 4	1 ± 1	114 ± 33	3 ± 3	5 ± 3
hsa-miR-3146	2 ± 2	4 ± 4	1 ± 1	322 ± 116	2 ± 2	18 ± 7
hsa-miR-3149	65 ± 15	68 ± 4	78 ± 16	59 ± 6	54 ± 13	48 ± 15
hsa-miR-3150b-3p	70 ± 73	74 ± 73	27 ± 17	46 ± 11	66 ± 56	91 ± 50
hsa-miR-3162-5p	3 ± 3	2 ± 3	1 ± 1	2 ± 1	2 ± 0	27 ± 16
hsa-miR-3164	0 ± 0	2 ± 1	1 ± 1	183 ± 43	4 ± 4	11 ± 5
hsa-miR-3178	693 ± 73	646 ± 58	726 ± 153	892 ± 181	1,256 ± 352	2,549 ± 1,059
hsa-miR-3182	44 ± 10	38 ± 1	45 ± 8	44 ± 25	33 ± 4	123 ± 59
hsa-miR-3185	9 ± 2	8 ± 2	4 ± 2	8 ± 0	14 ± 3	32 ± 8
hsa-miR-3195	19 ± 3	14 ± 3	12 ± 4	15 ± 6	26 ± 11	28 ± 19
hsa-miR-3196	260 ± 43	293 ± 32	167 ± 21	278 ± 36	219 ± 49	740 ± 137
hsa-miR-3197	29 ± 12	55 ± 4	14 ± 3	145 ± 64	62 ± 33	132 ± 90
hsa-miR-3591-3p	123 ± 44	156 ± 21	115 ± 7	103 ± 19	69 ± 33	146 ± 60
hsa-miR-3607-3p	31 ± 3	41 ± 8	22 ± 2	17 ± 7	59 ± 9	31 ± 14
hsa-miR-3607-5p	161 ± 7	179 ± 30	99 ± 28	143 ± 49	331 ± 88	215 ± 266
hsa-miR-3609	95 ± 19	93 ± 13	82 ± 10	63 ± 14	94 ± 19	85 ± 52
hsa-miR-3610	33 ± 5	33 ± 3	27 ± 13	134 ± 46	10 ± 2	28 ± 12
hsa-miR-3612	1 ± 1	4 ± 3	1 ± 2	235 ± 84	0 ± 0	16 ± 7
hsa-miR-3613-3p	19 ± 4	10 ± 1	14 ± 7	21 ± 17	14 ± 9	18 ± 9
hsa-miR-3620-5p	40 ± 17	44 ± 12	98 ± 21	142 ± 42	31 ± 9	149 ± 31
hsa-miR-3621	11 ± 11	7 ± 3	4 ± 0	10 ± 10	1 ± 1	25 ± 17
hsa-miR-3622b-5p	4 ± 1	3 ± 2	2 ± 2	3 ± 3	3 ± 2	20 ± 12
hsa-miR-3651	11 ± 8	16 ± 4	9 ± 0	22 ± 4	18 ± 9	42 ± 15
hsa-miR-3652	4 ± 4	8 ± 7	33 ± 9	38 ± 16	2 ± 1	7 ± 2

<b>MiR</b>	<b>3 H CONTROL</b>	<b>3 H TPEN</b>	<b>12 H CONTROL</b>	<b>12 H TPEN</b>	<b>24 H CONTROL</b>	<b>24 H TPEN</b>
hsa-miR-3656	159 ± 2	135 ± 26	254 ± 59	308 ± 107	113 ± 27	365 ± 40
hsa-miR-3661	4 ± 2	4 ± 3	2 ± 2	3 ± 4	7 ± 4	19 ± 14
hsa-miR-3663-3p	29 ± 12	36 ± 7	30 ± 10	23 ± 12	21 ± 4	23 ± 7
hsa-miR-3665	739 ± 283	948 ± 86	799 ± 54	1,442 ± 80	908 ± 151	2,545 ± 350
hsa-miR-3667-5p	19 ± 3	20 ± 1	23 ± 15	6 ± 5	3 ± 2	15 ± 6
hsa-miR-3673	1 ± 1	2 ± 1	0 ± 0	153 ± 34	2 ± 1	18 ± 5
hsa-miR-3676-3p	147 ± 105	234 ± 66	89 ± 12	109 ± 30	90 ± 23	12 ± 3
hsa-miR-3676-5p	97 ± 4	88 ± 37	98 ± 20	211 ± 102	86 ± 5	291 ± 61
hsa-miR-3935	6 ± 4	15 ± 7	13 ± 1	31 ± 3	4 ± 1	25 ± 7
hsa-miR-3940-5p	100 ± 12	132 ± 3	150 ± 40	164 ± 70	105 ± 32	252 ± 102
hsa-miR-3960	1,187 ± 199	1,365 ± 44	1,072 ± 69	1,580 ± 55	966 ± 305	3,014 ± 260
hsa-miR-4254	9 ± 2	9 ± 6	30 ± 16	24 ± 13	10 ± 1	8 ± 2
hsa-miR-4267	1,540 ± 1,341	1,758 ± 1,759	621 ± 237	1,120 ± 515	4,242 ± 3,592	5,950 ± 1,298
hsa-miR-4270	22 ± 5	19 ± 3	15 ± 6	29 ± 1	11 ± 4	66 ± 10
hsa-miR-4280	16 ± 5	31 ± 21	9 ± 9	29 ± 22	7 ± 5	13 ± 8
hsa-miR-4281	214 ± 84	198 ± 24	224 ± 38	136 ± 1	106 ± 12	147 ± 56
hsa-miR-4284	52 ± 11	91 ± 25	46 ± 11	101 ± 13	55 ± 18	256 ± 24
hsa-miR-4286	47 ± 8	49 ± 22	75 ± 37	57 ± 14	50 ± 14	67 ± 25
hsa-miR-4288	624 ± 301	605 ± 203	924 ± 387	428 ± 371	353 ± 158	1,000 ± 771
hsa-miR-4289	104 ± 65	159 ± 22	105 ± 23	49 ± 28	88 ± 26	98 ± 54
hsa-miR-4298	252 ± 41	251 ± 13	295 ± 78	140 ± 38	141 ± 32	113 ± 14
hsa-miR-4301	84 ± 32	96 ± 49	117 ± 68	180 ± 100	210 ± 148	613 ± 289
hsa-miR-4306	86 ± 13	76 ± 3	89 ± 10	53 ± 9	79 ± 4	39 ± 11
hsa-miR-4314	1 ± 1	2 ± 2	0 ± 0	139 ± 31	0 ± 1	13 ± 7
hsa-miR-4317	29 ± 7	23 ± 23	30 ± 20	13 ± 15	13 ± 14	71 ± 60
hsa-miR-4321	20 ± 18	25 ± 11	6 ± 4	14 ± 10	10 ± 5	21 ± 15
hsa-miR-4324	2,900 ± 555	2,742 ± 223	3,156 ± 449	2,397 ± 742	2,170 ± 291	2,239 ± 459

<b>MiR</b>	<b>3 H CONTROL</b>	<b>3 H TPEN</b>	<b>12 H CONTROL</b>	<b>12 H TPEN</b>	<b>24 H CONTROL</b>	<b>24 H TPEN</b>
hsa-miR-4325	28 ± 7	29 ± 15	38 ± 28	25 ± 30	18 ± 8	75 ± 58
hsa-miR-4329	12 ± 19	1 ± 1	1 ± 2	4 ± 2	1 ± 1	4 ± 3
hsa-miR-4419b	228 ± 31	233 ± 36	220 ± 94	191 ± 127	91 ± 32	75 ± 30
hsa-miR-4421	2 ± 0	2 ± 1	0 ± 1	99 ± 29	1 ± 2	11 ± 2
hsa-miR-4429	368 ± 33	340 ± 61	459 ± 113	441 ± 98	221 ± 76	217 ± 105
hsa-miR-4433-3p	17 ± 4	25 ± 2	30 ± 3	40 ± 10	18 ± 5	80 ± 33
hsa-miR-4440	3 ± 0	2 ± 2	17 ± 7	19 ± 16	2 ± 2	2 ± 0
hsa-miR-4442	72 ± 28	82 ± 8	71 ± 34	32 ± 10	33 ± 6	39 ± 13
hsa-miR-4443	2,051 ± 586	2,466 ± 42	2,259 ± 204	4,197 ± 276	2,223 ± 229	2,815 ± 216
hsa-miR-4444	46 ± 9	44 ± 12	55 ± 12	9 ± 4	26 ± 5	8 ± 2
hsa-miR-4447	67 ± 30	89 ± 10	90 ± 33	44 ± 29	62 ± 20	177 ± 153
hsa-miR-4454	211 ± 94	238 ± 23	215 ± 68	393 ± 103	382 ± 33	1,158 ± 478
hsa-miR-4455	251 ± 44	215 ± 19	321 ± 106	136 ± 30	177 ± 12	99 ± 13
hsa-miR-4459	353 ± 47	423 ± 30	366 ± 79	253 ± 66	225 ± 62	277 ± 49
hsa-miR-4462	6 ± 4	6 ± 2	33 ± 14	26 ± 12	2 ± 2	6 ± 2
hsa-miR-4463	40 ± 10	51 ± 2	71 ± 11	119 ± 17	37 ± 6	267 ± 36
hsa-miR-4466	101 ± 21	97 ± 14	67 ± 11	109 ± 8	77 ± 10	190 ± 34
hsa-miR-4472	64 ± 14	87 ± 5	70 ± 40	38 ± 15	41 ± 6	224 ± 154
hsa-miR-4481	12 ± 6	16 ± 10	118 ± 37	114 ± 49	5 ± 1	5 ± 1
hsa-miR-4482-5p	2 ± 2	1 ± 1	0 ± 0	128 ± 48	2 ± 1	9 ± 6
hsa-miR-4484	247 ± 57	225 ± 33	172 ± 20	429 ± 81	149 ± 20	1,680 ± 111
hsa-miR-4485	44 ± 20	96 ± 64	35 ± 11	1,217 ± 362	158 ± 27	1,703 ± 1,335
hsa-miR-4486	19 ± 6	34 ± 2	22 ± 3	42 ± 9	17 ± 8	44 ± 25
hsa-miR-4488	274 ± 60	308 ± 13	307 ± 26	336 ± 33	354 ± 79	644 ± 81
hsa-miR-4492	21 ± 6	19 ± 7	14 ± 3	36 ± 6	31 ± 4	108 ± 6
hsa-miR-4497	393 ± 107	466 ± 12	484 ± 92	531 ± 58	629 ± 110	1,333 ± 250
hsa-miR-4499	69 ± 11	50 ± 15	57 ± 9	33 ± 3	28 ± 4	31 ± 12

<b>MiR</b>	<b>3 H CONTROL</b>	<b>3 H TPEN</b>	<b>12 H CONTROL</b>	<b>12 H TPEN</b>	<b>24 H CONTROL</b>	<b>24 H TPEN</b>
hsa-miR-4500	14 ± 9	10 ± 8	31 ± 31	12 ± 18	7 ± 6	67 ± 65
hsa-miR-4505	27 ± 6	35 ± 2	26 ± 6	63 ± 9	46 ± 9	259 ± 30
hsa-miR-4507	22 ± 4	26 ± 8	64 ± 26	91 ± 32	23 ± 9	113 ± 17
hsa-miR-4508	387 ± 51	341 ± 52	427 ± 19	577 ± 102	595 ± 131	1,565 ± 615
hsa-miR-4514	22 ± 8	19 ± 9	10 ± 7	10 ± 2	44 ± 16	177 ± 107
hsa-miR-4516	472 ± 157	585 ± 112	415 ± 33	645 ± 27	442 ± 109	1,439 ± 262
hsa-miR-4521	886 ± 204	1,055 ± 185	785 ± 67	504 ± 83	645 ± 144	61 ± 19
hsa-miR-4530	117 ± 26	128 ± 12	91 ± 17	126 ± 27	93 ± 29	499 ± 186
hsa-miR-4532	32 ± 11	31 ± 4	17 ± 8	22 ± 9	32 ± 5	165 ± 104
hsa-miR-4534	81 ± 6	66 ± 15	87 ± 21	72 ± 32	50 ± 10	63 ± 15
hsa-miR-4632-5p	25 ± 11	28 ± 15	121 ± 48	157 ± 35	13 ± 5	32 ± 14
hsa-miR-4638-5p	1,549 ± 875	1,737 ± 368	957 ± 676	1,198 ± 1,088	533 ± 410	2,963 ± 3,573
hsa-miR-4644	24 ± 5	29 ± 16	23 ± 6	24 ± 10	11 ± 5	49 ± 10
hsa-miR-4646-5p	50 ± 8	46 ± 6	55 ± 15	15 ± 7	24 ± 6	21 ± 2
hsa-miR-4648	1 ± 2	1 ± 1	0 ± 0	87 ± 14	5 ± 3	7 ± 3
hsa-miR-4649-5p	5 ± 3	6 ± 2	18 ± 13	41 ± 22	4 ± 3	52 ± 7
hsa-miR-4651	7 ± 1	12 ± 7	84 ± 33	86 ± 52	3 ± 2	10 ± 3
hsa-miR-4660	1 ± 2	4 ± 4	1 ± 1	317 ± 91	2 ± 1	21 ± 9
hsa-miR-4667-5p	47 ± 5	59 ± 12	47 ± 20	28 ± 19	18 ± 6	52 ± 20
hsa-miR-4668-5p	27 ± 20	4 ± 1	4 ± 1	29 ± 41	10 ± 1	31 ± 10
hsa-miR-4669	3 ± 2	3 ± 3	5 ± 3	31 ± 4	4 ± 5	5 ± 4
hsa-miR-4687-3p	155 ± 34	191 ± 24	160 ± 25	157 ± 36	118 ± 20	301 ± 172
hsa-miR-4690-5p	1,397 ± 739	2,599 ± 1,568	1,050 ± 261	2,301 ± 342	2,467 ± 1,775	2,483 ± 628
hsa-miR-4695-5p	13 ± 6	20 ± 6	16 ± 6	15 ± 7	10 ± 7	18 ± 14
hsa-miR-4707-5p	49 ± 13	66 ± 5	43 ± 6	56 ± 24	38 ± 5	100 ± 34
hsa-miR-4710	9 ± 4	12 ± 7	50 ± 12	61 ± 36	5 ± 2	13 ± 6
hsa-miR-4712-3p	11 ± 13	9 ± 11	7 ± 3	6 ± 8	9 ± 10	48 ± 57

<b>MiR</b>	<b>3 H CONTROL</b>	<b>3 H TPEN</b>	<b>12 H CONTROL</b>	<b>12 H TPEN</b>	<b>24 H CONTROL</b>	<b>24 H TPEN</b>
hsa-miR-4717-3p	7 ± 3	6 ± 3	27 ± 4	33 ± 8	4 ± 1	2 ± 0
hsa-miR-4724-5p	1 ± 1	1 ± 1	1 ± 1	12 ± 20	1 ± 1	1 ± 1
hsa-miR-4728-5p	13 ± 2	27 ± 5	20 ± 4	19 ± 1	13 ± 2	21 ± 5
hsa-miR-4732-5p	21 ± 6	32 ± 10	18 ± 5	11 ± 3	6 ± 2	10 ± 3
hsa-miR-4734	2,588 ± 3,267	1,951 ± 2,090	603 ± 251	1,991 ± 736	3,131 ± 3,228	7,247 ± 3,484
hsa-miR-4739	258 ± 34	282 ± 27	264 ± 36	125 ± 26	168 ± 55	170 ± 35
hsa-miR-4743-5p	23 ± 10	36 ± 5	19 ± 8	13 ± 4	6 ± 3	20 ± 10
hsa-miR-4763-3p	9 ± 4	13 ± 3	50 ± 25	51 ± 13	5 ± 2	13 ± 6
hsa-miR-4764-3p	26 ± 36	78 ± 19	17 ± 7	34 ± 36	29 ± 36	343 ± 296
hsa-miR-4778-5p	581 ± 154	643 ± 135	744 ± 165	634 ± 269	222 ± 47	293 ± 91
hsa-miR-4787-5p	156 ± 19	221 ± 31	191 ± 4	346 ± 31	267 ± 33	1,208 ± 91
hsa-miR-4800-3p	5 ± 4	6 ± 1	3 ± 2	9 ± 4	4 ± 3	85 ± 28
hsa-miR-4800-5p	43 ± 12	31 ± 5	45 ± 22	85 ± 19	14 ± 3	41 ± 10
hsa-miR-5001-5p	22 ± 12	38 ± 8	29 ± 3	55 ± 7	26 ± 9	129 ± 70
hsa-miR-5088	4 ± 3	2 ± 0	4 ± 2	135 ± 45	4 ± 3	13 ± 7
hsa-miR-5096	395 ± 107	1,459 ± 1,964	250 ± 63	632 ± 148	476 ± 134	1,283 ± 824
hsa-miR-5100	50 ± 8	57 ± 8	47 ± 22	82 ± 19	74 ± 6	133 ± 35
hsa-miR-5194	1 ± 2	5 ± 2	4 ± 2	403 ± 140	1 ± 1	60 ± 20
hsa-miR-5196-5p	13 ± 7	13 ± 6	10 ± 2	9 ± 1	6 ± 5	118 ± 65
hsa-miR-5572	7 ± 3	9 ± 3	16 ± 10	26 ± 22	7 ± 4	17 ± 9
hsa-miR-5581-5p	0 ± 1	4 ± 4	0 ± 0	115 ± 48	2 ± 3	14 ± 6
hsa-miR-5739	19 ± 5	22 ± 12	8 ± 3	263 ± 109	9 ± 6	58 ± 25
hsa-miR-5787	119 ± 7	131 ± 16	105 ± 7	116 ± 12	91 ± 35	307 ± 145
hsa-miR-6073	13 ± 3	26 ± 5	18 ± 8	24 ± 26	24 ± 24	241 ± 194
hsa-miR-6075	4 ± 3	6 ± 5	2 ± 2	3 ± 3	4 ± 1	24 ± 19
hsa-miR-6076	47 ± 3	53 ± 5	43 ± 8	27 ± 6	29 ± 6	24 ± 5
hsa-miR-6082	25 ± 5	36 ± 7	21 ± 3	13 ± 2	20 ± 10	23 ± 12

<b>MiR</b>	<b>3 H CONTROL</b>		<b>3 H TPEN</b>		<b>12 H CONTROL</b>		<b>12 H TPEN</b>		<b>24 H CONTROL</b>		<b>24 H TPEN</b>	
hsa-miR-6085	69	± 15	75	± 14	57	± 4	87	± 18	61	± 2	266	± 59
hsa-miR-6086	45	± 12	62	± 9	37	± 13	23	± 2	22	± 4	24	± 12
hsa-miR-6087	1,005	± 42	1,239	± 167	836	± 86	1,024	± 5	764	± 142	2,070	± 138
hsa-miR-6088	138	± 48	122	± 8	179	± 31	121	± 20	71	± 14	181	± 53
hsa-miR-6089	1,276	± 92	1,416	± 45	1,306	± 63	1,761	± 231	1,455	± 212	2,847	± 637
hsa-miR-6090	1,123	± 432	1,418	± 144	976	± 275	1,408	± 78	902	± 342	2,232	± 841
hsa-miR-6124	163	± 30	144	± 15	117	± 31	163	± 23	71	± 10	184	± 44
hsa-miR-6125	288	± 26	263	± 36	204	± 28	240	± 45	210	± 33	617	± 119
hsa-miR-6126	147	± 44	163	± 51	117	± 30	382	± 44	159	± 30	801	± 154
hsa-miR-6127	20	± 10	11	± 2	37	± 17	43	± 3	5	± 4	32	± 12
hsa-miR-6128	0	± 1	1	± 1	0	± 1	61	± 19	1	± 1	10	± 3
hsa-miR-6132	7	± 2	7	± 4	6	± 3	13	± 2	8	± 3	60	± 19
hsa-miR-6133	532	± 202	352	± 279	253	± 96	373	± 180	583	± 269	720	± 162
hsa-miR-6165	55	± 16	64	± 7	58	± 10	41	± 8	27	± 7	51	± 28
hsa-miR-6509-5p	2	± 2	2	± 1	7	± 1	93	± 25	2	± 0	7	± 5
hsa-miR-6510-5p	1,094	± 231	1,233	± 104	850	± 161	985	± 46	776	± 195	1,439	± 358
hsa-miR-6511a-5p	3	± 3	5	± 4	6	± 1	3	± 3	5	± 7	20	± 21
hsa-miR-6511b-5p	6	± 3	4	± 3	6	± 2	7	± 4	3	± 4	20	± 19
hsa-miR-6716-5p	2	± 1	3	± 2	1	± 1	217	± 89	4	± 1	27	± 4
hsa-miR-6722-3p	45	± 9	57	± 14	124	± 49	141	± 77	17	± 2	85	± 60
hsa-miR-6723-5p	5	± 3	3	± 1	6	± 2	9	± 1	9	± 6	21	± 18
hsa-miR-6724-5p	50	± 20	35	± 8	31	± 11	46	± 5	24	± 3	69	± 18

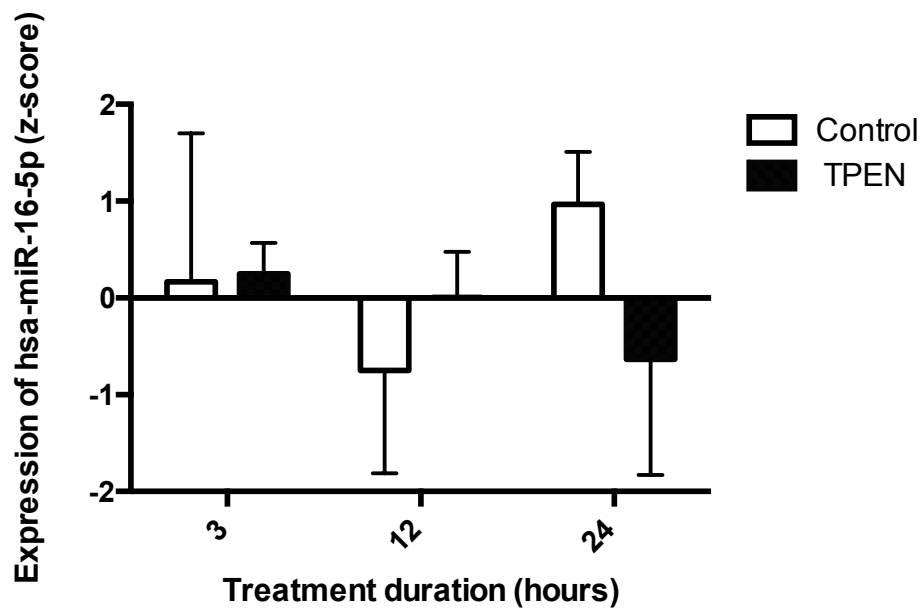


**Figure A.1: Hsa-miR-16-5p expression measured by microarray (z-scores of log transformed signal intensities).**

MDA-MB-231 cells were treated with DMSO (control) or TPEN (10  $\mu$ M in DMSO) for 3, 12 and 24 h (n=3). 2-way ANOVA indicated no significant differences between groups ( $p < 0.05$ ).

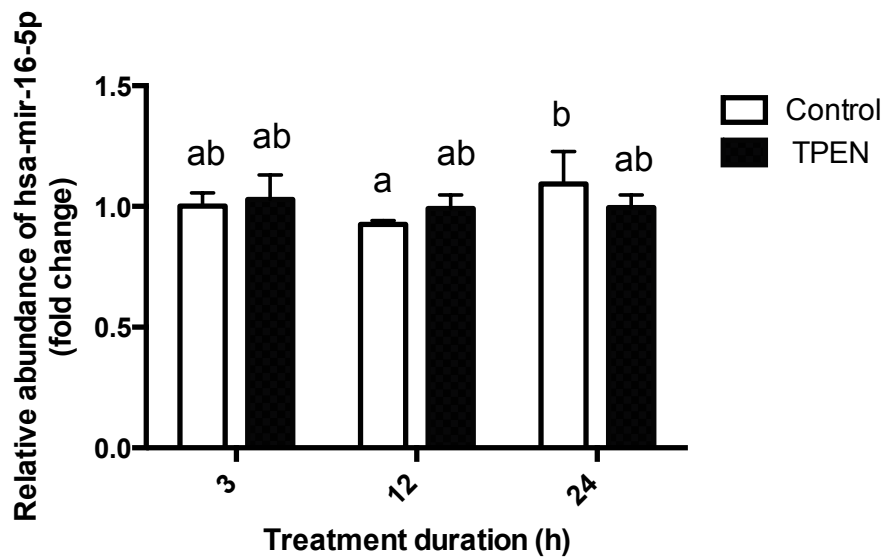


**Figure A.2: Hsa-miR-16-5p expression during qRT-PCR experiment 1.**

MDA-MB-231 cells were treated with control (DMSO) or TPEN (10  $\mu$ M in DMSO) for 3, 12 and 24 h. Values are mean  $\pm$  SD (n = 6 except TPEN at 12 h, where n = 5 due to removal of an outlier). Expression is reported relative to the control sample at 3 h. Different letters indicate significant differences between means ( $p < 0.05$ ).

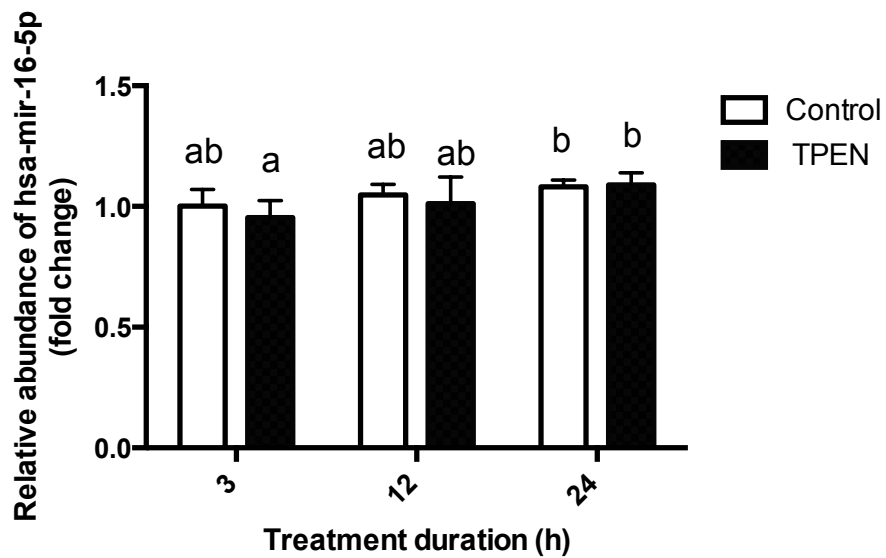


**Figure A.3: Hsa-miR-16-5p expression during qRT-PCR experiment 2.**

MDA-MB-231 cells were treated with control (DMSO) or TPEN (10  $\mu$ M in DMSO) for 3, 12 and 24 h. Values are mean  $\pm$  SD (n = 6 except TPEN at 3 and 12 h, where n = 5 due to removal of outliers). Expression is reported relative to the control sample at 3 h. Different letters indicate significant differences between means ( $p < 0.05$ ).

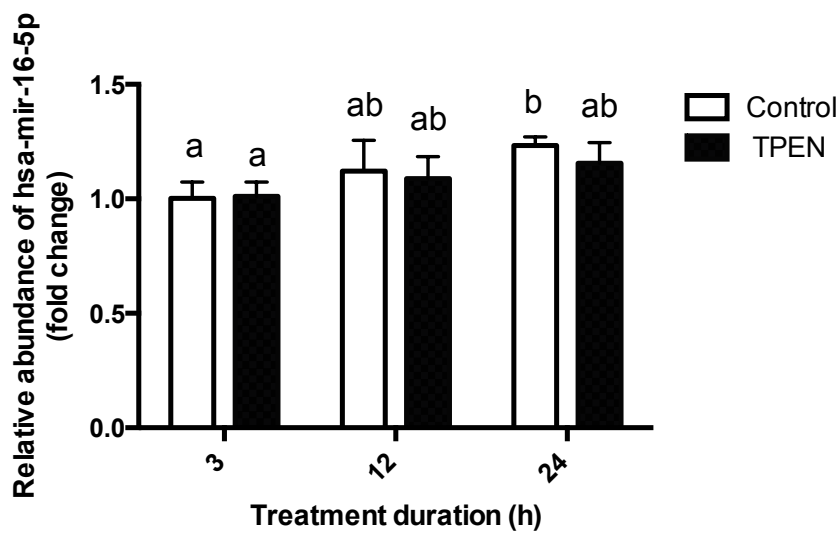


**Figure A.4: Hsa-miR-16-5p expression during qRT-PCR experiment 3.**

MDA-MB-231 cells were treated with control (DMSO) or TPEN (10  $\mu$ M in DMSO) for 3, 12 and 24 h. Values are mean  $\pm$  SD (n = 6). Expression is reported relative to the control sample at 3 h. Different letters indicate significant differences between means ( $p < 0.05$ ).

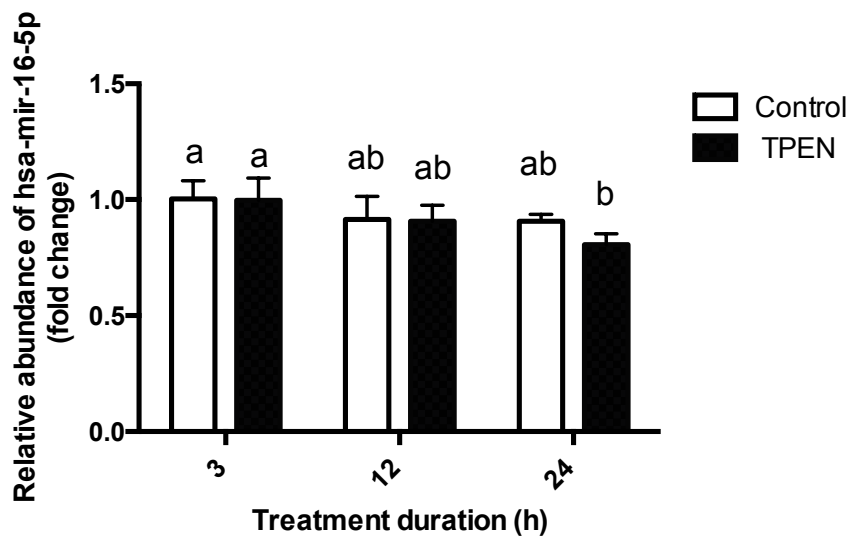


**Figure A.5: Hsa-miR-16-5p expression during qRT-PCR experiment 4.**

MDA-MB-231 cells were treated with control (DMSO) or TPEN (10  $\mu$ M in DMSO) for 3, 12 and 24 h. Values are mean  $\pm$  SD (n = 6 except Control at 3 h and TPEN at 12 h, where n = 5 due to removal of outliers). Expression is reported relative to the control sample at 3 h. Different letters indicate significant differences between means ( $p < 0.05$ ).

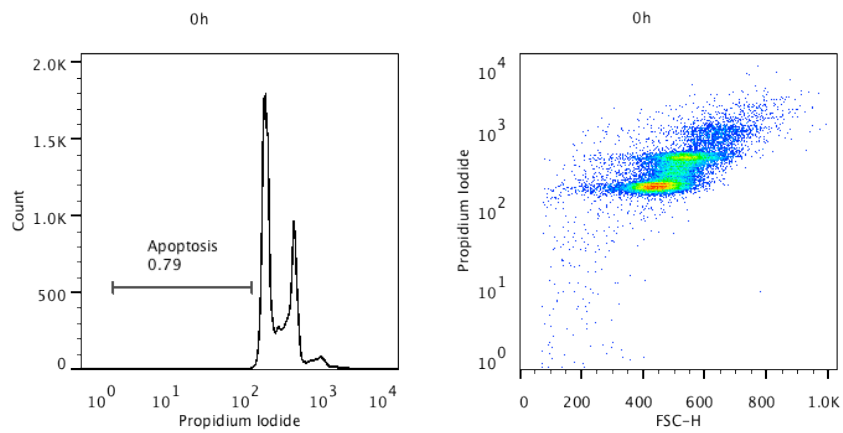


**Figure A.6: Baseline DNA fragmentation in MDA-MB-231 cells at 0 h.** Apoptosis was assessed by propidium-iodide flow cytometric assay. Dot plots and histograms of propidium-iodide labeled cells are shown.

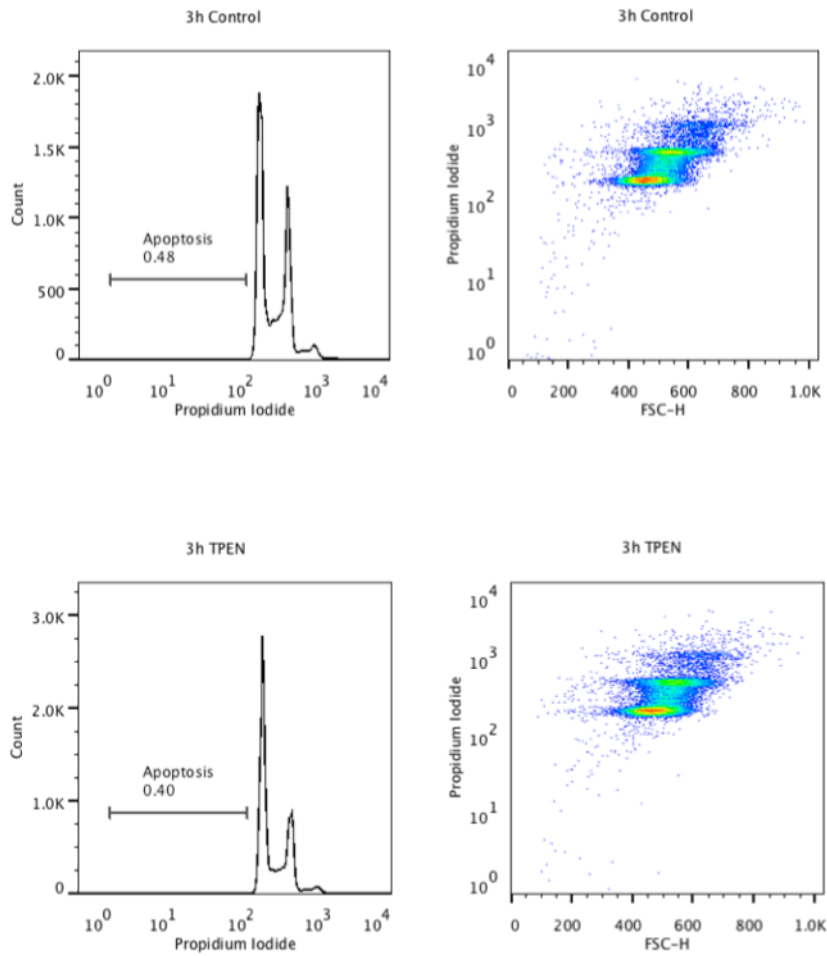


**Figure A.7: DNA fragmentation in MDA-MB-231 cells treated with TPEN at 3 h.** MDA-MB-231 cells were treated with control (DMSO) or TPEN (10  $\mu$ M in DMSO) for 3 h and apoptosis was assessed by propidium-iodide flow cytometric assay. Dot plots and histograms of propidium-iodide labeled cells are shown.

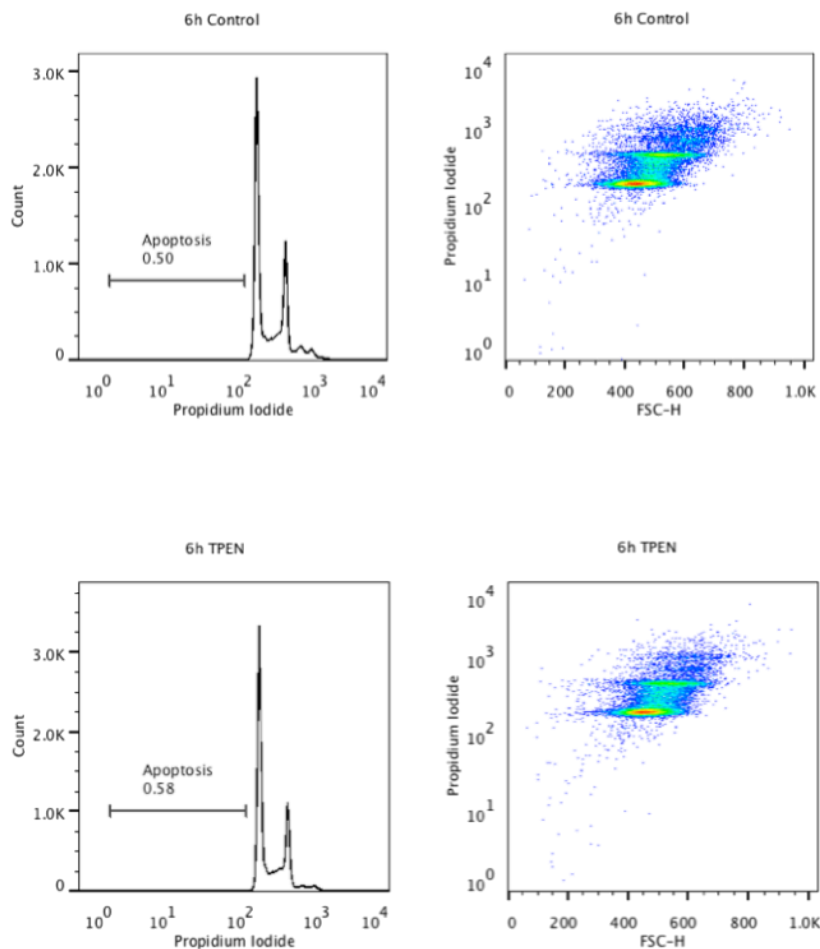


**Figure A.8: DNA fragmentation in MDA-MB-231 cells treated with TPEN at 6 h.** MDA-MB-231 cells were treated with control (DMSO) or TPEN (10  $\mu$ M in DMSO) for 6 h and apoptosis was assessed by propidium-iodide flow cytometric assay. Dot plots and histograms of propidium-iodide labeled cells are shown.

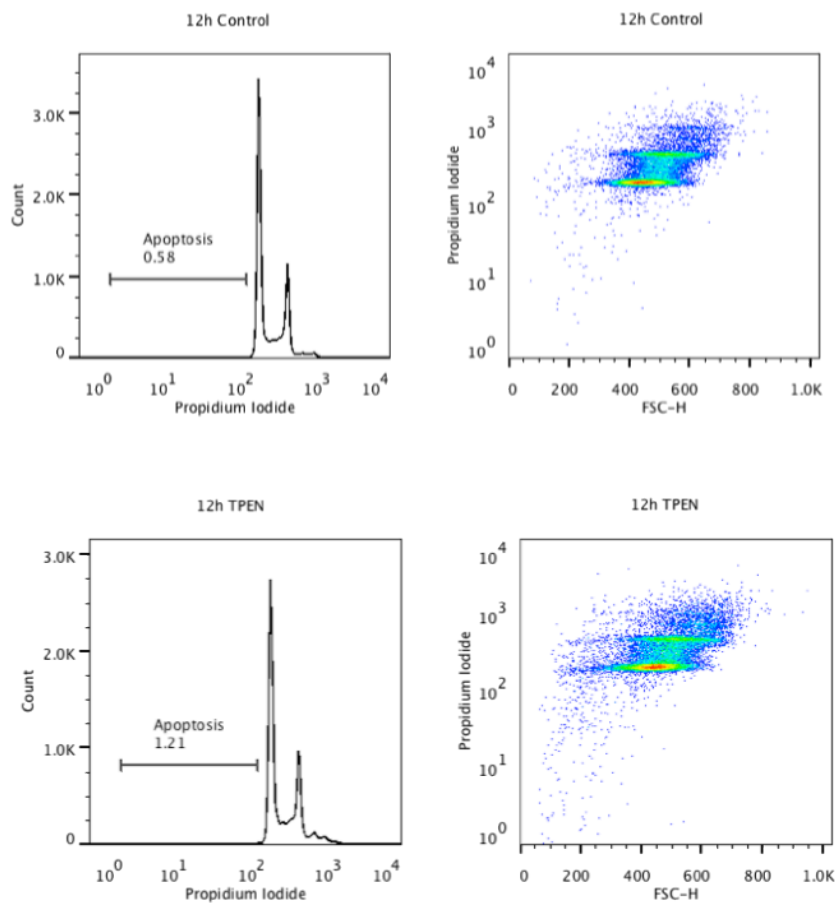


**Figure A.9: DNA fragmentation in MDA-MB-231 cells treated with TPEN at 12 h.** MDA-MB-231 cells were treated with control (DMSO) or TPEN (10  $\mu$ M in DMSO) for 12 h and apoptosis was assessed by propidium-iodide flow cytometric assay. Dot plots and histograms of propidium-iodide labeled cells are shown.

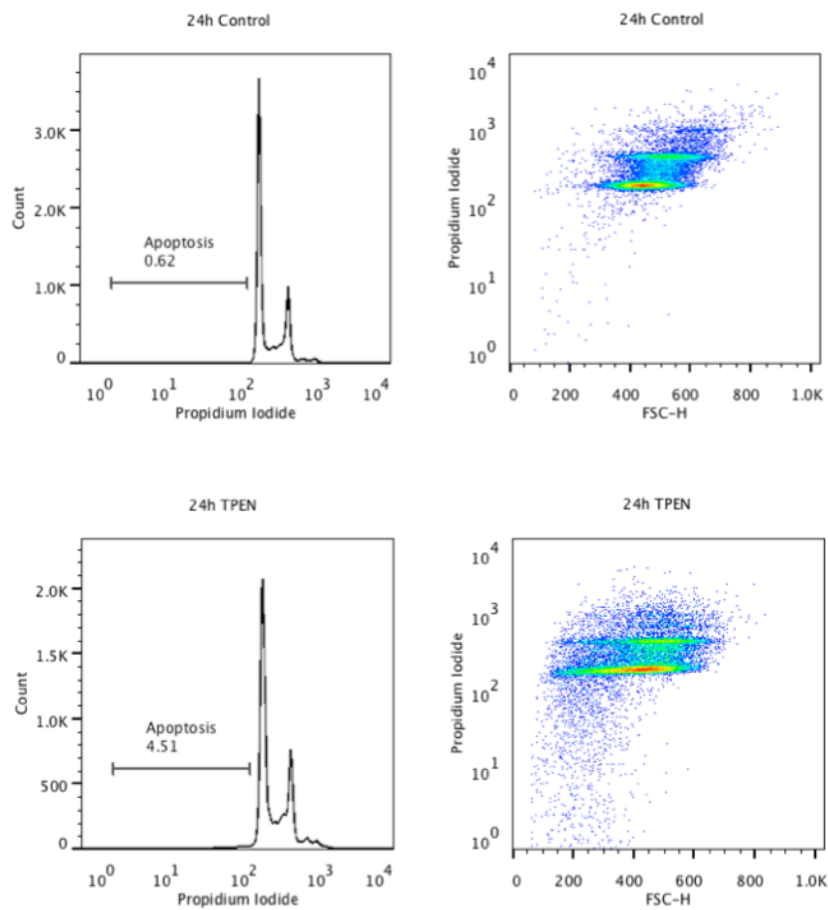


**Figure A.10: DNA fragmentation in MDA-MB-231 cells treated with TPEN at 24 h.** MDA-MB-231 cells were treated with control (DMSO) or TPEN (10  $\mu$ M in DMSO) for 24 h and apoptosis was assessed by propidium-iodide flow cytometric assay. Dot plots and histograms of propidium-iodide labeled cells are shown.

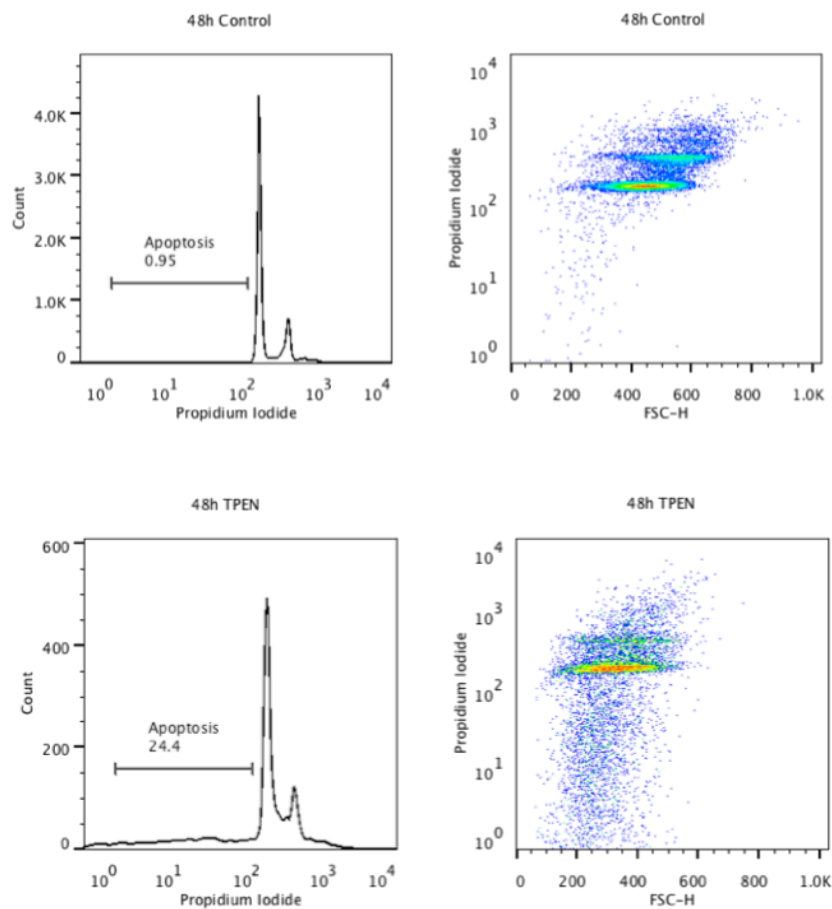


**Figure A.11: 48-h TPEN-induced DNA fragmentation in MDA-MB-231 cells.**

MDA-MB-231 cells were treated with control (DMSO) or TPEN (10  $\mu$ M in DMSO) for 48 h and apoptosis was assessed by propidium-iodide flow cytometric assay. Dot plots and histograms of propidium-iodide labeled cells are shown.

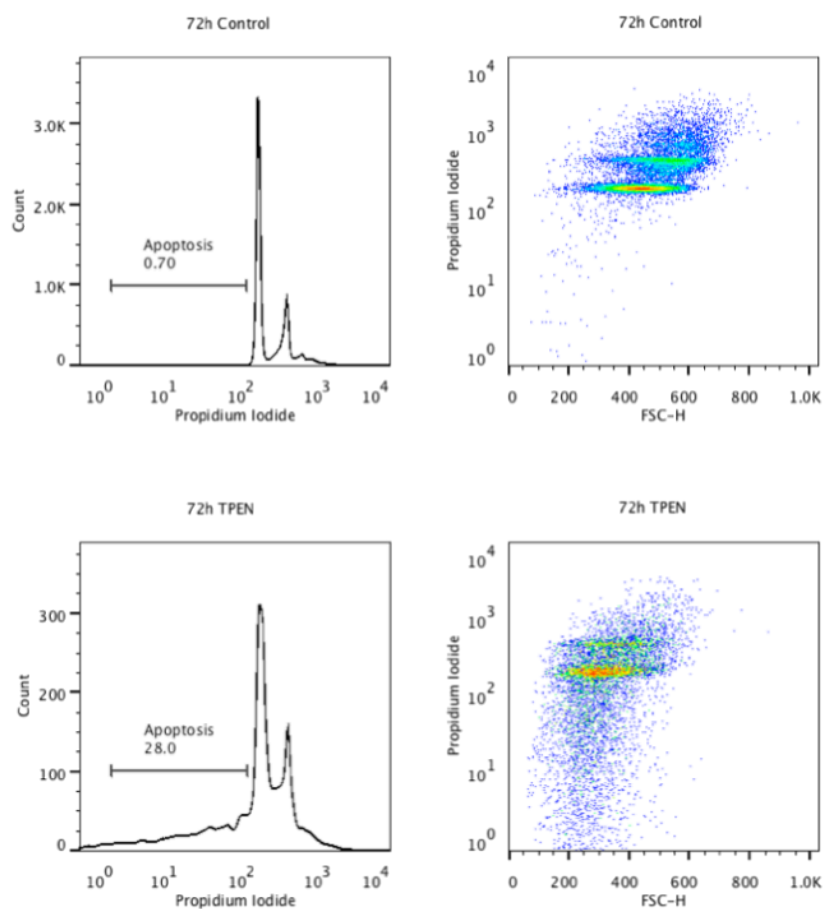


**Figure A.12: 72-h TPEN-induced DNA fragmentation in MDA-MB-231 cells.** MDA-MB-231 cells were treated with control (DMSO) or TPEN (10  $\mu$ M in DMSO) for 72 h and apoptosis was assessed by propidium-iodide flow cytometric assay. Dot plots and histograms of propidium-iodide labeled cells are shown.